UNIVERSITY OF NEAPLES

"FEDERICO II"

PhD PROGRAM IN NEUROSCIENCE
XXXVI CYCLE

PhD thesis title:

GAIN OF FUNCTION EFFECT CAUSED BY INNER PORE VARIANTS IN Kv7.2, Kv7.3 AND Kv7.5 POTASSIUM CHANNELS IDENTIFIED IN PATIENTS WITH DEVELOPMENTAL AND/OR EPILEPTIC ENCEPHALOPATHY

Coordinator
Prof. Maurizio Taglialatela

Tutor
Prof. Maurizio Taglialatela

Candidate
Nappi Mario
DR995200

Academic Year 2023/2024

Abbreviations

AG: Activation gate

AnkG: ankyrin G

AHP: afterhyperpolarization

AIS: axon initial segment

AP: action potential

ASD: autism spectrum disorder

SLFNE: Self-limited Familial Neonatal Epilepsy

SLFIE: Self-limited Familial Infantile Epilepsy

CaM: Calmodulin

CHO: Chinese Hamster Ovary

CHOL cholesterol

CTL: control

Cryo-EM cryogenic electron microscopy

DAG: diacylglycerol

DD: developmental disorder

DEE: Developmental Epileptic Encephalopathy

DMPC 1,2-Dimyristoyl-sn-glycero-3-phosphocholine

DN: dominant-negative

NO-DEE: Neonatal Onset – Developmental Epileptic Encephalopathy

EC50: half maximal effective concentration

GoF: gain-of-function

IC50: half maximal inhibitory concentration

ID: intellectual disability

I_{KM}: M-current

IP_3: inositol triphosphate

LoF: loss-of-function

MD molecular dynamics

NDD: neurodevelopmental delay

PKC: protein kinase C

PIP_2: Phosphatidylinositol 4,5-bisphosphate

POPC: 1-palmitoyl-2-oleoyl-sn-glycero-3-phosphocholine

POPE: 1-palmitoyl-2-oleoyl-sn-glycero-3-phosphoethanolamine

POPG: 1-Palmitoyl-2-oleoyl-sn-glycero-3-(phospho-rac-(1-glycerol))

PLC: phospholipase C

Po: maximal probability of opening

RMSD root mean square deviation

TEA: tetraethylammonium

V_{rest}: resting membrane potential

VSD: Voltage Sensing Domain

$V_{½}$: half-activation potential

1. INTRODUCTION

1.1 ION CHANNELS: CLASSIFICATION, FUNCTIONAL PROPERTIES AND ROLE IN NEURONS

All living cells are surrounded by a thin, approximately 40 angstrom thick, lipid bilayer called the cell membrane. Although plasma membrane is a basic prerequisite for life (Deamer et. al., 2002), it generates a major problem: it creates a barrier for many solutes, including ions. Cell membrane interior is an oily substance and ions are more stable in water than in oil, but ions are essential for many physiological processes, from maintaining proper intracellular osmolarity to generating electrical signals.

Ion channels evolved, hand-in-hand with membranes, to overcome this problem: these are, indeed, pore-forming proteins that allow the flow of ions across membranes. Ion channels are present both in plasma membranes and in membranes of intracellular organelles (Hille, 2001).

Currently, ion channels constitute an abundant and complex category of proteins: in the human genome, more than 300 genes code for ion channels.

Most ion channels are selective to one or more types of ions; moreover, one of the main roles of ion channels is to control the selective flow of ions in response to a stimulus. It is possible to classify ion channels on the basis of their selectivity into ion channels for chloride, potassium, sodium, calcium, protons or multiple cations. Ion channels may be also classified by the nature of their gating or the species of ions passing through those gates. The main gating modes of ion channels include gating due to protein binding to a neurotransmitter (Ligand-gated ion channels) or to changes in the membrane potential (Voltage-gated potassium channels). Other modes of gating involve interaction with second messengers on the intracellular side.

Generally, the various ion channels are classified into macro groups on the basis of their selectivity, and then subclassify on the basis of the gating mechanism, as follows:

- **Chloride channels** This superfamily consists of 13 members. Most of that are voltage-dependent, but CFTR is ATP-dependent.
- **Potassium channels**, that can be classified in:

    - Voltage-gated potassium channels
    - Calcium-activated potassium channels
    - Inward-rectifier potassium channels
    - Two-pore-domain potassium channels
- **Sodium channels** (NaVs), consisting in 10 members, most of that are voltage-dependent;
- **Calcium channels** (CaVs), including 10 voltage-dependent members and 4 ligand-gated channels;
- **Proton channels**
- **Non-selective cation channels**.

Since the first direct recording of single ion channel current (Neher and Sakmann 1976), which earned the Nobel Prize for the two German physiologists Sakmann and Neher in Physiology or Medicine in 1991, the individual functional properties of numerous ion channels have been described (Gałecka et. al., 2021). Each ion channel has its own conductance, a measure that indicates how much charge moves across the membrane, and a certain probability that the pore is in open conformation. Single-channel behavior can be described by the following equation:

$$i = \gamma P_o$$

where *i* is the single-channel current, *γ* is the single-channel conductance, P_o is the probability of finding the pore open. For a voltage gated ion channel, P_o is a function of the membrane potential [$P_o(V_m)$] (see below).

Considering these parameters, the macroscopic current of a cell can be described as:

$$I = N \gamma P_o$$

Where *N* is the number of ion channels in the membrane.

Membrane potential, on the other hand, can be defined as a product of the separation of charges across the membrane generates an electrochemical potential and electrical potential across membranes. Electrochemical potential of a ion differentially distributed across a non-permeable membrane is described by the Nernst equation:

$$E_x = \frac{RT}{zF} ln \frac{[x]_O}{[x]i}$$

where *R* is the gas constant, *T* is temperature, *z* is the valence of the ion, *F* is the faraday constant and $[x]$ is the concentration of the ion on a specific side of the

membrane. Ion channels regulate membrane potential by changing the permeability of the membrane for a specific ion species.

In fact, the membrane potential depends on the difference in the electrochemical potential of an ion and on the permeability of the membrane for that ion, as described by the Goldman equation:

$$Vm = \frac{RT}{F} ln \frac{P_K[K^+]_o + P_{Na}[Na^+]_o + P_{Cl}[Cl^-]_o}{P_K[K^+]_i + P_{Na}[Na^+]_i + P_{Cl}[Cl^-]_i}$$

Generally the resting potential of a cell membrane is -80 mV.

The permeability (P_x) of a membrane can be defined as the passive diffusion rate of permeable molecules across the membrane.

An action potential occurs when the membrane potential rapidly rises and falls (Fig. I.1) (Hodgkin and Huxley, 1952).

In neurons, action potentials play a central role in cell-to-cell communication by allowing the propagation of signals along the neuron's axon toward synaptic buttons. Then, these signals can be transferred to other neuron, to muscle cells or glands.

In other types of cells, their main function is to activate intracellular processes. In muscle cells, for example, an action potential is the first step in the chain of events leading to contraction.

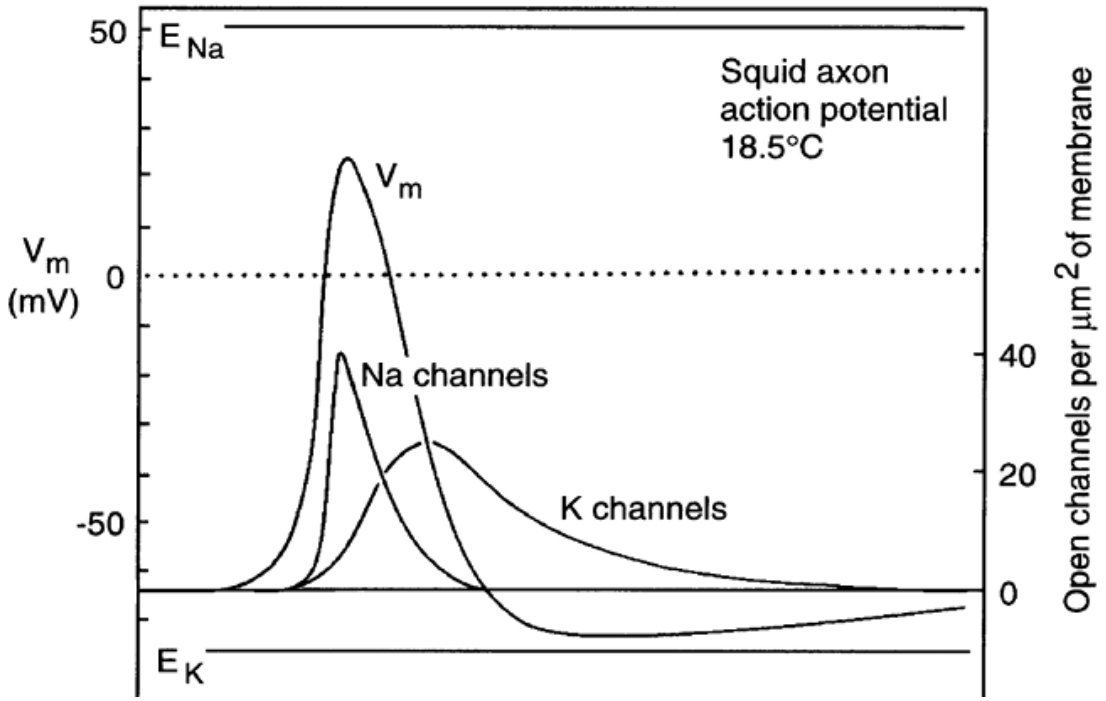

Figure I1.1 *Ionic currents in squind axon contributing to neuronal action potential (Hille, 2001)*

Hodgkin and Huxley demonstrated that ion's membrane permeability is voltage-dependent; I_{Na} is fast-activating, but I_K is more slow-activating current (Fig. I1.1, Hille, 2001) During the action potential, the depolarization soon increases the Na^+ permeability, inducing a Na^+ inward current, with sequential depolarization of the membrane from -70 mV to +30 mV (E_{Na}); this change in membrane potentials increase the K^+ permeability too, activating the K^+ outward current that determine the hyperpolarization of the membrane until resting values potentials and inactivating Na^+ currents. Ion channels are essential, for rapid changes in membrane permeability, to generate action potentials, a fundamental mechanism in intercellular communication.

1.2 POTASSIUM CHANNEL: PORE STRUCTURE AND ION SELECTIVITY

K^+ channels are a heterogeneous and ubiquitous group of membrane proteins that selectively conduct K^+ ions, in or out the cell membrane, depending on the electrochemical gradient. At physiological conditions, the concentration of K^+ ions is 25-fold higher in the intracellular solutions than in the extracellular compartment, so the opening of K^+ channels permits the inward flux rate between 10^6 and 10^8 ions per second (Hille, 2001).

All K^+ channels are characterized by 1) a pore that permits ion flux, 2) selectivity filter that allows the flux of K^+ ions but no other species and 3) a gating mechanism that is necessary to switch between closed and open conformations. In that chapter we are focusing on the structure of the pore of potassium channels and on ions conduction mechanism.

1.2.1 PORE STRUCTURE

The general structure of the pore in cation channels is pretty well-conserved among species and evolution (MacKinnon, 1995).

The first cation pore structure that was elucidated with X-ray crystallography technique was the structure of the KcsA bacterial potassium channel (Doyle et.

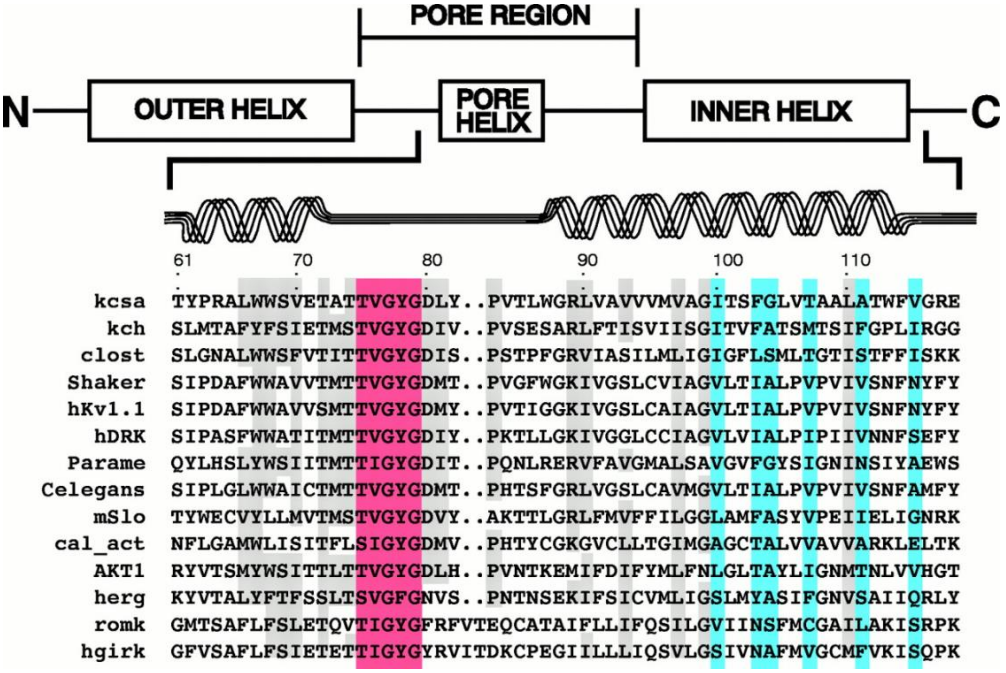

***Figure I2.1**: Sequence alignment of selected K+ channels. In magenta is reported conserved selectivity filter sequence (Adapted from Fig.1, Doyle et. al., 1998)*

al., 1998) by MacKinnon's group. This discovery led to Roderick MacKinnon being awarded the Nobel Prize in Chemistry in 2003.

KcsA (K channel of streptomyces A) is a prokaryotic potassium channel, found in the *Streptomyces lividans* bacteria, that is activated by intracellular changes in pH.

KcsA represents the simplest topology for a K^+ channel. The pore and the selectivity filter structures are very similar to other K^+ channels, including eukaryotic K^+ channels (Fig. I2.1, Doyle, 1998). For this reason, KcsA crystal structure was used as a template to study the structure of several K^+ channels for many years (Roux B., 2005). This structure consists of four identical pore-

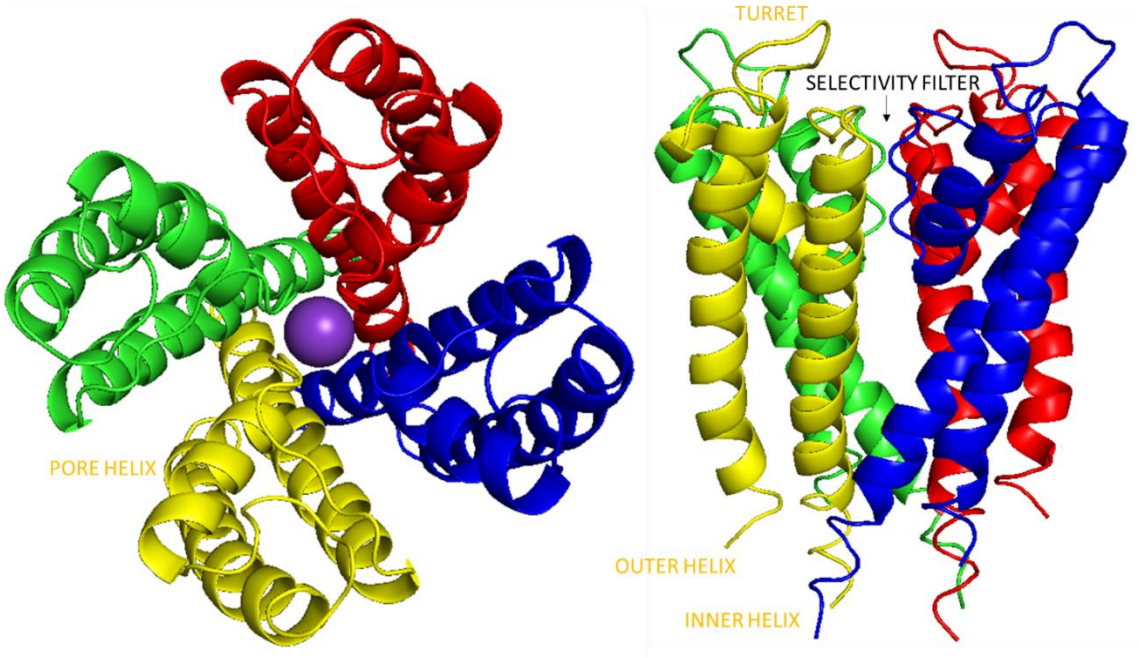

Figure I2.2 *KcsA channel structure top view (left) and lateral view (right). Each of the four subunit are indicated with a different color. Potassium ion into the filter is rapresnted in purple (left)(Doyle et. al., 1998).*

forming subunits and a selectivity filter tuned to select the potassium ions. Each subunit has two transmembrane α-helices connected by the roughly 30 amino acid pore region, which consists of the turret, pore helix, and selectivity filter. A subunit is inserted into the tetramer, in a way that one transmembrane helix (inner helix) faces the central pore while the other (outer helix) faces the lipid membrane. The inner helices are inclined, relative to the membrane, about 25° and are slightly bent so that the subunits open like the petals of a flower facing outward from the cell. The open petals include the structure formed by the pore region near the extracellular surface of the membrane (Fig. I2.2). This region

contains the K^+ channel signature sequence, which forms the selectivity filter (Fig. I2.1).

The essential features of subunit packing can be appreciated by observing the relationship between the four internal helices and the four pore helices. The four internal helices pack against each other as a bundle near the intracellular side of the membrane. The pore helices are sandwiched between the poles of the teepee and are directed, in an amino-carboxylic direction, towards a point near the center of the channel. This helical pore arrangement provides many of the inter-subunit contacts that hold the tetramer together and are critical for the functioning of the ion-conduction pore.

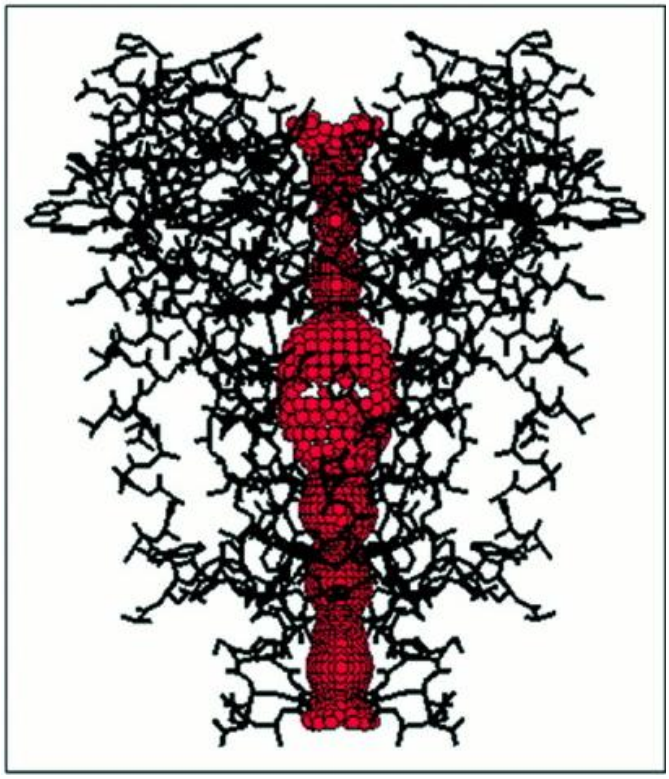

Figure I2.3 *KcsA channel pore. The internal cavity of the pore is shown in red (Doyle et. al., 1998).*

The total length of the resulting conduction pore, in its closed state, is 45 angstroms. When viewed longitudinally, the pore can be divided into three regions: the selectivity filter, the water cavity and the inner pore (fig. I2.3). The diameter of the selectivity filter is approximately 3 angstroms. The rest of the pore diameter varies from 8 to 18 angstroms. The outer helices of the pore expose a negative charge on the channel surface, due to the presence of negatively charged side chains (such as Y82 and T85). These negative charges, placed on the channel surface, attract cations to induce and facilitate their flow through the pore. Furthermore, since an ion, moving through a narrow pore, faces the

maximal energy barrier at the center of the membrane (Parsegian, 1975), the central cavity overcomes this problem: the aqueous cavity is located longitudinally in the center of the pore, and its presence appears to lower the electrostatic barrier, facilitating the flow of ions through the pore (Fig I2.3, Doyle et. al., in 1998), thus demonstrated how the structure of KcsA is optimized to overcome the main thermodynamic barriers that would prevent the flow of potassium ions. These observations can be also extended to the pore of other potassium-selective ion channels.

1.2.2 SELECTIVITY MECHANISM AND CONDUCTION OF POTASSIUM IONS

Considering that the radius of sodium is smaller than the potassium, even in hydrated form, how is it possible to have an ion channel that is selectively 1000 times permeable for potassium than for sodium (Thomas et. al., 2008)? This issue was clarified when the first potassium channel structure was solved using X-ray crystallography approach (Zhou et. al., 2001).

The answer is in the peculiar selectivity filter. The selectivity filter consists in 5 residues located between the outer helix and the pore helix (Fig I2.1), forming the highly-conserved Threonine-Valine-Glycine-Tyrosine-Glycine (or TVGYG) motif. The threonine is more internal of the pore, whereas the last glycine faces the extracellular side of the membrane. The carbonyl groups of these amino acids of all four subunits face the central cavity of the pore and are the ones that form the

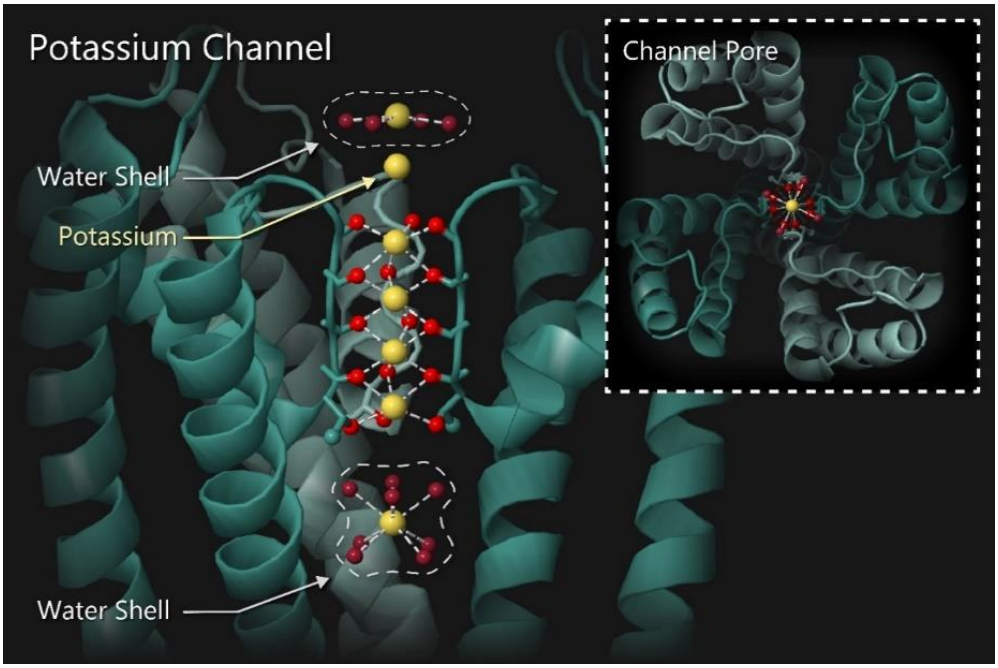

Figure I2.4 *Hydrated and dehydrated potassium ions occupation into the selectivity filter of KcsA (https://pdb101.rcsb.org/motm/38).*

core of the selectivity filter. Assuming that the ions are flowing from inside to outside, the potassium ion is hydrated into the central cavity and is surrounded by 8 symmetrical water molecules (Zhou et. al., 2001). The four carbonyl groups

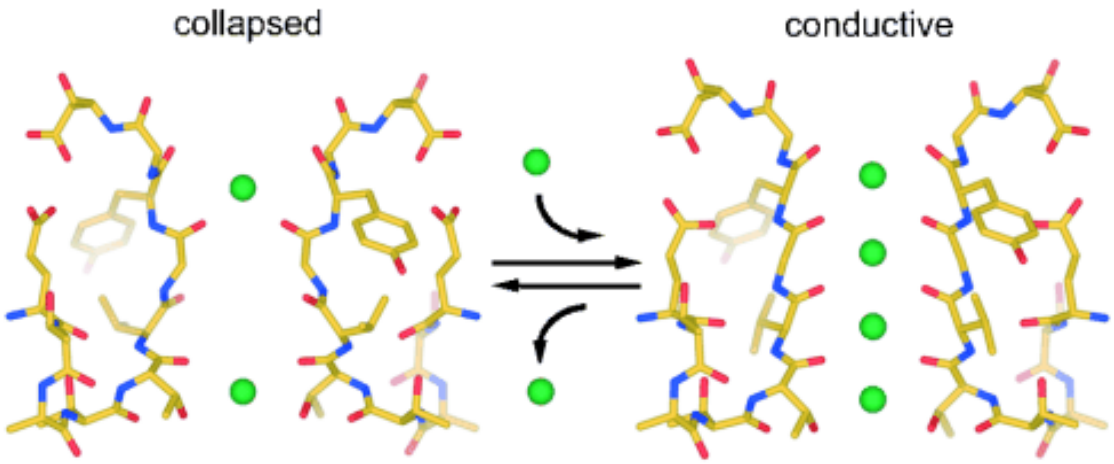

Figure I2.5 *Non-conductive and conductive potassium filter configurations in KcsA (Doyle et. al., 1998).*

of T75 are far enough to dehydrate a hydrated potassium ion coming from the aqueous cavity. Subsequently, the potassium ion will pass through the selectivity filter by interacting with the carbonyl groups of V76, G77, Y78, G79, occupying four different positions, sometimes referred to as S1-S4 and also called “cation binding sites”, until it is released into the extracellular side and rehydrated again (Fig I2.4). A single K^+ ion would interact strongly with the carbonyl oxygens and remain tightly bound to the selectivity filter. On the other side, when potassium ions are coming from the extracellular side, G79 (or S0) is responsible for dehydration of the potassium ions (Zhou et. al., 2001). This way, every cation binding site consist in a “coordination cage” that is specific for dehydrated potassium ions (Fig. I2.4).

Moreover, the T75 or G79 carbonyls are far enough to allow dehydration of a potassium hydrated ion, but not for a sodium hydrated ion, since the radius of the sodium hydrated ion is too high (Table I1). A similar hypothesis was already postulated in the early 1970s (Bezanilla and Armstrong, 1972), but was confirmed only after the resolution of KcsA structures. Structural studies of KcsA and NaK (a channel that conducts both K^+ and Na^+) crystallized in the presence of Na^+ (and Li^+) suggest that instead of binding in the center of the eight-oxygen cage, Na^+ binds in a plane formed by four oxygens, in between two K^+ binding sites (Alam and Jiang 2009b;). Therefore, K^+ channels preferentially pass K^+ over Na^+ because either binding is energetically unfavorable and because it encounters a

very high-energy barrier to permeate through the pore (Noskov et al. 2004; Zhou and MacKinnon 2004; Lockless et al. 2007; Alam and Jiang 2009b).

Ion	Ionic radius (Angstrom)	Hydrated radius (Angstrom)
Na^+	1.02	2.76
Tl^+	1.40	2.30
K^+	1.38	2.32
Rb^+	1.48	2.28
Cs^+	1.67	2.26

Table I1 *Ionic and Hydrated radius, in Angstrom, of some of the selectivity filter permeable and non-permeable ions*

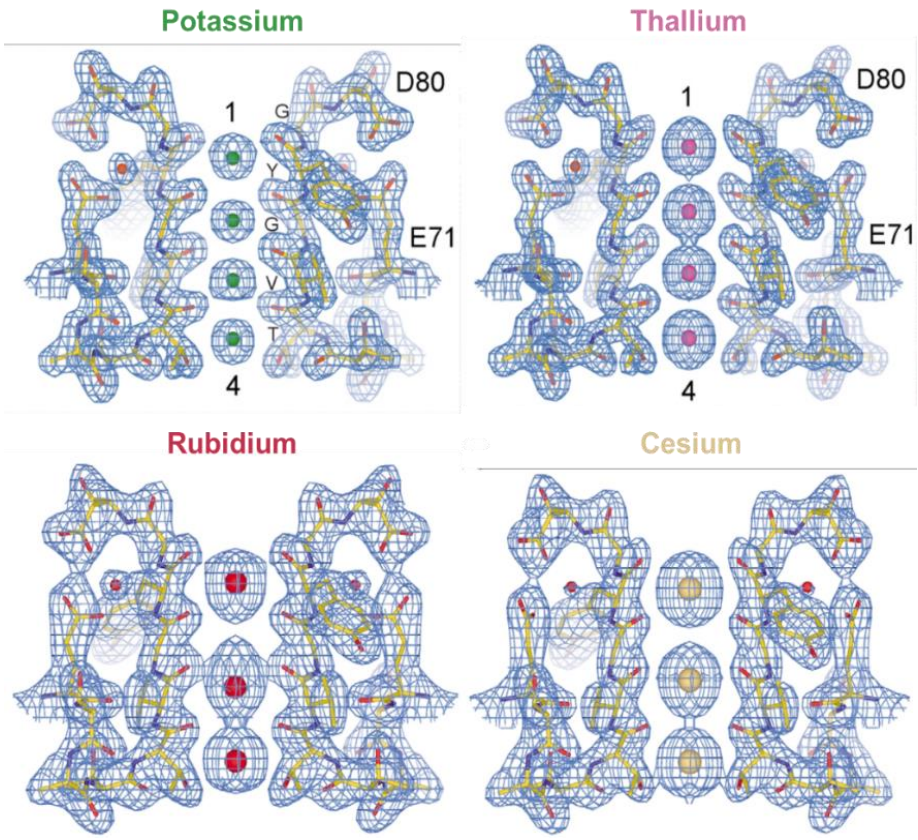

Figure I2.6 *Disposition in the conductive selectivity filter of potassium, thallium, rubidium and cesium ions (Zhou and MacKinnon, 2003).*

This mechanism relies on a strikingly delicate energy balance. Potassium conduction for KcsA is 10^7 to 10^8 ions per second, and can be considered pretty hight. To allow rapid ion conduction, the strong attraction between the ions and the channel must be exquisitely counterbalanced by the electrostatic repulsive forces between the ions. Probably, one ion from one side of the selectivity filter is coupled to the simultaneous exit of another ion on the opposite side (Roux, 2005).

If the concentration of K^+ ions bathing the crystals is lowered sufficiently (below normal intracellular levels), then a reduction in the number of ions from four to two occurs (occupyng S1-S3 or S2-S4 sites), and is associated with a structural change to a “collapsed” filter conformation, which is pinched closed in the middle and is not conductive. It seems that the occupancy of all the four cation binding site in the filter is crucial for the stabilization of a conductive conformation of the selectivity filter (Fig. I2.5; Zhou et. al., 2001).

The conformational shift induced by potassium ions carries thermodynamic implications for the binding strength of four potassium ions within the "conductive" filter. This suggests that a portion of the binding energy of the third ion must be utilized as mechanical work to induce the “conductive” conformational alteration in the filter. To grasp this concept intuitively, it's crucial to acknowledge that, in order for ions to be present in the filter, they must counteract its inclination to collapse and expel one of them. In essence, the "conductive" conformation with four ions is subjected to tension, leading to a reduced affinity for potassium ions. This reduced affinity is a favorable attribute for an ion channel since weaker binding promotes heightened conduction rates. (MacKinnon, 2004). This principle aligns with the "induced fit" hypothesis, which enzymologists had proposed many years earlier to elucidate high specificity coupled with low substrate affinity in enzyme catalysis (Jencks, 1987).

KcsA and, in general, potassium channels, are also permeable to other cations, such as Tallium, Rubidium and Cesium (Hille, 1972; Clay and Shlesinger, 1983). Zhou and MacKinnon compared, with K^+, the ion distribution and occupancy of Tl^+, Rb^+ and Cs^+ in the selectivity filter of KcsA. They concluded that Tl^+ and K^+ bind at essentially identical positions, and both are distributed nearly evenly over four positions, sites S1–4. The filter conformation and distribution of K^+ and Tl^+ corresponds to the high-concentration K^+ structure. The near identity of the structures in Tl^+ and K^+ and the same ion distribution profiles indicate that Tl^+ is a good K^+ analog for estimating ion occupancy in the selectivity filter. On the other hand, even if the protein structures in high-concentration Rb^+ or Cs^+ are very similar to the high-K^+ or the high-Tl^+ structures, there are only three major occupied ion positions (only S1, S3 and S4) in the selectivity filter, instead of four, occupied by these two ions. They conclude that their larger ionic radius clearly affects their distribution and their structural periodicity disposition inside the filter,

even though the filter structure is very similar to the hight-K^+ conductive configuration. (Fig I2.6, Zhou and MacKinnon, 2003).

1.2.3 STRUCTURAL REARRANGEMENTS OF POTASSIUM CHANNEL PORES DURING GATING

The X-ray structure of KcsA revealed that the pore domain is in a close configuration; indeed the terminal cross of the inner helices occlude ion flow. The X-ray structure of the open channel state was determined by MacKinnon and collaborators in MthK, a bacterial channel with high homology to KcsA. The open conformation of KcsA was obtained by comparison of KcsA sequence to MthK structure in the open conformation (homology sequencing). KcsA can open if exposed to low pH levels on the cytosolic side, but have also a low voltage dependence.

During the transition between the closed and open state, the inner helices, which in the closed state are crossed, undergo a displacement towards the outside, forming a hole of 20 angstroms width, which allows the passage of ions. (Jiang et al., 2002) In MthK this shift uses a flexible glycine (G83) residue as a pivot. This glycine is highly conserved among potassium channels (Rosenhouse-Dantsker and Logothetis, 2006). Pore opening generally induces profound structural changes in the most C-terminal region of the inner helix of the pore in other potassium channels as well. Many details, however, regarding this mechanism cannot be generalized to potassium channels.

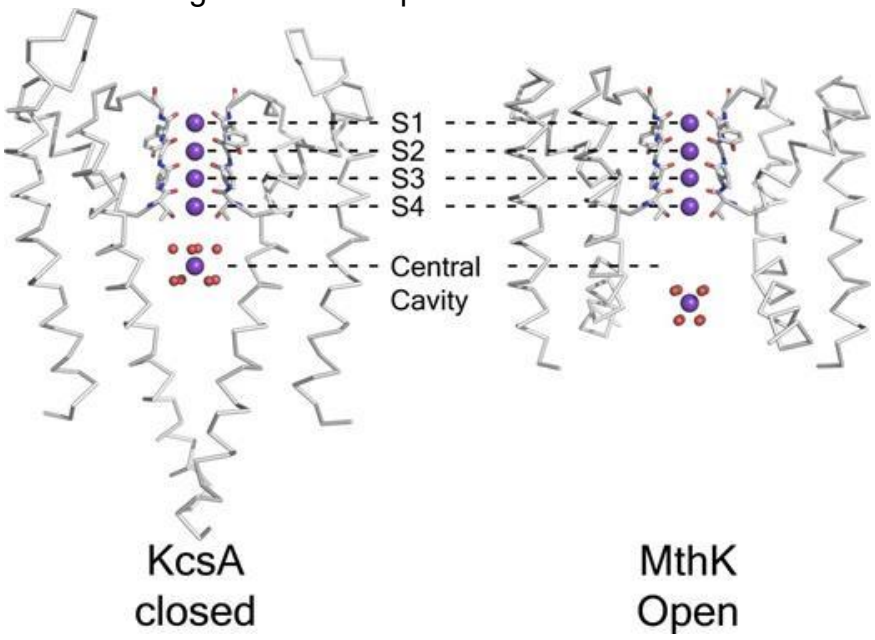

Figure I2.7 *Opening conformational changes in bacterial potassium channels (Guo et al., 2014).*

1.3 POTASSIUM CHANNELS

1.3.1 PHYLOGENY AND CLASSIFICATION

Potassium channels form the largest and the most diverse ion channel family (Jan and Jan 1997). Molecular identification of the first potassium channel was achieved by positional cloning, based on the phenotype of the *Drosophila* mutant Shaker (Papazian et. al., 1987). Since then, more than 200 genes encoding various potassium channels have been cloned. For many, but not all potassium channels, post-transcriptional alternative splicing of their transcripts further increases the diversity of potassium channels *in vivo*. (Yang and Jan, 2013). The K^+ channel-forming subunits of metazoans show similarities to the KcsA channel, but are encoded by a large family of genes. The evolution of K^+ channels has been traced back to the prokaryotic world, where K^+ channel proteins are common in eubacteria and archaea (Jan and Jan, 1992; Derst and Karschin, 1998; Anderson and Greenberg, 2001; Martinac et al., 2008). Phylogenetic studies and structure/function properties of channel proteins have led to the hypothesis that the complex K^+ channels in animals and plants evolved from a simple bacterial precursor channel (Anderson and Greenberg, 2001). It is postulated that the precursor channel protein, that should be highly related to KscA, resembling the pore module of modern K^+ channels (Thiel et. al., 2013). The human genome contains ~80 potassium channel genes. Those gene can be divided, structurally, into three categories (Fig I3.1). The first structural category consists in inward-rectifying channels that, like the KcsA channel, have a simple subunit structure in which two membrane-spanning domains flank a pore-forming

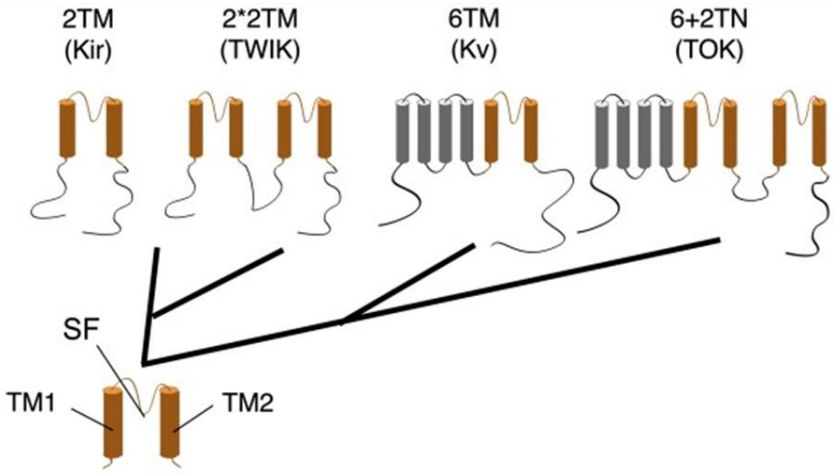

Figure I3.1 *Potassium channels families and structural differentiation (Thiel et al., 2013).*

domain. A second structural category has six transmembrane segments for each subunit. This class can further be subclassified into two families based on the gating mechanism. The class of six transmembrane (6TM) K^+ channels includes the voltage-gated Kv and the Ca^{2+}-activated K^+ channels. In voltage-gated channels, the fourth membrane domain contains an abundance of basic residues that appear to congregate on one side of the membrane helix. This helix acts as a voltage sensor, regulating the opening of the pore in response to membrane

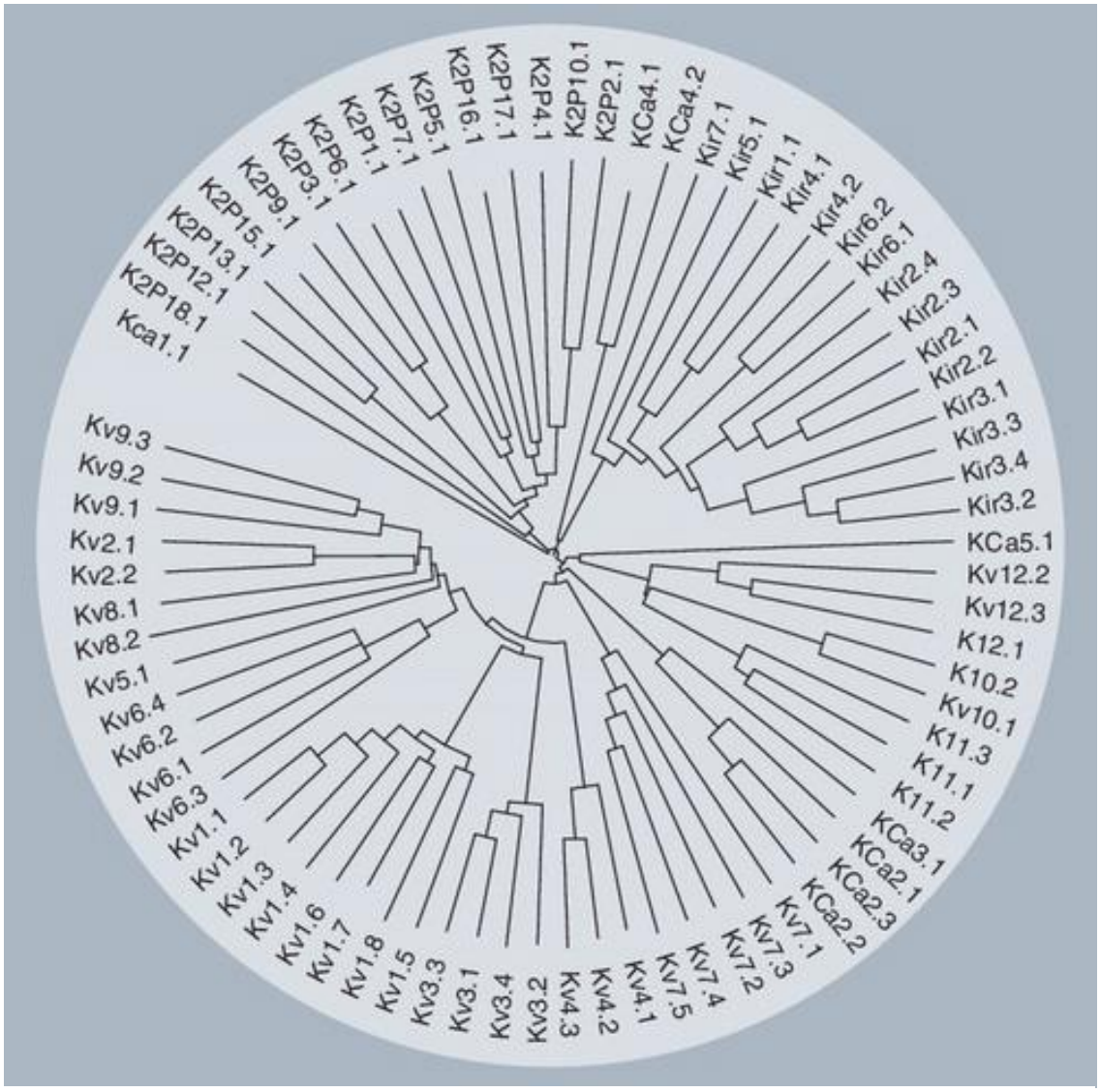

Figure I3.2 *Potassium channels members and phylogenetic tree (Chou et al., 2014).*

voltage changes. The last two segments resemble those in the KcsA channel and surround a pore-forming domain. A third structural class of K^+ channel subunits possesses four membrane domains and two pore-forming domains, which resemble two interconnected KcsA subunits (Moulton et. al., 2003) (Fig I3.1; Fig I3.2). In this chapter we describe inward rectifiers, calcium-activated and two-

pore potassium channels, while the next will be dedicated to the description of voltage-gated potassium channels.

1.3.2 INWARD RECTIFIERS (K_{IR}) POTASSIUM CHANNELS

The subunits of inwardly rectifying K^+ channels consist of two transmembrane segments known as M1 and M2, which can be likened to the outer and inner helix of KcsA, respectively. These channels are categorized into seven subfamilies (Kir1-7), with Kir2 and Kir3 having 6 and 4 members, Kir4 and Kir6 each having two members, and the rest having only one member (Tab I2.1). The N-terminal and C-terminal ends of K_{IR} channels are positioned on the cytoplasmic side of the membrane and are interconnected. Each -N terminus contains a single-strand (βA) that forms a β-sheet with two β-strands (βL and βM) in a -C terminus. This cytoplasmic three-β-strand subunit shapes a cylinder on the cytoplasmic side of the pore, also known as the "cytoplasmic pore" (Fig. I3.3).

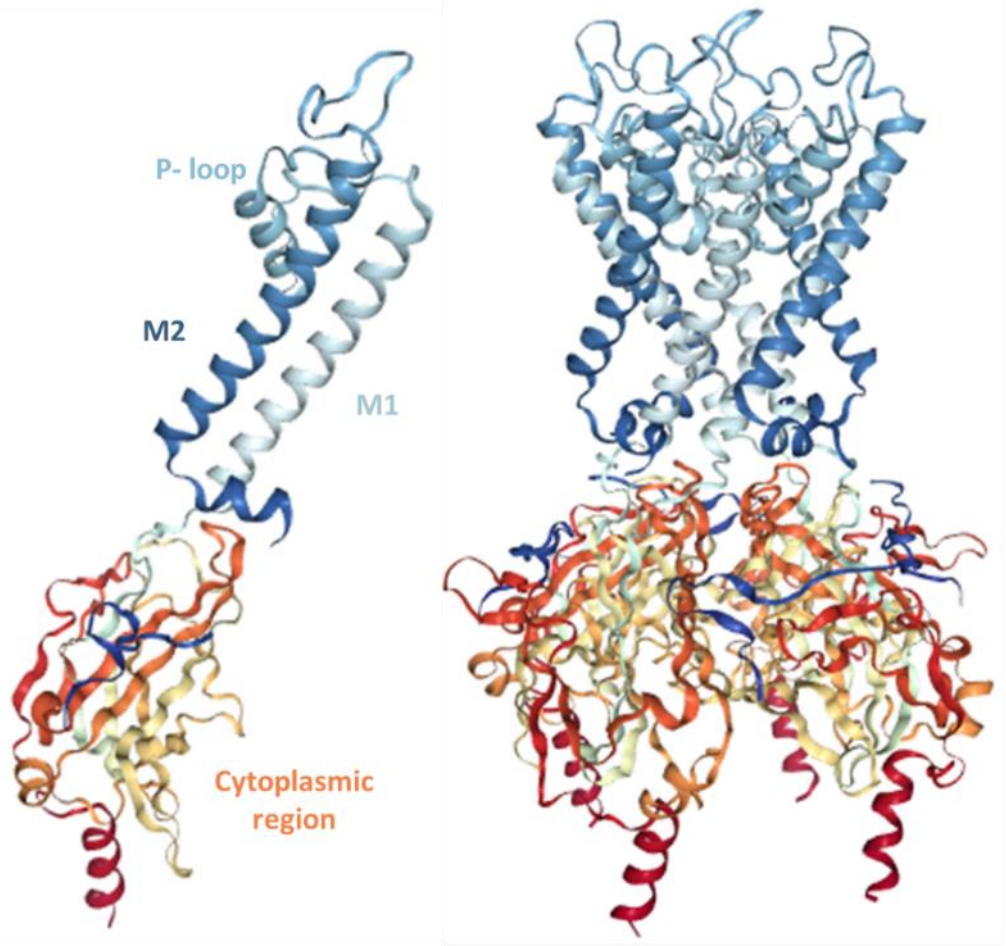

Figure I3.3 *Structure of Kir2.2 subunit and functional channel in open state (PDB 6M86).*

These channels conduct potassium predominantly in the inward direction (inward rectification). This property is attributable to blockade of outward current by intracellular cations, such as Mg^{2+}, or polyamine (Taglialatela et. al., 1995). Different inwardly rectifying potassium channels exhibit different degrees of inward rectification. Kir2 families show strong inward rectification, while Kir1, Kir3, and Kir6 families show weak inward rectification (Hibino et. al., 2010). The C-terminus of the Kir3 subfamily can interact with the $G_{\beta\gamma}$ protein, which determine channel opening.

Gene	Protein	Aliases
KCNJ1	Kir1.1	ROMK1
KCNJ2	Kir2.1	IRK1
KCNJ12	Kir2.2	IRK2
KCNJ4	Kir2.3	IRK3
KCNJ14	Kir2.4	IRK4
KCNJ17	Kir2.5	IRK5
KCNJ18	Kir2.6	IRK6
KCNJ3	Kir3.1	GIRK1, KGA
KCNJ6	Kir3.2	GIRK2
KCNJ9	Kir3.3	GIRK3
KCNJ5	Kir3.4	GIRK4
KCNJ10	Kir4.1	$K_{ir}1.2$
KCNJ15	Kir4.2	$K_{ir}1.3$
KCNJ16	Kir5.1	BIR 9
KCNJ8	Kir6.1	KATP
KCNJ11	Kir6.2	KATP
KCNJ13	Kir7.1	$K_{ir}1.4$

Table I3.1 *K_{ir} channel classification*

Kir6 is modulated by the intracellular ATP concentration. ATP-sensitive potassium channels are formed by four subunits of Kir6 and four subunit of ATP-binding cassette family proteins (ABC), that can form an octameric complex. ABC

proteins confer ADP sensibility to Kir6 channels that modulate positively the open probability.

1.3.3 CALCIUM-ACTIVATED K^+ CHANNELS (K_{Ca})

K_{Ca} channels counts among its members the large conductance BK_{Ca} (also known as $K_{Ca}1.1$), the small conductance SK_{Ca} (including $K_{Ca}2.1$-2.3; 4.1, 4.2, 5.1), and intermediate conductance IK_{Ca} (also identified as $K_{Ca}3.1$)(Tab I3.2). The activation of calcium-activated K^+ channels occurs in response to an increase in cytoplasmic concentration of Ca^{2+}. Additionally, K_{Ca} channels exhibit voltage-dependent characteristics. These channels play diverse physiological roles, such as regulating neuronal firing, blood flow, and proliferation.

Gene	Channel	Aliases
KCNMA1	KCa1.1	BK, Slo1, Maxi-K
KCNN1	KCa2.1	SK1
KCNN2	KCa2.2	SK2
KCNN3	KCa2.3	SK3
KCNN4	KCa3.1	IKCa, SK4
KCNT1	KCa4.1	Slack, Slo2.2
KCNT2	KCa4.2	Slick, Slo2.1
KCNU1	KCa5.1	Slo3

Table I3.2 *K_{Ca} channel classification*

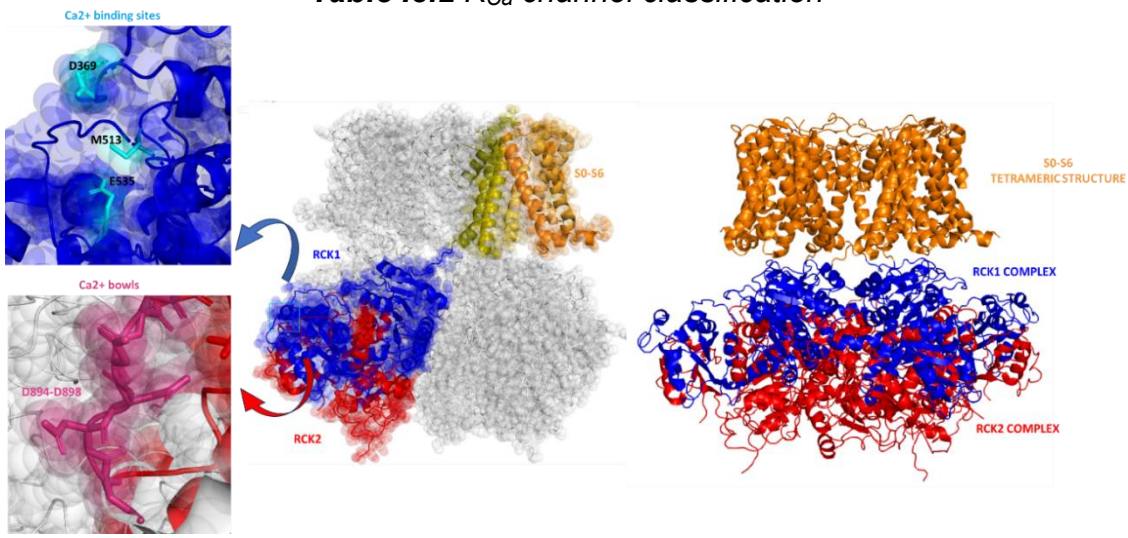

Fig. I3.4 *K_{Ca} 1.1 subunit representation into the channel complex, with Ca^{2+} binding sites and calcium bowls. Tetrameric structure is on the right (PDB: 8GH9).*

The subunit of BK_{Ca} channels, also known as $K_{Ca}1.1$, Slo1 or KCNMA1, shares a structural resemblance to voltage-gated potassium channels, featuring six transmembrane domains and a pore domain positioned between the S5 and S6 segments. However, BK subunits have an additional N-terminal transmembrane domain (S0). Within the channel, this subunit exposes the N-terminus of BK channels on the extracellular side, while the C-terminus is situated on the intracellular side. On the intracellular side, $K_{Ca}1.1$ contains a pair of “regulators of K^+ conductance” (RCK) domains, which assemble in an octameric ring structure

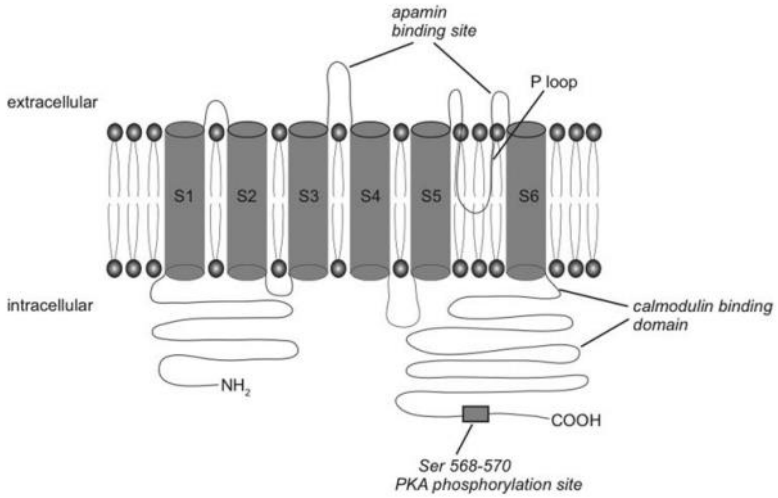

Fig. I3.5 *K_{Ca} 2.1 subunit structure (Faber et. al., 2009).*

in the functional channel and binds Ca^{2+}. In RCK1 there are calcium binding site, and in RCK2 there are the so called "calcium bowls" (Fig. I3.4). These RCK domains house primary binding sites for Ca^{2+} and are crucial for the regulation of BK_{Ca} by calcium. The principal subunits can combine with accessory beta subunits, and four beta subunits have been identified, each exhibiting a distinct tissue expression pattern. These beta subunits modulate the biophysical properties of the mature channel, including Ca^{2+} sensitivity, voltage-dependency, and pharmacological characteristics. $K_{Ca}1.1$ is implicated in various physiological processes such as muscle contractions, neuroendocrine release, neurotransmitter release, and synaptic plasticity. Research on knockout animal models has revealed significant roles of $K_{Ca}1.1$ in motor control and cerebellar ataxia (Sausbier et al., 2004). SK_{Ca} channels also closely resemble the structure of voltage-gated potassium channels, as they are composed of subunits featuring six transmembrane domains (Fig. I3.5). The SK_{Ca} subfamily (KCNN1-3) comprises three types of pore-forming subunits ($K_{Ca}2.1$-3). Each subunit is distinguished by a cytoplasmic tail at the C-terminus, which includes a 91-amino

acid region that constitutively binds Calmodulin in the absence of calcium (Fig 1.3.6).

The activation of SK_{Ca} channels occurs when the Calmodulin associated with the

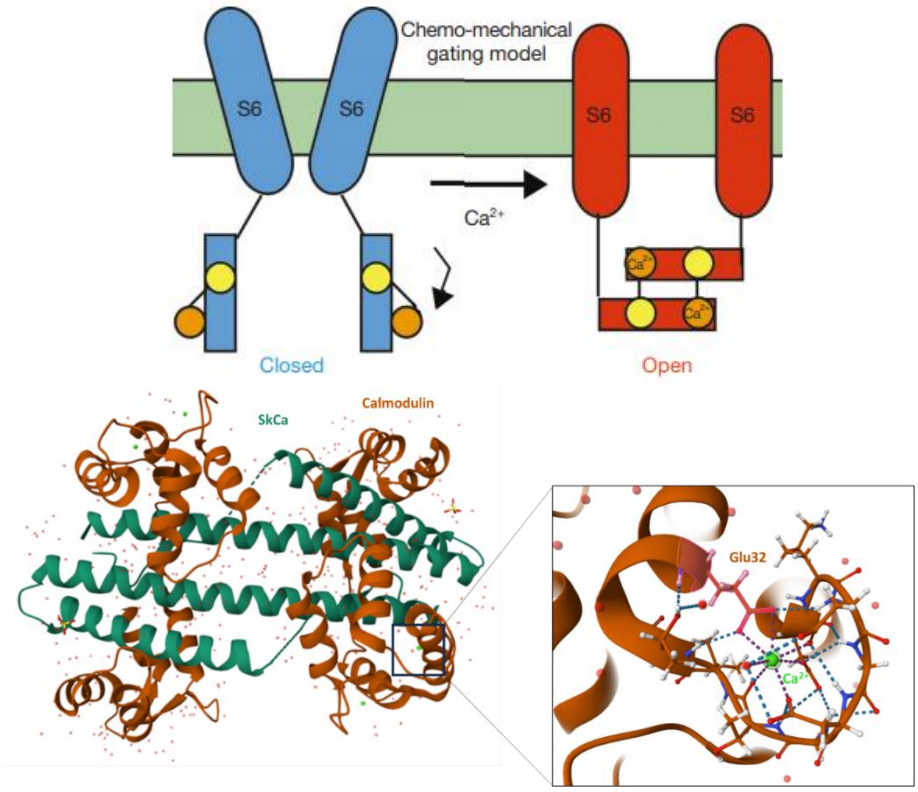

Fig. I3.6 *Conformational changes during $K_{Ca}2.1$ gating (Schumacher et. al., 2001) Bottom figure is reporting the intracellular region of K_{Ca} 2.1(green) when it's binding Ca^{2+}-Calmodulin complex (PDB: 4QNH).*

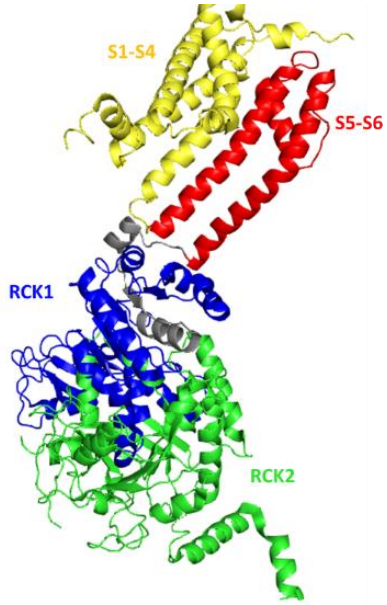

Fig. I3.7 *Chicken Slo2.2 subunit structure in the open conformation (PDB 5U70).*

channel binds Ca^{2+}, causing a conformational change in the channel that prompts a transition to the open state (Fig. I3.6, Schumacher et al., 2001). $SK_{Ca}2.1$-3

subunits exhibit widespread expression in the brain, particularly in the cortex and hippocampus (Stocker and Pedarzani, 2000). Pharmacological inhibition of SK_{Ca} increases the excitability of hippocampal neurons and facilitates the induction of synaptic plasticity (Schumacher et al., 2001). Alterations in $K_{Ca}2.3$ have been linked to conditions such as schizophrenia, anorexia nervosa, and ataxia (Lam et. al., 2013). $K_{Ca}4.1$ and $K_{Ca}4.2$, encoded by the KCNT1 and KCNT2 genes, respectively, are highly sensitive to intracellular sodium concentrations, so much so that we refer to the channels as sodium-activated potassium channels. Under conditions of symmetric K^+ concentrations, $K_{Ca}4.1$ channels have an EC_{50} of 41 mM for activation by intracellular Na^+.

This channel resembles the $K_{Ca}2.1$ channel by containing very large carboxy termini in addition to the transmembrane domains. The large carboxy termini contain RCK domains (Bhattacharjee and Kaczmarek, 2005 ; Salkoff et al., 2006). These RCK domains are thought to be essential for sodium binding and concomitant gating for this class of potassium channel (Jiang et al., 2002; Hite et. al., 2015, Fig. I3.7).

1.3.4 TWO-PORE K^+ CHANNEL

Functional K2P channels are formed by two subunits, each featuring four transmembrane domains (M1-M4) and two pores (P1 between M1 and M2, and

Gene	Channel	Family	Aliases
KCNK1	K2p1.1	TWIK	TWIK-1
KCNK2	K2p2.1	TREK	TREK-1
KCNK3	K2p3.1	TASK	TASK-1
KCNK4	K2p4.1	TREK	TRAAK
KCNK5	K2p5.1	TASK	TASK-2
KCNK6	K2p6.1	TWIK	TWIK-2
KCNK7	K2p7.1	TWIK	
KCNK9	K2p9.1	TASK	TASK-3
KCNK10	K2p10.1	TREK	TREK-2
KCNK12	K2p12.1	THIK	THIK-2
KCNK13	K2p13.1	THIK	THIK-1
KCNK15	K2p15.1	TASK	TASK-5
KCNK16	K2p16.1	TALK	TALK-1
KCNK17	K2p17.1	TALK	TALK-2, TASK-4
KCNK18	K2p18.1	TRESK	TRIK, TRESK

Table I3.3 *K2p channel classification*

P2 between M3 and M4). The extracellular loop between M1 and M2 contains the self-interacting domain (SID), crucial for homodimer formation. This family comprises 15 members, classified in 7 families, with widespread tissue distribution, particularly in the brain, placenta, lung, and liver (Lesage et al., 2000). Two-pore K^+ channels (K2P) are weak inward rectifiers, rapidly activating and non-inactivating, open at all membrane potentials, leading to their designation as "leak channels".

1.4 VOLTAGE GATED K^+ CHANNELS AND STRUCTURAL/FUNCTIONAL RELATIONSHIP

The electrical proprieties of excitable cells are determined in large part by the voltage gated K^+ channels (VGKCs, Triggle, Gopalakrishnan, Rampe, Zheng, 2006).

The first voltage-gated potassium channel was identified and cloned in *Drosophila*, since a mutation in this gene caused aberrant movements in the fruit fly, including shaking of the leg under anesthesia (Jan and Jan, 1988). For this reason, this channel was called “Shaker”, and was then identified as the homologous to human Kv1.1.

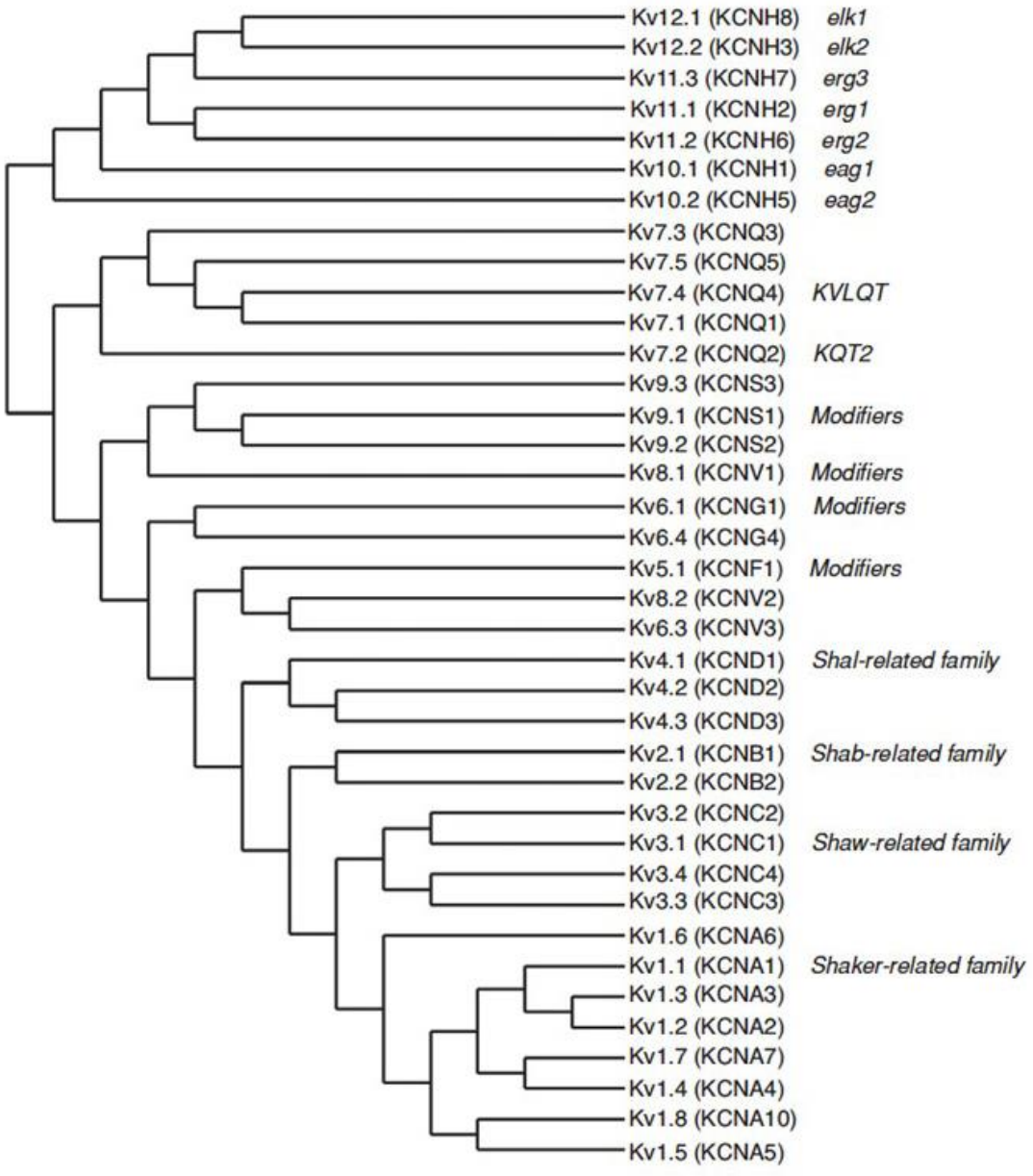

Figure I4.1 *Voltage-gated potassium channels families and nomenclature (Gonzalez et. al., 2012).*

In Human, there are 38 genes encoding for voltage-gated potassium channel subunits, that are classified in 12 subfamilies (Kv1-Kv12, Fig. I4.1). The first family is called Shaker-related, referring (like other families) to the orthologous gene in *Drosophila*. That family accounts for 8 members (Kv1.1-8). Then, we have the Shab-related family, that includes just two members, Kv2.1 and Kv2.2. Morover, the Shaw related family is composed of 4 members (Kv3.1-4) and the Shal-related family by only three members (Kv4.1-3). Modifiers families (Kv5, Kv6, Kv8 and Kv9) are instead responsible to co-assemble with Shab related family members, conferring those heteromeric channel an incredible functional and structural heterogeneity.

Kv7 family is compose of five members (Kv7.1-5) and will be discussed in the next chapter. Finally, three other families Kv10, Kv11 and Kv12 (or eag, erg and elk) are composed of two members (such as the Kv10 family) or three (such as Kv11 and Kv12).

In addition to alpha pore forming subunits, auxiliary subunits, called Kv-Beta (Kvβ) subunits, have been identified. These β-subunits assemble with main subunits with a 1:2 or 1:1 stoichiometry (Li et. al., 2006). The β subunits of the potassium channels are rather heterogeneous from a structural point of view. This assembling can alter current density and kinetics of channels.

1.4.1 VOLTAGE SENSOR ACTIVATION AND CHANNEL GATING

In general, Kv channels are tetrameric proteins that can be formed by one or more types of subunits.

Each Kv channel subunit consists of six transmembrane segments, called S1-S6, and both N- and C- terminus of these proteins are located on the intracellular side.

S1-S4 segments forms the voltage sensor domain (VSD). The S4 domain contains a highly conserved motif consisting of a series of four positively charged amino acids that act as a voltage sensor, separated by two non-charged amino acids. Generally, these amino acids are called R1-R4. The number of arginines or lysines may vary along the S4 segment among different members. Some Kv possess up to 6 positive charges (R1, R2, R3, R4, K5, R6) (Fig. I4.2).

The S5 and S6 segments, on the other hand, form the pore domain (PD). Those segments structurally closely resemble the KcsA subunit. (Fig. I4.2).

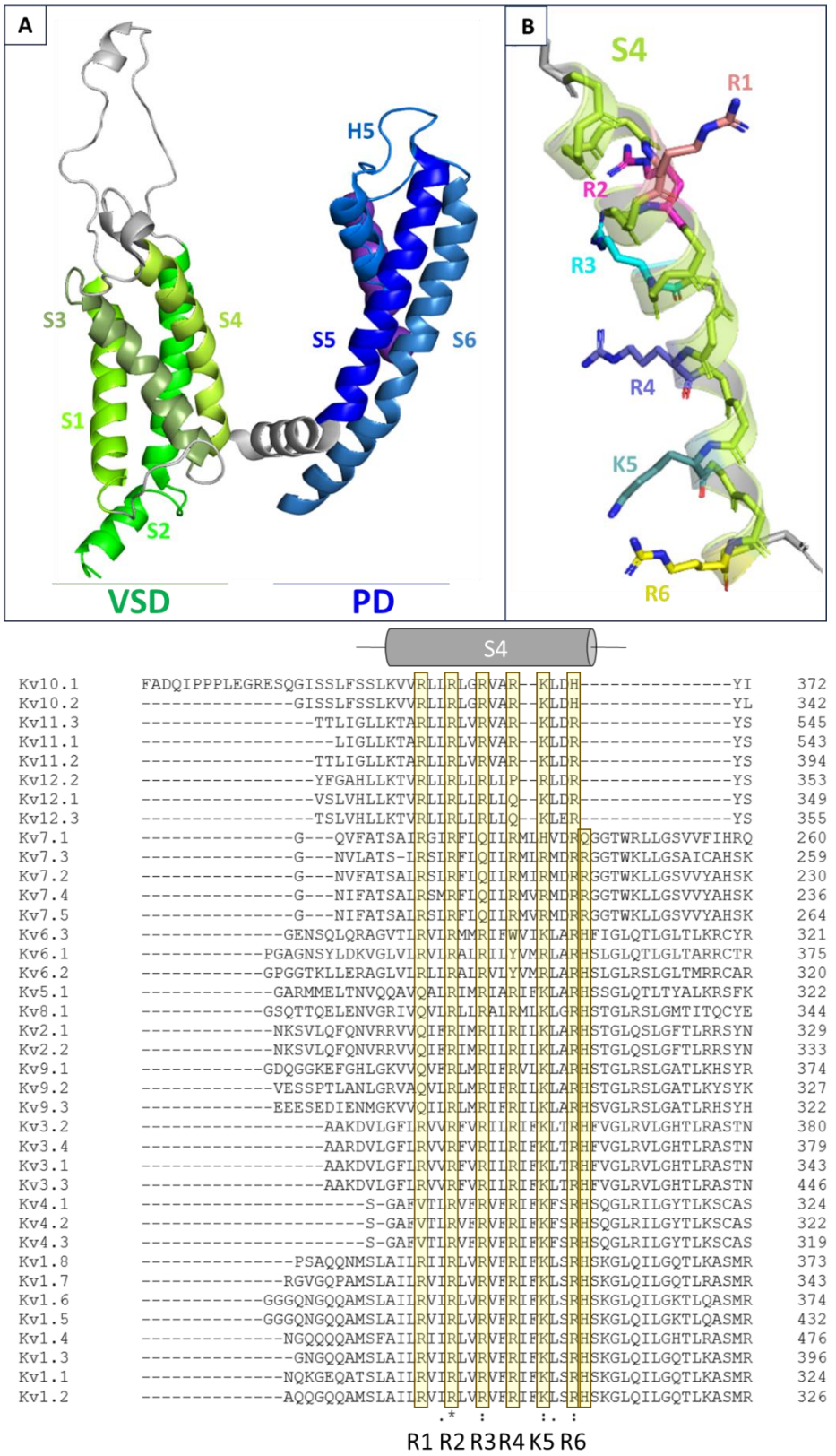

Figure I4.2 *Mammalian Kv1.2 subunit that resemble general resting closed structure of Kv channels (PDB: 3LUT). (A) In green is reported VSD and in blue pore domain, with potassium ion position into the filter in purple. Gray color is reporting linkers. (B) Positive amino acid disposition in S4 segment. Sequence report positive charge conservation among Kv in S4 segment. Labeled refer to Kv1.1.*

These two segments are connected to each other by a short α-helix, called H5, and by a loop, called P-loop, which contains the GYG motif that characterizes the selectivity filter. In their tetrameric form, the four VSD are located outside the pore domain, while segments S5 and S6 of the four subunits are organized centrally to form the pore (Fig. I4.3). This disposition led to the hypothesis that the voltage sensors are semi-independent modules (Long et al., 2005).

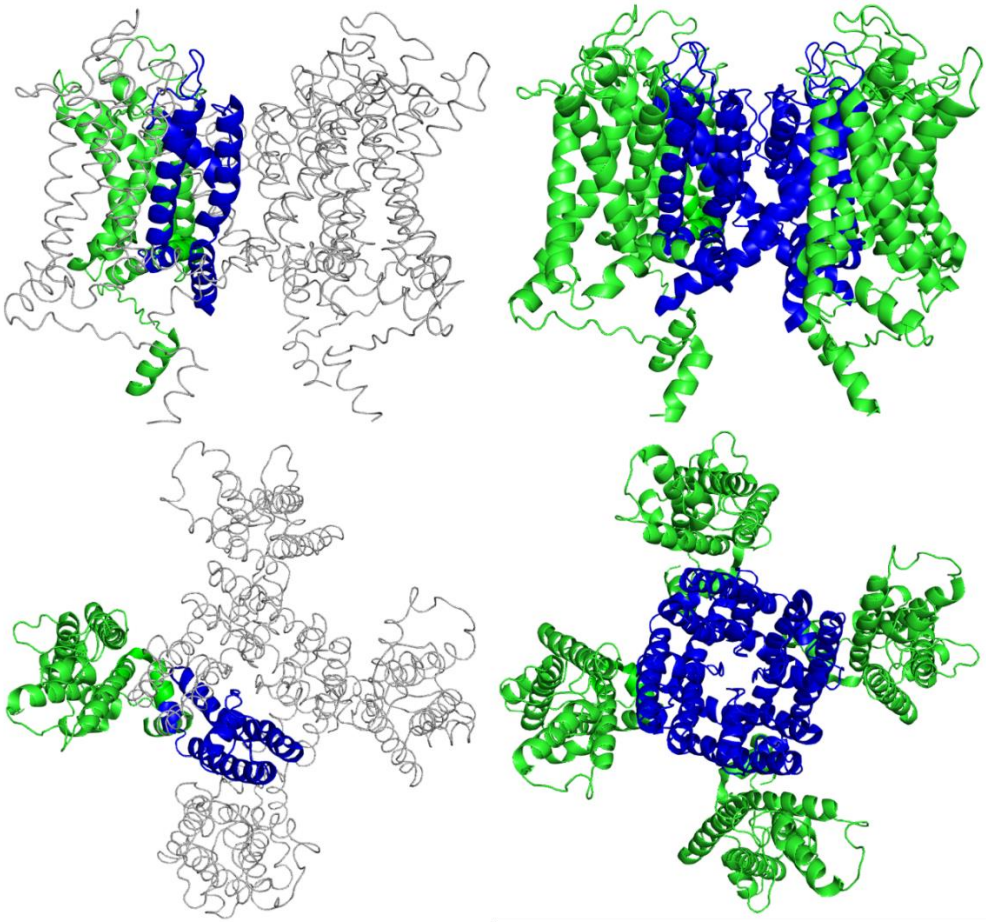

Figure I4.3 *Lateral (upper) and top (bottom) view of subunit localization and tetrameric structure of resting closed Kv1.2/2.1 paddle chimera channel structure (PDB 6EBM). Green indicates voltage sensors and blue pore domains.*

The presence of net charges within voltage sensors had already been hypothesized by Hodkin and Huxley in 1952 (Hodgkin and Huxley, 1952). The VSD domains are sensitive to the electric field of the membrane, and alterations of the latter determine its movement inside the membrane (Seoh et. al., 1996), generating new electrostatic interactions with negatively charged amino acids, present in the S1-S3 domains and stabilizing the open channel conformation (Bezanilla et. al., 2000).

The movement of these charges inside the membrane can be measured as a "gating current", transients electric currents distinct from ion conduction (Armstrong and Bezanilla, 1973)

Several mutagenesis studies have shown how the neutralization of positive charges located into the S4 determines alterations in the functionality of the channel under examination (Miceli et. al., 2017) and the disappearance of gating currents (Aggarwal and MacKinnon, 1996).

These amino acids therefore confer sensitivity to channels to voltage variations across the membrane.

In the resting condition, the pore domain is closed, as the C-terminal tails of the S6 segments form a narrow passage, which crosses the intracellular side,

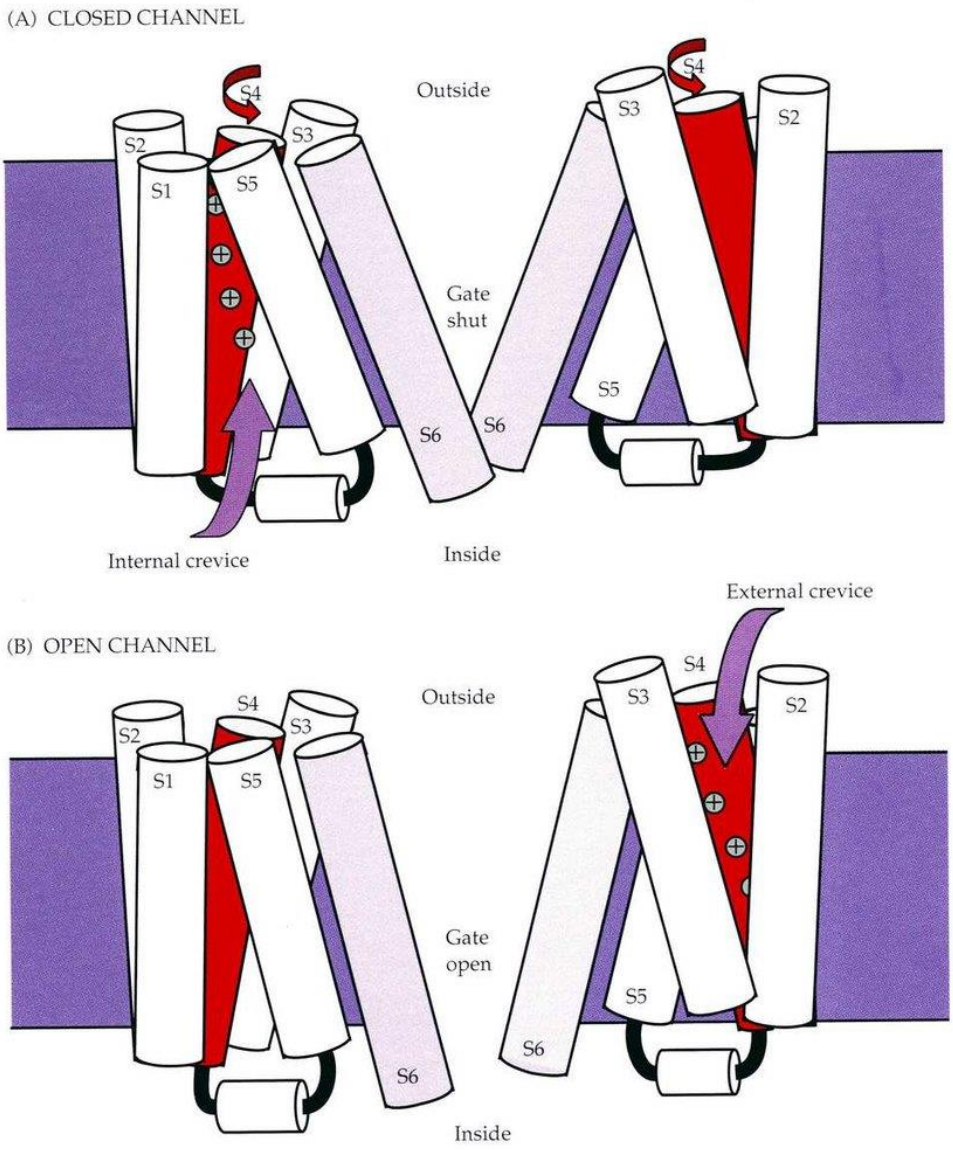

Figure I4.4 *Schematic representation of conformational change of S4 during gating and pore opening (Hille, 2001).*

preventing ion flow through the channel (Liu et. al, 1997). At the same time, the voltage sensor is in the resting configuration, lying downward (Figure I4.6).

Describing in general the activation mechanism of the voltage sensor, we could say that membrane depolarization induces an upward rotation of the S4 segment (Fig. I4.4) similarly to the movement of a screw being unscrewed inside the hole in which it lodges. That structural reorganization is transmitted to the S6 segments via the S4-S5 linker. The movement of the S6 segment causes the “relaxation” of its C-terminal ends which kept the channel closed, thus permitting the flow of K^+ ions (Kim et al., 2016).

It is also thought that the opening of the pore domain is allowed by a particularly mobile region, called PVP region (in Kv1, Kv3 and Kv4 families), which produces a curvature in the S6 and makes it particularly sensitive to conformational changes on its C-terminal end (Fig. I4.7).

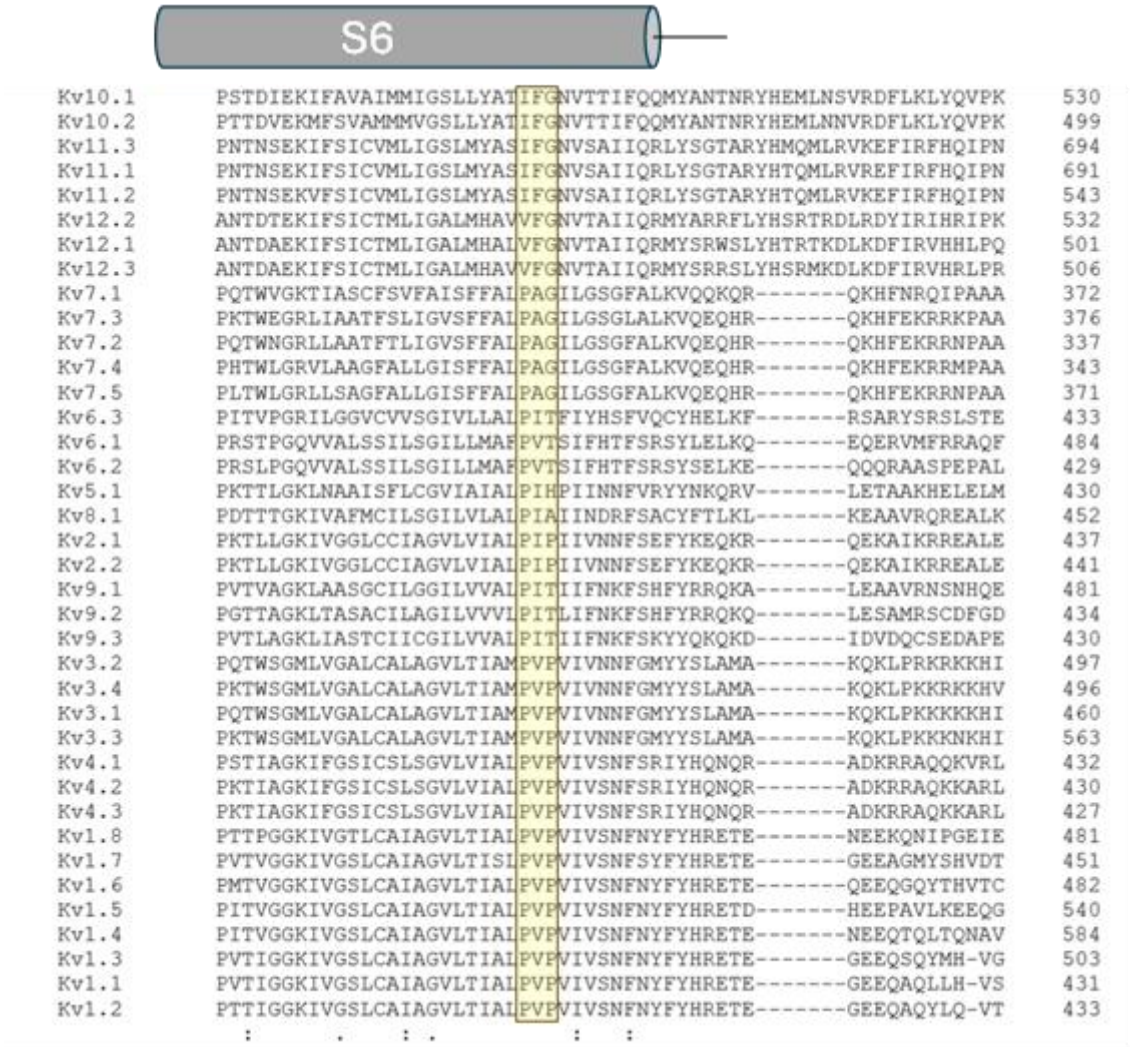

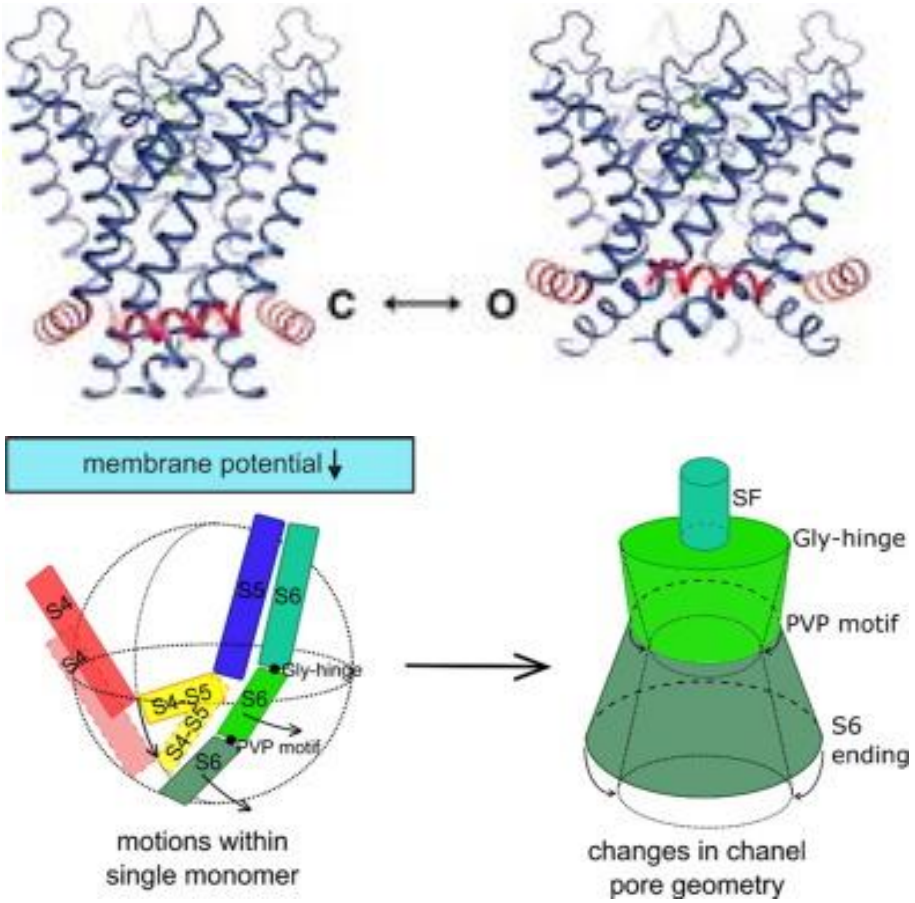

Figure I4.6 *Conformational change of the pore, from the closed to the open state (Tao et. al., 2010, Wawrzkiewicz-Jałowiecka et. al., 2017).*

The specific sequence of amino acids interactions that allows activation of a voltage-dependent potassium channel is relative to the family or specific member under consideration. This will be discussed in detail for the Kv7 family in the next chapter. The process of opening the pore is called "opening". The opening process involves the activation gate (AG). "Deactivation" is the opposite process: the activation gate closes, usually in response to the membrane repolarization (Ahern, 2016). "Inactivation" is when ion flow is blocked by a mechanism that differs from channel deactivation (Bähring and Covarrubias, 2011). Whilst the mechanism of activation of VGKCs is similar among different classes of the Kv superfamily, the mechanism of inactivation does not concern all the voltage-dependent potassium channels and differs among the various members of this family.

1.4.2 INACTIVATION MECHANISMS IN VGKCS

The voltage-dependent potassium channels can inactivate in two ways: C-type inactivation or selectivity filter gating or for N-type inactivation (Fig. I4.8)

C-type inactivation is believed to be the result of a conformational change in filter selectivity (Kim et al., 2016). C-Type inactivation was predicted by structural studies in KcsA when this is exposed to low potassium concentration (Zhou et al., 2001). It is believed that several VGKCs inactivate in a C-type way, like Shaker-related family (Hoshi et. al, 1991). Functional studies on KcsA have identified that mutation E71A disrupt C-type inactivation (Cordero-Morales et al., 2006) and

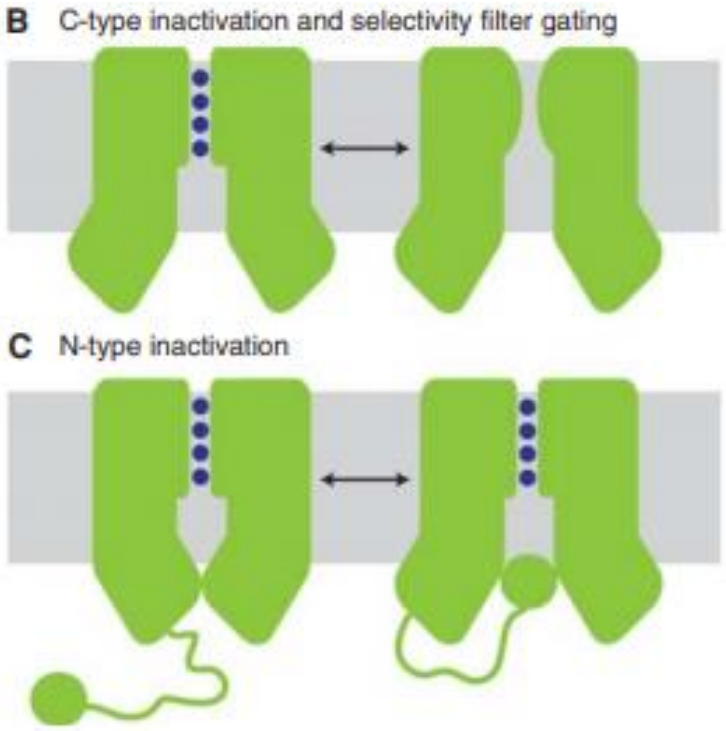

Figure I4.8 *Inactivation mechanisms in Kv channels (Kim et al., 2016).*

mutagenesis studies on Shaker and Kv1.2 in the corresponding position suggest that these residues can play a similar role in voltage gated potassium channels (Cordero-Morales et al., 2011). In KcsA, two C-type inactivated conformations of KcsA have been described, I1 and I2. When the selectivity filter is in the I1 conformation, the inner gate is partially opened and when the selectivity filter is, instead, in the I2 conformation, the inner gate is fully opened. That suggests us that selectivity filter conformation is coupled with activation gate (Cuello et al., 2010). That's also true for Shaker channel and other Shaker-related channels (Ong et. al., 2022).

Recently, the structure of the Shaker channel with C-type inactivated filter was revealed by the high-resolution cryo–electron microscopy and computer simulations (Fig. I4.9; Tan et. al., 2022).

They used the W434F mutant of Shaker, that accelerates and stabilizes the C-type inactivation of the channel (Perozo et. al., 1993, Pless et. al., 2013).

They report that, in that mutant, the external pore quickly leads to rearrangement of the P-loop. This dilation of the ion selectivity filter results into a C-type inactivated conformation (Fig. I4.9).

C-type inactivation is defined as slow inactivation (Kiss and Korn, 1998).

On the other side, N-type inactivation is called fast inactivation and also occurs in Shaker-related family (Zagotta et. al., 1990). This mechanism involves a N-terminus peptide that can physically obstruct the intracellular side of the pore of the channel. The N-terminus peptide have an high affinity for the pore in the open conformation (Yao et. al., 2000) and removing the amino-terminal peptide abolish this type of inactivation (Hoshi et al., 1990), that can be rescued by the addition of the same sequence peptide in solution (Zagotta et al., 1990).

Mutational analysis provided evidence that N-terminus peptide binds the intracellular side of the pore (Gonzales et. al., 2011).

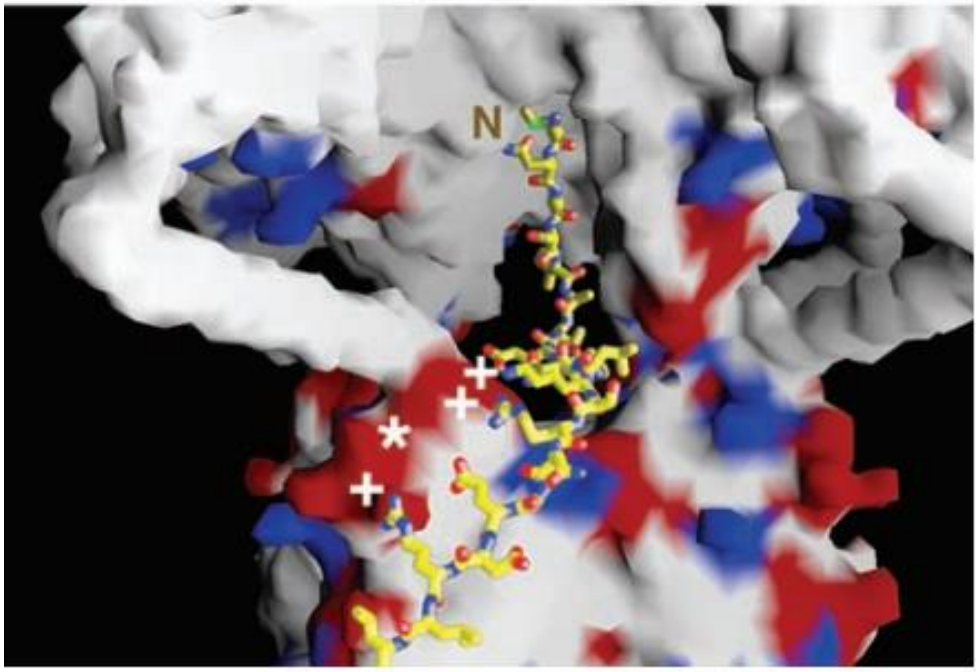

Figure I4.10 *Structural organization of the peptide during N-type inactivation of Shaker channel (Long et. al., 2005).*

Inactivation peptide snakes into the inner pore interacting with a negative surface on the bottom of the pore (Fig. I4.10) (Long et al., 2005).

Thus, Kv1 channels are inactivated by both a slow C-type and a fast N-type mechanism (Hoshi et. al., 1990). The potassium channels Kv2, Kv3 and Kv4 also exhibit inactivation, but the mechanism is not as clear. Recent studies suggest that in Kv2.1 and possibly in Kv4, inactivation involves altered coupling between

the voltage sensors and the pore, leading to closure of the internal pore (Fernández-Mariño et. al., 2023).

1.4.3 BIOPHYSICAL PROPERTIES OF VGKCS

Voltage-gated ion channels can be also classified by their biophysical properties. The majority of them can be divided into two groups: Delayed Rectifiers (or D-type) and A-type potassium channels.

Delayed Rectifier Voltage gated K^+ channels include two categories: slowly inactivating, such as Kv1.1, Kv1.2, Kv1.3, Kv1.5, Kv1.6, Kv1.7, Kv1.8 and Kv2 subfamily, that shows a little time-dependent inactivation, or non-inactivating, such as Kv3.1, Kv3.2, and Kv10.1.

Opening of these channels typically start membrane potential is close to -40 mV.

A-type potassium channels are rapidly inactivating voltage gated potassium channels and this group includes Kv1.4, Kv3.3, Kv3.4, Kv4.1, Kv4.2, Kv4.3 (González et. al., 2012).

This type of channel shows a strong time and voltage-dependent inactivation (Fig. I4.11).

Kv5-6 and Kv8-9 subfamilies can be classified as modifier/silencer; these subunits can assemble with Kv2 subfamily members but are unable to form functional channels alone (Bocksteins et al., 2016).

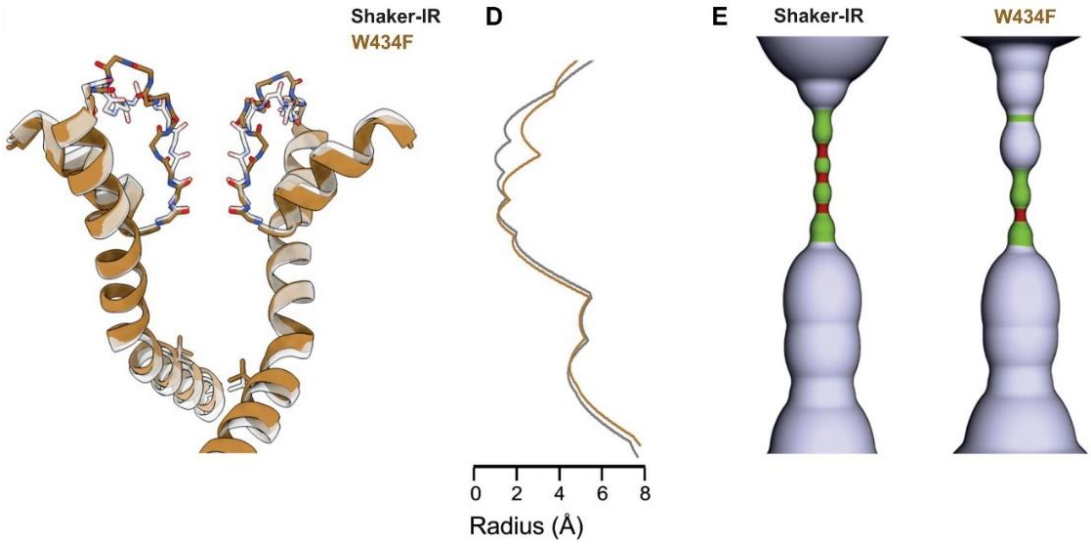

Figure I4.9 *on the left, selectivity filter rearrangement and collapse during C-type inactivation of Shaker channel (Tan et. al., 2022). In the middle, pore radius of active and C-type inactivated Shaker's selectivity filter and on the right, the corresponding representation of pore areas.*

Kv11 represents the only voltage dependent inwardly-rectifying channels subfamily and this property arises following a rapid voltage dependent inactivation of channels (Trudeau et al., 1995).

Kv12 subfamily and Kv10.2 are voltage gated potassium channels that are classified as “slowly activating” (Zhang et al., 2009).

In mammalian neurons, the main potassium currents are voltage-dependent currents (Fig I4.12). These potassium currents can in turn be divided into four components: I_D, I_A, I_K and I_M (Storm, 1988) and pharmacology is used to distinguish various components of the overall potassium current (Mitterdorfer et al., 2002).

I_D are fast activating currents, slowly inactivating and are sensitive to 4-aminopyridine at 30 micromolar. I_A current is fast activating and fast inactivating, and is sensitive to 4-aminopyridine at 3 mM. I_K and I_M currents are slowly activating, not inactivating and sensitive to TEA at 3-25 mM (Fig. I4.12).

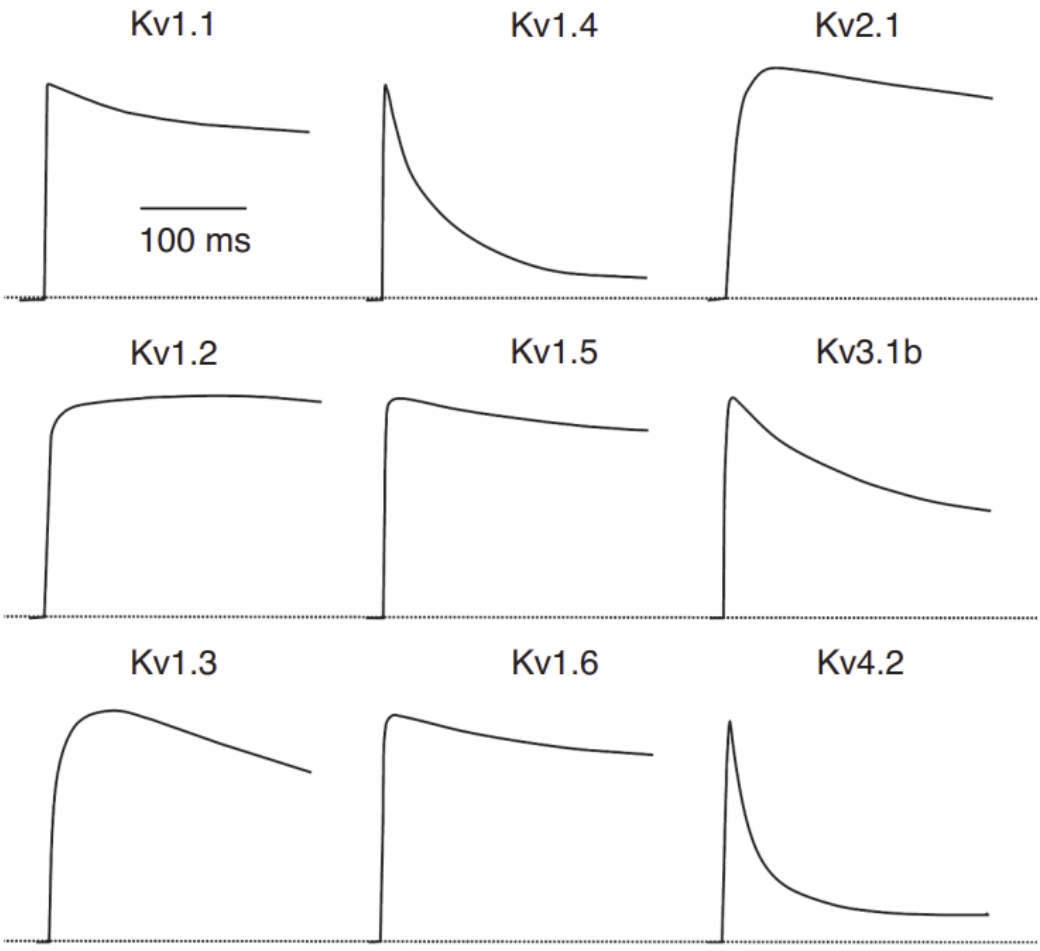

Figure I4.11 *Current responses of different Kv members to a +40 mV membrane depolarization (from -80 mV; Gonzales et. al., 2012).*

During action potential, potassium current is made by I_D and I_A components.
I_M current is involved in the regulation of excitability but it is also involved in the action potential repolarization (Gu et. al., 2005; Tsingounis et. al., 2010).
I_M current is a typical subthreshold activated potassium current and plays a critical role in the regulation of the neuronal excitability, maintaining resting potentials at low stable values. In the next chapter we will investigate Kv7 channels that, in neurons, underlie the M-current.

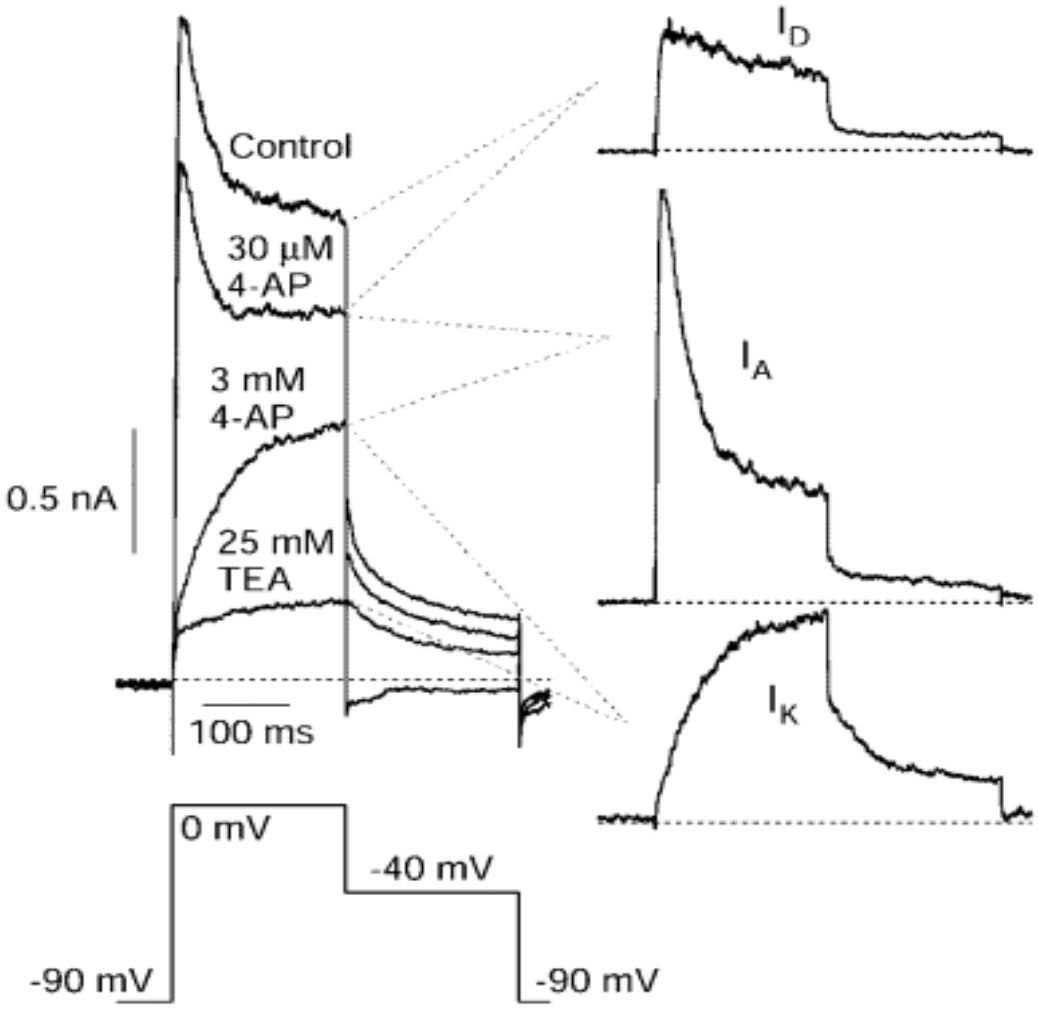

Figure I4.12 *K+ currents components in mammalian neuronal model (Ion channels of excitable membranes, Hille).*

1.5 Kv7 CHANNELS: STRUCTURE AND REGULATION

1.5.1 STRUCTURE OF Kv7 CHANNELS

The arrangement of subunits within the Kv7 subfamily closely resembles the general structure of voltage-gated potassium channels (as discussed in Chapter 4). These subunits exhibit a typical six-transmembrane configuration with N- and C-termini located on the intracellular side. The S4 segment features positive charges, interspersed with two uncharged residues, forming the voltage sensor core. This motif for Kv7.2-5 is -RXXRXXQXXRXXRXXR-. In Kv7.1, the fifth positive charge is represented by an histidine instead of an arginine (Fig I3.1). The selectivity filter includes the canonical -TVGYG- sequence. In contrast to other VGKCs, such as Kv1.1, there is no evidence that the selectivity filter may be in a nonconductive state, and, in general, with the exception of Kv7.1, they do not undergo inactivation. Members of the Kv7 subfamily, also known as KCNQ, include Kv7.1-5 (*KCNQ1*-5), are capable of forming homotetramers or heterotetramers with other Kv7 family members. Notably, Kv7 subunits possess a conserved long intracellular C-terminal region that binds accessory proteins and regulate subunit assembly, channel trafficking and activity (Soldovieri et al., 2011).

The N-terminal region is pretty short but contains a phosphorylation site for Src kinase. Src recognizes two tyrosine residues, one in the N-terminus (Y67 in Kv7.3) and one in C-terminal region (Y349 in Kv7.3). Phosphorylation in these sites suppress the Kv7.3-mediated current. (Li et al., 2004).

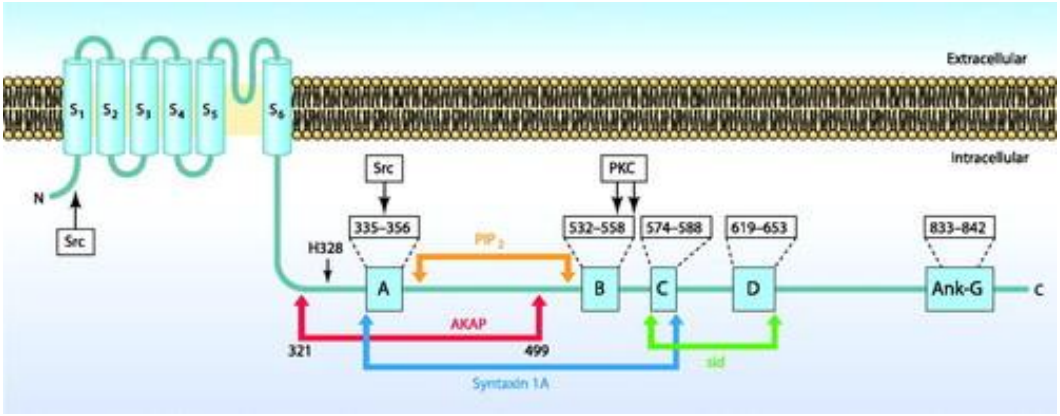

Figure I5.1 *KCNQ C-terminal interacting-sites (Soldovieri et al., 2011).*

The secondary structure of the C-terminal region of a Kv7 subunit presents four α-helices called A, B, C and D (Fig. I5.1). A and B regions contain Calmodulin binding sequences. Some studies have demonstrated that Calmodulin is essential for Kv7 folding and trafficking (Etxeberria et al., 2008) and confers $[Ca^{2+}]_i$ sensitivity to Kv7 channels. (Hernandez et al., 2008). C and D helices are involved in assembly and subunit-specific tetramerization (Schwake et al., 2003). PKC can be recruited on the C-terminal domain by AKAP79. The removal of two putative phosphorylation sites in helix B can prevent the PKC-induced inhibition of channel activity (Hoshi et al., 2003). Moreover, Ankyrin G binding site is crucial for localization in the axon initial segment for Kv7.2 and Kv7.3 (Pan et. al., 2006). Interestingly, that motif is not present in the neuronal Kv7.5, that localizes into the dendrites and soma (Fidzinski et. al., 2015). Syntaxin-1A also binds selectively to the Kv7.2 A helix. When co-expressed, Syntaxin-1A seems to modulate directly the activity of Kv7.2 channels, lowering the activation kinetics (Regev et. al., 2009). The interactions between Syntaxin-1A and Kv7.2 are probably mediated by the Syntaxin-binding protein 1, encoded by STXBP1 gene (Devaoux et.al., 2017).

1.5.2 TRANSCRIPTIONAL CONTROL, ASSEMBLING, HETEROMERIZATION AND TRAFFICKING OF Kv7 CHANNELS

The expression of KCNQ genes is controlled by several transcription factors. Expression is facilitated by Sp1 (Mucha et al., 2010) and NFAT (Zhang and Shapiro, 2012), while negative regulation is exerted by the repressor element 1-silencing transcription factor (REST, NRSF) (Iannotti et al., 2013; Mucha et al., 2010). During and after transcription, the Heat Shock Proteins HSP40 and HSP70 may play an important role in promoting the biosynthesis and folding of Kv7.4 at the endoplasmic reticulum membrane (Gao et. al., 2013). The heteromerization process could then be mediated by J-domain-containing chaperone proteins, recruited from the same system as HSP70 (J-proteins) (Li et. al., 2017). It has also been suggested that Calmodulin may play a role in the folding process of the C-terminal region as well as in the heteromerization of Kv7 channels and in the trafficking process (Liu and Devaux, 2014). Helix D could also promote the assembly process through self-assembling ability (Howard et. al., 2007).

Kv7 channels can form functional heterotetramers in different combinations. It is known that the main configuration that can be found in adult neurons is the Kv7.2/Kv7.3 heterotetramer (Wang et. al., 1998). Heterotetramers formed by Kv7.3/Kv7.5 (Shroeder et. al., 2000) but also Kv7.2/Kv7.5 and Kv7.2/Kv7.3/Kv7.5 are also present at the neuronal level (Soh et. al., 2022). Combinations of Kv7.4/Kv7.5, predominantly expressed at the vascular level, have also been reported (Bal et. al., 2008). There is also evidence that the process of heteromer formation is random (Stewart et. al., 2012). The trafficking process is highly member- and cell-specific. The specific mechanism of exocytosis of Kv7 channels is still unknown. It is known that, in neurons, the membrane localization of the axon initial segment of Kv7.2 and Kv7.3 is mediated by the protein Ankirin-G (Pan et. al., 2006) and assisted by Neurofascin186 (Nfasc186, Ghosh et. al., 2020).

1.5.3 THE ACTIVATION OF THE VOLTAGE SENSOR IN Kv7s

As anticipated, the activating movement of the voltage sensor from a resting state consists of a screwing up movement of the S4 segment within the membrane. This is due to depolarizing changes in the membrane potential

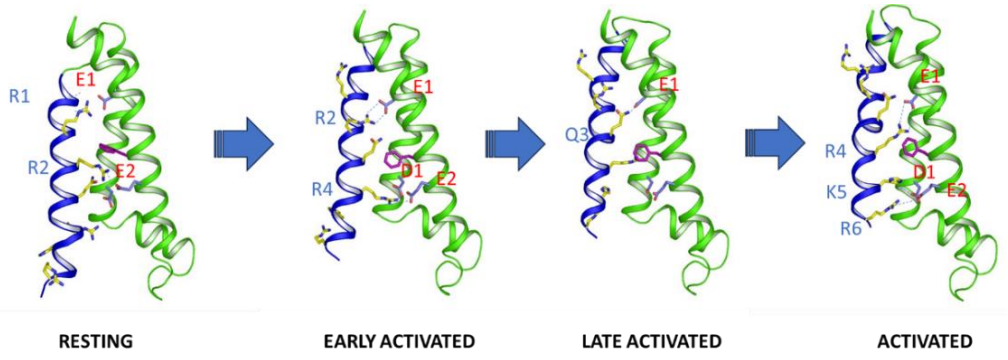

states	E1	E2	D1
RESTING	R1	R2	-
EALY ACTIVATED	R2	R4	-
LATE ACTIVATED	Q3	-	-
ACTIVATED	R4	R6	K5

Figure I5.2 *Aminoacid interactions during the process of activation of Kv7.1 voltage sensor domain. Labeled position are the ones that are responsible for electrostatic interaction during the specific phase. Model was adapted from Kuenze et. al., 2019; Table was adapted from Soldovieri et. al., 2019.*

that induce a rearrangement of arginine organization within the membrane, which rearrange their covalent bonds with negatively charged residues in S2 and S3 segments, as shown in Figure I5.2 (Soldovieri et. al., 2019, Kuenze et. al., 2019).

1.5.4. Kv7 PIP_2- AND CALMODULIN-MEDIATED MODULATION

Phosphatidyl-inositol-4,5-bisphosphate ($PI(4,5)P_2$ or PIP_2) has been shown to play a crucial role in the functional regulation of ion channels, including Kv7 channels (Fig. I5.3) (Kruse et. al., 2012; Winks et. al., 2005).

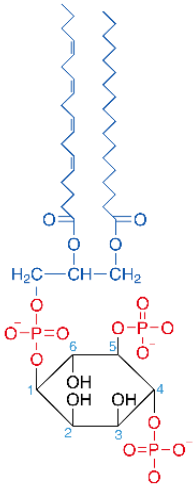

Figure I5.3 *PIP_2 chemical structure.*

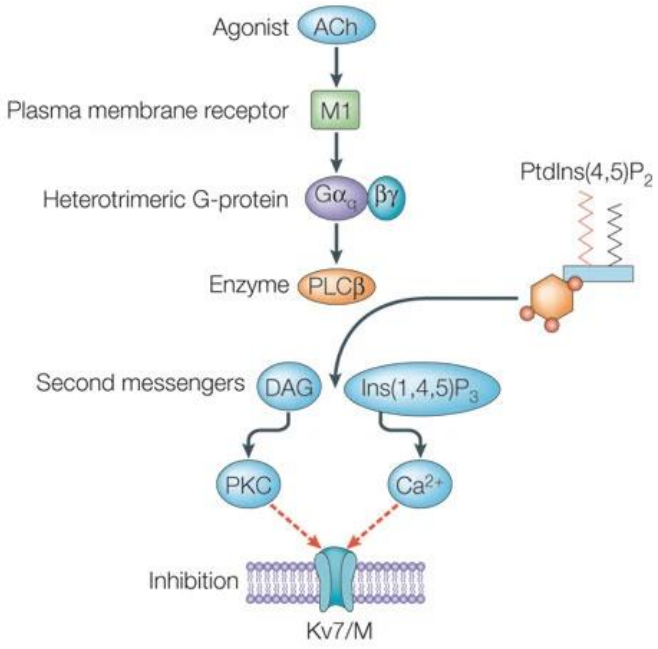

Figure I5.4 *PIP_2 degradation pathway upon M1 activation (Delmas and Brown, 2005).*

Kv7 subunit	PIP_2-interacting Residue	Reference
Kv7.1	R116; K183; R181; R195; K186; R249	Sun and MacKinnon, 2020
Kv7.2	R87; R89; R214; K230; K327	Ma et. al., 2023
Kv7.4	P1: R93; R159; K172; R219; R220; K225 P2: R93; R95; R220; K236; K333	Zheng et. Al., 2022

Table I5.1 *PIP_2 binding amino acid in Kv7.1, Kv7.2 and Kv7.4.*

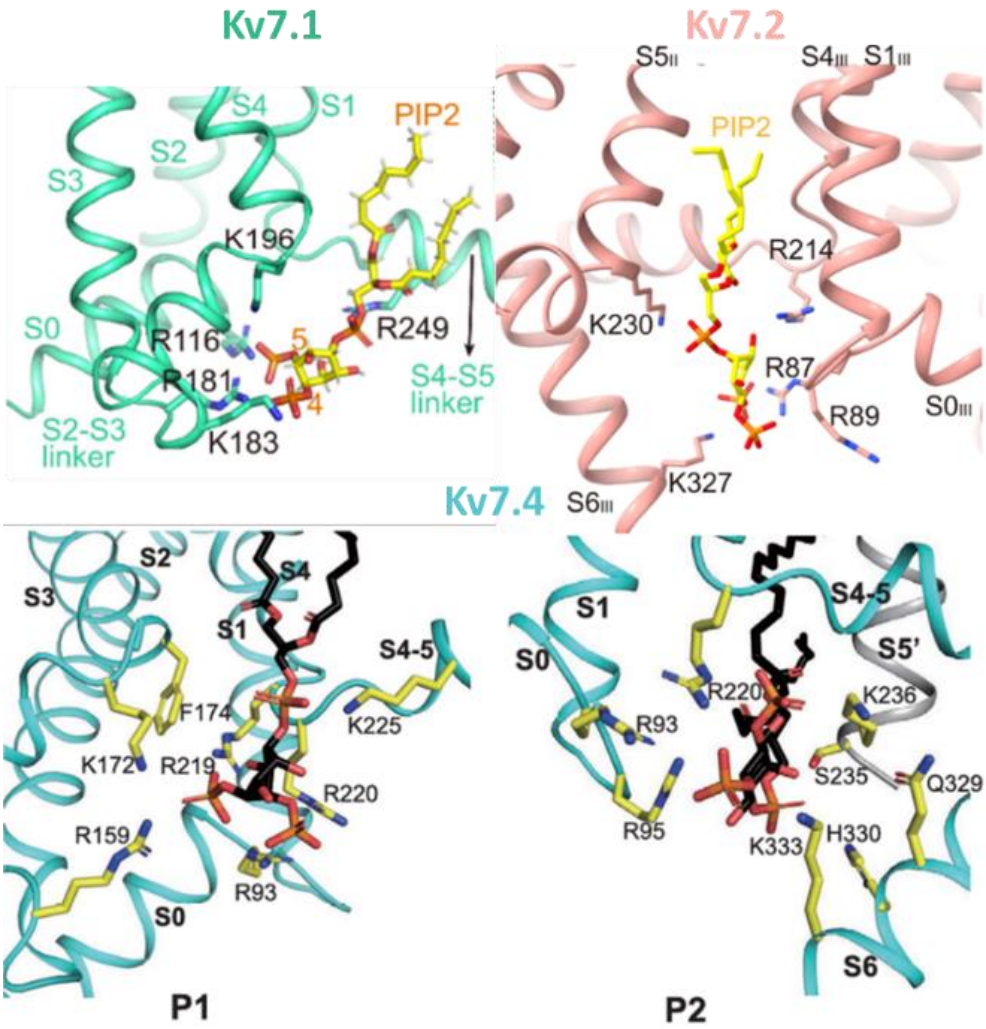

Figure I5.5 *PIP2 binding sites in Kv7.1, Kv7.2 and Kv7.4, with P1 and P2 binding sites (from Sun and MacKinnon, 2020; Ma et. al., 2023; Zheng et. al., 2022).*

These conclusions were reached following the observation that muscarinic receptors, upon their activation, e.g., upon binding to the Oxotremorine (Oxo-M), can modulate Kv7 activity. Indeed, activation of Gq/11 subunit, and phospholipase-Cβ (PLCβ) selectively catalyzes the hydrolysis of the PIP_2 on the glycerol side of the phosphodiester bond. There is the formation of a weakly enzyme-bound intermediate, inositol 1,2-cyclic phosphodiester, and

release of diacylglycerol (DAG). The intermediate is then hydrolyzed to inositol 1,4,5-trisphosphate (IP3) (Kadamur and Ross, 2013). It has been observed that depletion of PIP_2, but not increase of IP3 or DAG (or others

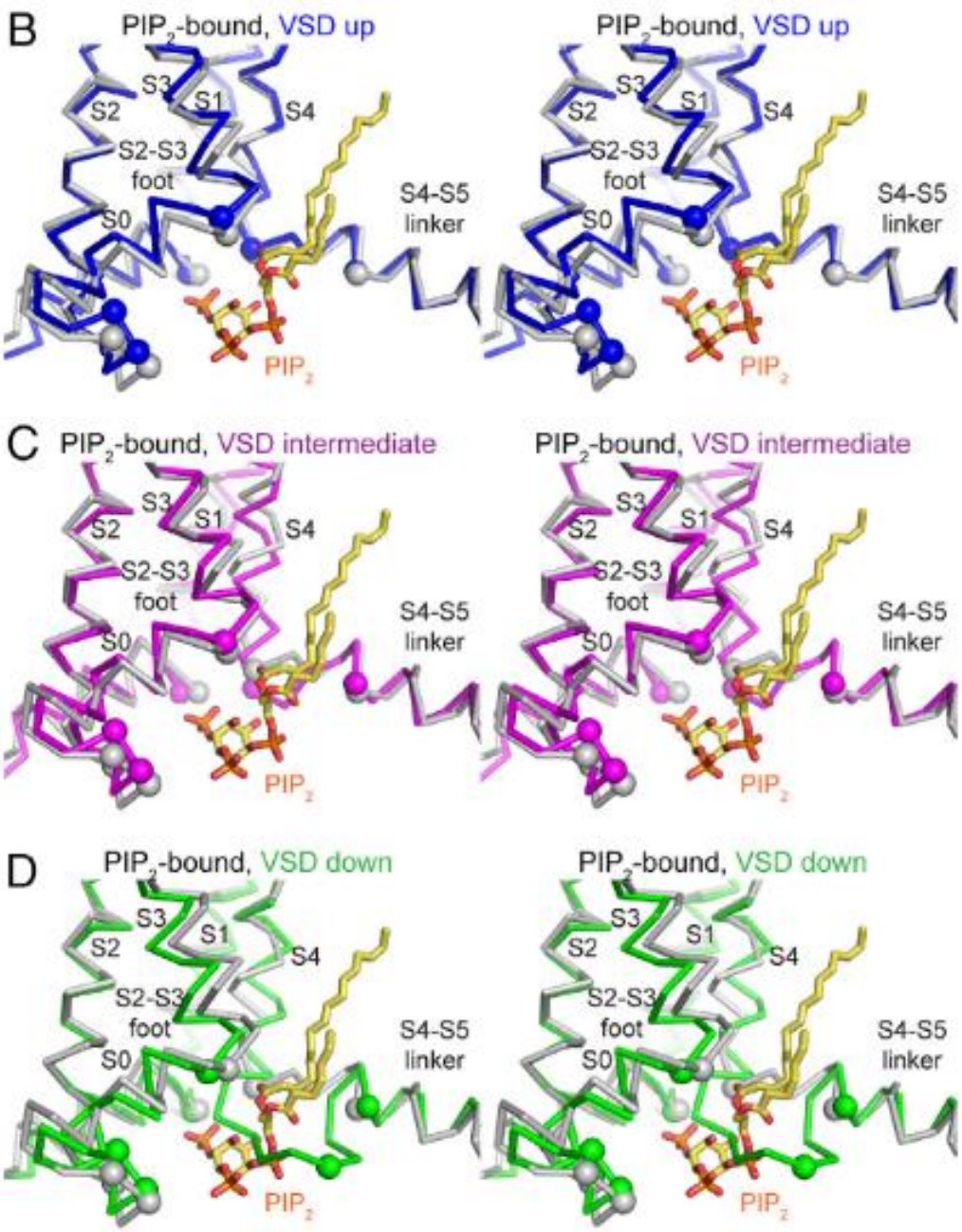

Figure I5.6 *Occupation of PIP_2 of PIP_2-binding site at different VSD conformation. Of note, the binding site in resting conformation of VSD is not accessible by PIP_2 (Mandala et. al., 2023).*

downstream events) is responsible for the decrease in M-current levels (Delmas and Brown, 2005). Single-channel investigations have shown that modulation by PIP_2 is essential to stabilize or increase the probability of Kv7 opening. Moreover, this effect is subtype specific, as they have an intrinsic affinity for intracellular PIP_2. (Li et. al., 2005). The intrinsic opening

probability of each member of the Kv7 family has been shown to depend closely on its affinity for PIP_2 (Hernandez et. al., 2008; Soldovieri et. al., 2011). It is known that PIP_2 is a positive regulator of the function of Kv7 channels in that it is thought to couple the movement of the voltage sensor with the opening of the pore (Zaydman et. al., 2013). Numerous mutagenesis studies have been aimed at identifying the PIP_2 binding site and mutations in several positively charged amino acids, on the intracellular side of the channel induced a loss of sensitivity to modulation of PIP_2 levels (Eckey et. al., 2014; Soldovieri et. al., 2016; Choveau et. al., 2018), such that it has been proposed that PIP_2 may have multiple binding sites (Chen et. al., 2015; Pant et. al., 2021). These sites include the S2-S3 linker, S4-S5 linker, S6 and pre-Helix-A, (Zaydman and Cui, 2014). Recent cryo-EM studies of Kv7.1 (Sun and MacKinnon, 2017; Sun and MacKinnon, 2020; Mandala and MacKinnon, 2023), Kv7.2 (Ma et. al., 2023) and Kv7.4 (Zheng et. al., 2021; Li et. al., 2021) in the presence of PIP_2, have defined the PIP_2 binding site within Kv7 channels. For Kv7.4, one study indicates two different PIP_2 binding sites (Zheng et. al., 2021) (Table I5.1; Fig. I5.).

The Cryo-EM structure of Kv7.1, resolved at different membrane potentials, revealed that PIP_2 binds the binding pocket only when the voltage sensor is in an active state. At hyperpolarized membrane voltages, the voltage sensor is in the down conformation, which prevents PIP_2 from binding because the site is occluded. Depolarization pushes the S4 helix upward, which is accompanied by the formation of the PIP_2 binding site. The pocket structure is maintained when the channel pore is open or closed, as long as the voltage sensor is in the up conformation. In other words, when the voltage sensor is in the up conformation, PIP_2 can bind to this pocket and promote channel opening (Fig I5.6; Mandala and MacKinnon, 2023). Thus, the binding of PIP_2 is preceded by the activation of the voltage sensor, and is followed by the opening of the pore. PIP_2 is also thought to be crucial in mediating the effects of some activating drugs (Kim et. al., 2017). Calmodulin also plays a crucial role in the gating and pore-opening process of Kv7 channels (Wen and Levitan, 2002). Calmodulin is a multifunctional calcium-binding protein that plays a crucial role in the regulation of various cellular processes in eukaryotic cells. It is a small protein that is highly conserved across species. Calmodulin is known for its ability to bind calcium

ions and undergo conformational changes that allow it to interact with a wide range of target proteins and modulate their activity. CaM has a two-lobed structural architecture, with the N-terminal domain (N-lobe) and the C-terminal domain (C-lobe), and each lobe harbors two Ca^{2+} binding sites (Babu et. al., 1988). These sites are also called EF-hand calcium binding motifs. Each EF-hand motif can bind a calcium ion, and calcium binding induces conformational changes in Calmodulin (Gifford et. al., 2007).

Calmodulin, as mentioned above, binds helixes A and B in the C-terminal region of Kv7 channels (Fig. I5.7). In particular, this binds the domain in helix A characterized by the IQ CaM interaction motif (IQXXXRXXXXR). The other site in helix B is different for different members of the Kv7 family: in Kv7.1 and Kv7.5, CaM binds the motif and MXXXVXXXXF while in Kv7.2-4 it binds the LXXXIXXXXV motif (Yus-Najera et al, 2002) and three serine residues (Ser511, Ser523, Ser530) that can be phosphorylated by protein kinase C (PKC) (Yus-Najera et al, 2002). CaM regulation of Kv7 channels is still debated, some studies suggested that CaM confers Ca^{2+}-dependent inhibition of Kv7.2, Kv7.3 and Kv7.4 currents but Ca^{2+}-dependent enhancement of Kv7.1 currents (Chang et. al., 2018).

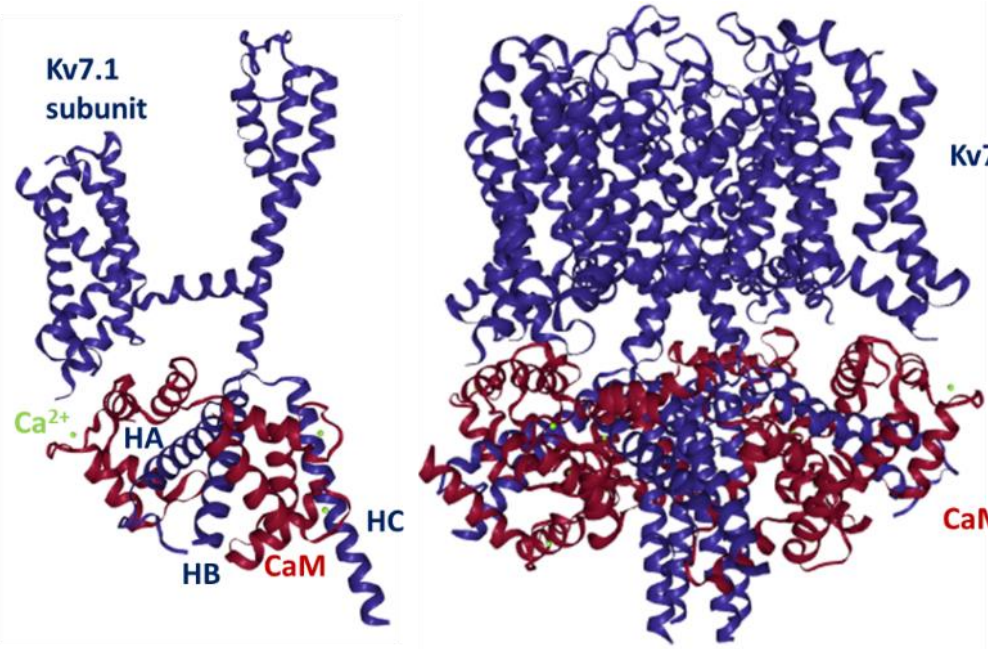

Figure I5.7 *CaM interacting with Kv7.1 single subunit (left) and tetrameric channel (right) (PDB: 5VMS).*

In general, upon depolarization, HA, HB, and their surrounding CaM undergo an almost 180° rotation around the so-called “RQHK” motif (Fig. I5.8) and after this rotation the HA and S6 helices form a joint continuous helix. All together these structural rearrangements induce an enlargement of the activation gate with the opening of the PD (Huang et. al., 2023). It is also thought that PIP_2 may cooperate with Calmodulin during the activation process of Kv7 channels (Fig. I5.7)(Tobelaim et. al., 2017; Lipinsky et. al., 2020; Kang et. al., 2020). Huang et. al. hypothesize that PIP_2 molecules disrupt VSD-CaM interactions, causing CaM release from the VSD. The release of CaM from the VSD likely triggers the rotation of HA, HB, HC and CaM, the folding of S6 and HA into a single continuous helix and the opening of the activation gate. The differences between Kv7.1 and the other members of the Kv7 family could be explained by the fact that the configuration of Calmodulin without calcium (also called ApoCaM) promotes

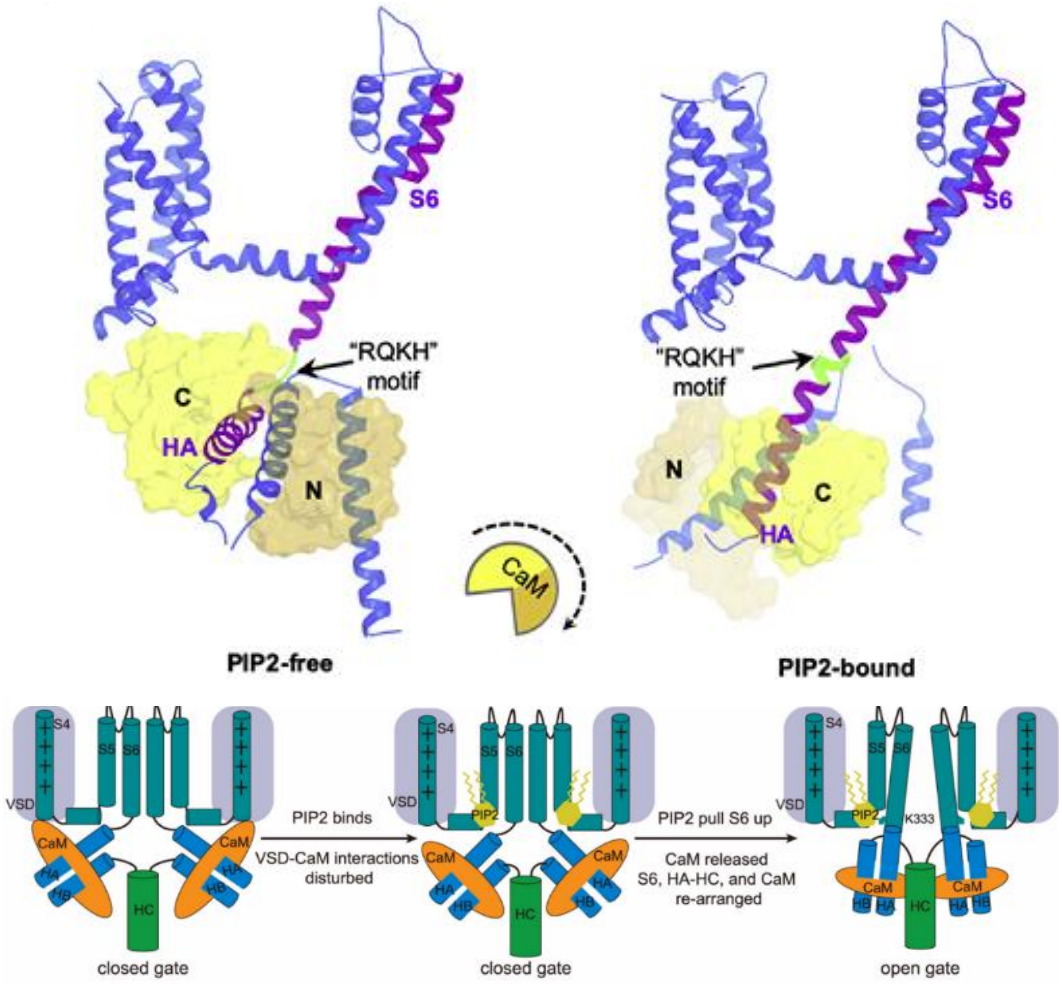

Figure I5.8 *Role of PIP_2-CaM interactions in pore opening (Sun and MacKinnon, 2020; Huang et. al., 2023).*

the opening of Kv7.2-Kv7.5 channels but opposes the activation of Kv7.1. (Chang et. al., 2018).

1.5.5 GATING PROCESS AND STRUCTURAL REARRANGEMENTS DURING PORE OPENING

Electromechanical coupling is the process by which changes in the membrane potential are translated into structural rearrangements of the voltage sensor. These movements are, then, transmitted along the protein to induce the opening of the pore and, finally, the flow of the ion (or ions) which the channel is selective to. After the S4 movement, in Kv7, these structural rearrangements involve S4-S5 linker, that is responsible to “drag” the bottom part of the S6 region, leading to the pore opening.

In particular, the occurring Van der Waals interactions between W248 and I268 and between L251 and F339 (in Kv7.1) are responsible for the stabilization of the open configuration of the pore (Fig. I5.9, Hou et. al., 2020). There are three main motifs that are crucially mediating that process: PAG, GSG and activation gate region (Fig. I5.10).

PAG motif is considered the motif around which the most C-terminal region of the S6 segment makes its movement, from closed to open, with an outward shift (Seebohm et. al., 2006). In contrast, the GSG motif represents

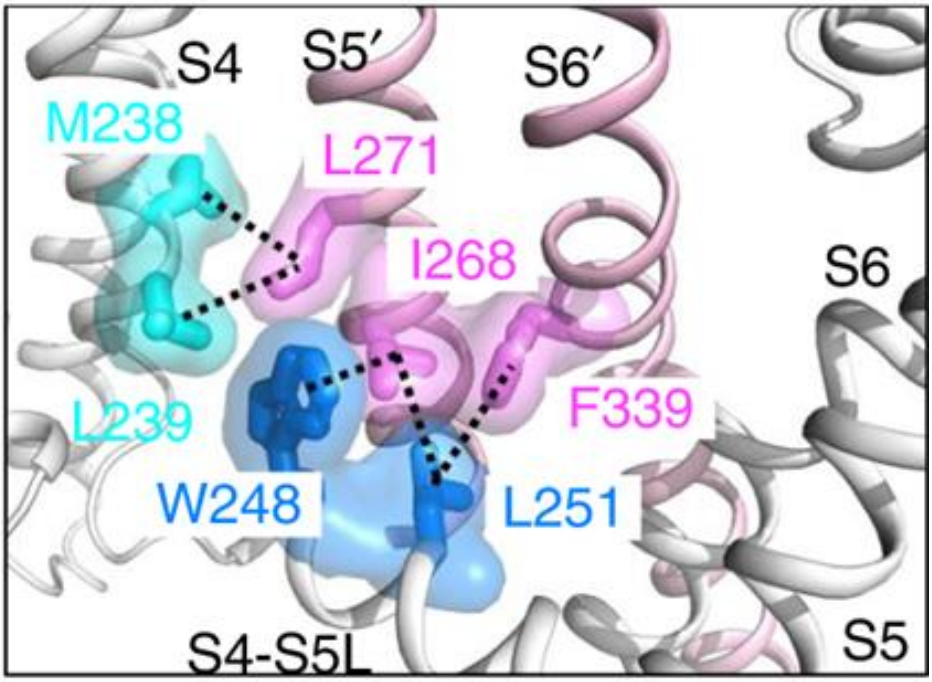

Figure I5.9 *Van-der-Waals intrasubunits interaction between S4-S5 linker aminoacids and distal S6 segment (Hou et. al., 2020).*

the narrowest point of the pore in closed conformation (Sun and MacKinnon, 2017). The activation gate, on the other hand, is the region of the pore that undergoes the greatest expansion in diameter as a result of pore opening (Figure I5.10, Ma et. al., 2022).

The pore opening process, interestingly, does not affect the structure of the selectivity filter, but involves a strong rearrangement that causes a large dilation in the pore diameter, especially on the intracellular side of the pore, allowing the flow of hydrated potassium ions. The narrowest region of the pore, that corresponds to the “GSG” motif (to the serine, in particular), dilates from around 1 angstrom diameter to 4 angstrom diameter, becoming large enough to allow the hydrated potassium ions flow, that have a diameter of 2,5 angstroms.

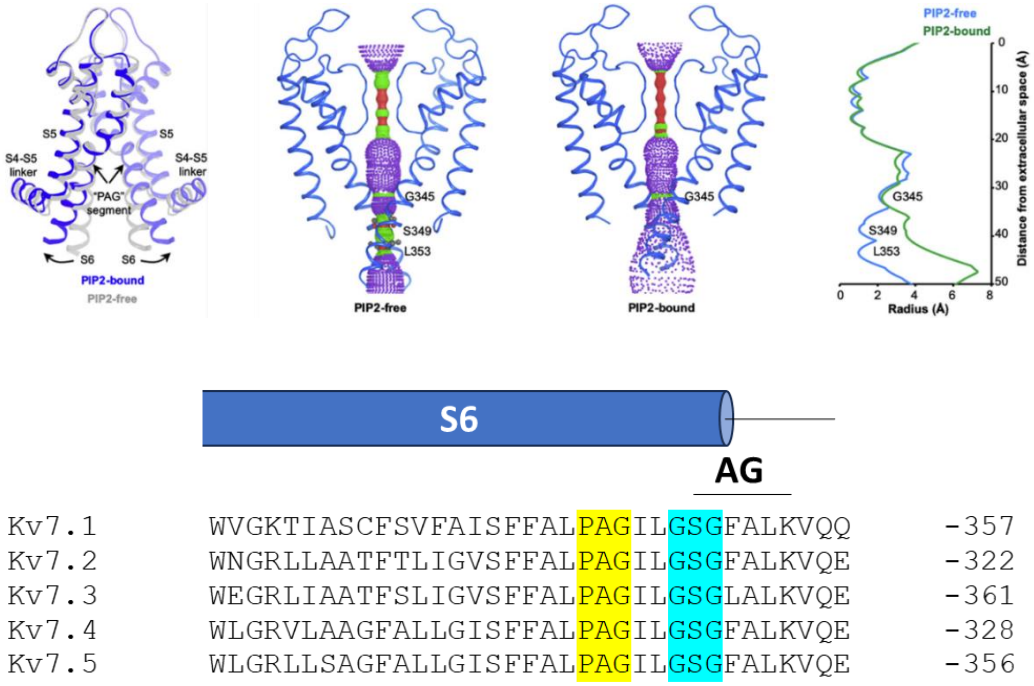

Figure I5.10 *Structural rearrangements of distal S6 segment underlying pore opening. On the right, pore radius representation and measurement in closed and open conformation are shown (Sun and MacKinnon, 2020). In the bottom part of the figure, Kv7 alignment of the distal region of S6 is reported. In yellow and light blue highlighted, respectively, “PAG” and “GSG” motifs in Kv7; “AG” indicates the region of the activation gate.*

1.6 NEURONAL Kv7 CHANNELS

Neuronal Kv7 channels (Kv7.2-3, 5) underlie M-current in neurons (K_M, see 1.4 chapter). The M-current was discovered, upon observation that activation of muscarinic receptor (and for this reason, also called “M current”) using voltage-clamped frog sympathetic neurons, cause the selective suppression of a distinct component from delayed rectifier potassium current (Brown and Adams, 1980). That current was then found in the brain, in particular in the hippocampus (Halliwell and Adams, 1982).

M-current is a slowly activating, non-inactivating, voltage-dependent potassium (K^+) current that activates in the range of the resting membrane potential. This current in neurons is involved in the regulation of resting membrane potential (Wladyka et al., 2006), into shaping the slow after hyperpolarization (sAHP, Tzsingounis et. al., 2010) and in spike frequency adaptation (Otto et. al, 2006).

Modulation of Kv7 channels in neurons crucially alters neuronal excitability and spiking frequency (Fig. I6.1). Moreover, Kv7 channels have also a compensatory role in hyperexcitability: NFAT transcription factor, in fact, following increased intracellular calcium concentrations, promotes the expression of Kv7 channels in an activity-dependent manner (Zhang and Shapiro, 2012), a mechanism that protects neurons from overexcitability and restores spiking rate within physiological limits.

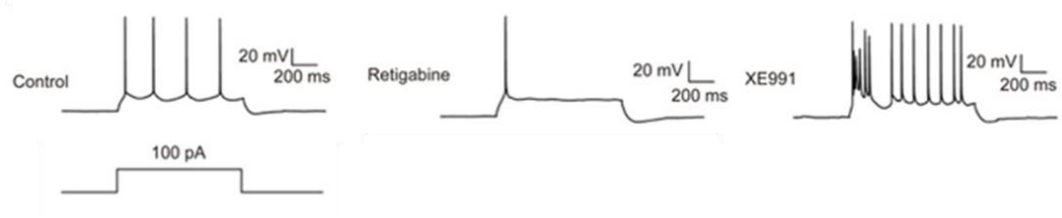

Figure I6.1 *Effect of M-current modulation on neuronal excitability by an activator (retigabine) and an inhibitor (XE991).*

1.6.1 SPATIO-TEMPORAL EXPRESSION PATTERN OF NEURONAL Kv7 CHANNELS

The M-current is thought to be predominantly mediated by Kv7.2/3 heteromers at the neuronal level. Kv7.2 is expressed throughout the entire encephalon, and is particularly expressed at the level of the cortex and hippocampus, and Kv7.3 follows the same pathway (Tinel et. al., 1998).

Kv7.2/Kv7.3 channels form heterotetramers *in vitro*, in heterologous expression patterns (Wang et. al., 1998). It has been observed that these two proteins also co-localize *in vivo*, indicating that Kv7.2/Kv7.3 heterotetramers are present in cortical and hippocampal neurons (Cooper et. al., 2000). Both Kv7.2 and Kv7.3 are ubiquitously expressed at the neuronal level, with no distinction between excitatory or inhibitory neuronal populations (Cooper et. al., 2001). These heterotetramers localize predominantly at the axon initial segment (AIS) level of Ranvier's nodes (Devaux et. al., 2004), although patch clamp recordings report M-current also in the soma of hippocampal neurons (Hu et. al., 2007). Kv7.5 can also form heterotetrameric functional channels with Kv7.3 and it is believed that Kv7.3/5 contributes to molecular heterogeneity of M-current during fetal period and after birth in medial prefrontal cortex and hippocampal formation (Schroeder et. al., 2000). Moreover, recently, Tzingounis' group demonstrated that Kv7.5 can form heteromers with Kv7.2 alone or assemble in Kv7.2/Kv.7.3/Kv7.5 complexes (Soh et. al., 2022). In contrast to Kv7.2 or Kv7.3, Kv7.5 would appear to be predominantly expressed at the dendritic level, in both cortical and hippocampal somatostatin neurons (Fidzinsky et. al., 2015). Kv7.5 is also abundantly expressed at the pre-synaptic level, in the calyx of Held, probably in homomeric form. Here it regulates the release frequency of glutamate-containing vesicles (Huang and Trussell, 2011). Temporally, in mice, Kv7.2 subunits exhibit significant expression from birth, with relatively stable or increasing levels postnatally, as documented by Tinel et al. (1998) and Safiulina et al. (2008). In contrast, the expression of Kv7.3 subunits is initially minimal at birth but gradually rises, eventually surpassing that of Kv7.2 subunits, according to studies by Tinel et al. (1998) and Zhang et al. (2016). Consequently, the more “efficient" channels composed of Kv7.2/3 heteromers increase as development proceeds, replacing those composed of the Kv7.2 subunit alone (Kanaumi et. al., 2008; Dirkx et. al., 2020). Those data are confirmed in human, by transcriptional analysis performed on human samples during and after fetal development. The graph in Fig. I6.2 shows the expression levels of neuronal Kv7 channels from the eighth week after conception to the first year of life. (https://www.brainspan.org/). These data seem to indicate that neuronal Kv7 expression is relevant during embryogenesis and confirm that the

expression of Kv7.2 is high at birth, while Kv7.3 and Kv7.5 are expressed more late during early infancy.

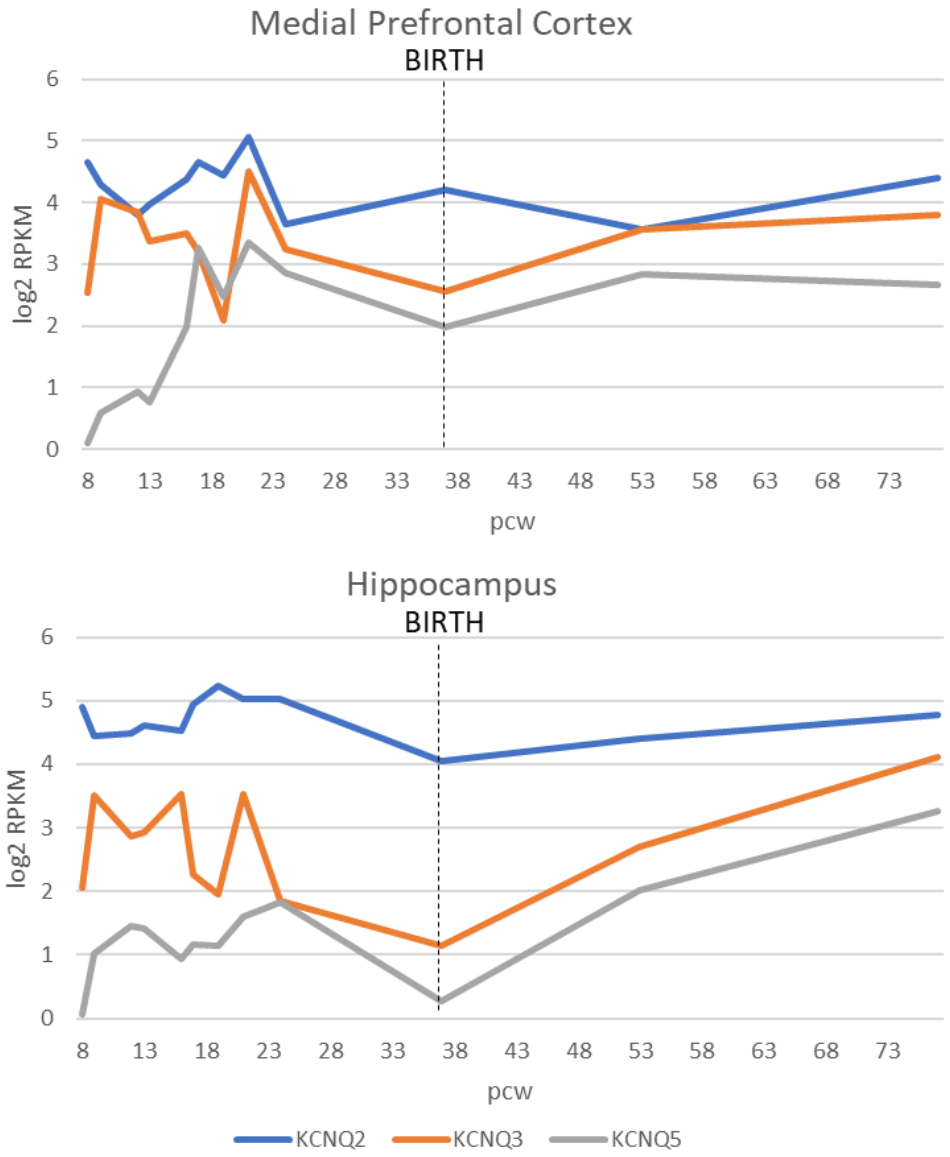

Figure I6.2 *Spatio-temporal expression pattern of KCNQ2 (blue), KCNQ3 (orange) and KCNQ5 (grey) in Human medial prefrontal cortex and hippocampus between 8 post-conception week and the first year of life. The dotted line represents the moment of birth (36 post-conception week). Data derived from https://brainspan.org/.*

1.6.2 KCNQ-RELATED DISORDERS

Epilepsy is a disorder of the brain characterized by an enduring predisposition to generate epileptic seizures (Fisher et al., 2014). An epileptic seizure is a transient behavioral change caused by an abnormal,

excessive, synchronous neuronal activity in the brain, occurring either with objective signs or subjective symptoms (Devinsky, et al., 2018).

Epilepsy is the third leading contributor to the global burden of disease for neurological disorders (Ngugi et al., 2010). Seizures can be the result of almost any insult that perturbs brain function. Causes of seizures can be acquired such as infectious diseases, or congenital, such as genetic mutations. To date, >500 genes associated with epilepsy have been identified (Devinsky et al., 2018). Of these, 27 percent encode for ion channels (Oyrer et. al., 2018). Diseases associated with genetic alterations of ion channels are termed "channelopathies". Although epilepsy is often a polygenic disorder, some forms of epilepsy are monogenic, with a single gene mutation responsible for the phenotypic features (Rastin et. al., 2023). In particular, mutations in the *KCNQ2*, *KCNQ3*, and *KCNQ5* genes are associated with a wide spectrum of human neuronal channelopathies in which epilepsy is often (but not always) present. In the following paragraphs, we will briefly summarize the phenotypic features of the genetically determined channelopathies associated to these genes.

1.6.3 GENOTYPE-PHENOTYPE CORRELATION FOR *KCNQ2* GENE

Mutations in *KCNQ2* are responsible for mostly neonatal onset epileptic disease with a phenotypic spectrum ranging from self-limited neonatal epilepsy (SLFNE) to developmental and epileptic encephalopathy (DEE). SLFNE is characterized by seizures starting between two and eight days of life and are typically multifocal seizures, lasting a few minutes, with normal interictal EEG (Miceli et. al., 2010; Nappi et. al., 2020). Then, seizures spontaneously disappear between the first month of life between the first and the sixth to 12th month of life in otherwise healthy infants, in a context of normal neuropsychological development and EEG features (Miceli et al., 2010), although 10-15% of patients report seizures later in life (Plouin et. al., 1994). In addition, pathogenic variants in *KCNQ2* gene has been identified in patients with self-limited familial neonatal infantile seizures (SLFNIS) or self-limited familial infantile seizures (SLFIS) (Zara et. al., 2013; Zhou et. al., 2006); both of these conditions differ from SLFNE in the age of onset of seizures, which can arise, respectively, between birth and the sixth

month of life or after the sixth month of life and then, in both cases, disappear spontaneously (Berkovich et. al., 2004).

The effect of pathogenic mutations in KCNQ genes has been a subject of interest in our group for many years. Functional investigations of numerous mutations in KCNQ channels have allowed the establishment of a genotype-phenotype correlation model (Fig I6.3). According to this model, the pathological range of conditions associated with mutations in *KCNQ2* with LoF varies from neonatal onset-DEE (NO-DEE) to the most benign and familial forms of SLFNE. Mutations in *KCNQ2* with a gain-of-function can, in turn, induce a spectrum of phenotypes ranging from the least severe, characterized by infantile spasms and intellectual disability, to the most severe, also characterized by neonatal-onset DEE intellectual disability and high risk of early mortality.

Mutations in *KCNQ2* are responsible for mostly neonatal onset epileptic diseases with significant phenotype heterogeneity, ranging from benign forms, such as self-limited familial neonatal epilepsy (SLFNE), to severe forms of neonatal onset developmental and epileptic encephalopathy (NO-DEE). *KCNQ2* is the most commonly mutated gene in patients with SLFNE. At the most severe end of the spectrum, *KCNQ2*-DEE characterized by multiple daily pharmaco-resistant seizures that begin in the first week of life and cease between 9 months and 4 years of age, developmental delay, neuroradiological abnormalities, and behavioral comorbidities including intellectual disability and autism cognitive decline (Fig. I6.3). (Weckhuysen et. al., 2012). In addition, mutations in *KCNQ2* gene were also reported in Ohtahara syndrome patients (Saitsu et. al., 2012) and associated with sudden unexpected death in epilepsy (SUDEP) (Wechkhuyen et. al. 2013). Mutations associated with more severe phenotypes, such as NO-DEE, are all missense mutations. Mutations causing SLFNE are distributed among all sequence of the channel and include missense, frameshift and premature stop codon variants, whereas variants causing DEE are all missense are localized within 4 hot spot regions: the S4 voltage-sensor, the pore, the proximal C-terminal domain that binds PIP_2 and Calmodulin (CaM A), and the more distal domain which binds Calmodulin (CaM B). The most benign phenotypes, such as SLFNE, are associated with variants that induce LoF of a single allele (or haploinsufficiency). These kinds of

mutations include frameshift mutations, deletions, insertion and splicing variants (which together account for 36% of the mutations in *KCNQ2* associated with SLFNE) (Nappi et. al., 2020), but also missense mutations. It has been suggested that, because of the excitatory effects of GABAergic neurotransmission during this developmental stage, the neonatal brain may be more vulnerable to mutations decreasing the inhibitory contribution of I_{KM} to neuronal excitability (Okada et. al., 2003).

Functional studies of missense variants in *KCNQ2* identified in patients with SLFNE revealed a slight reduction (by 25%-50%, Jentsch, 2000) of channel function (loss of function, LoF), suggesting haploinsufficiency as the primary pathogenic mechanism for *KCNQ2*-SLFNE. On the other hand, missense mutations causing DEE exert more severe functional defects on K+ current function, with a reduction of current more than 50% (LoF), suggesting that a dominant-negative effect could be responsible for the severe epileptic phenotype (Miceli et al 2013, Orhan et al 2014).

In addition to LoF, few *de novo* missense gain of function (GoF) variants in *KCNQ2* have been described. These variants induce an increase of channel activity by increasing maximal current density and/or a marked hyperpolarizing shift in the voltage dependence of activation. Several hypotheses have been put forward to explain the paradoxical increase in neuronal excitability associated with an enhanced Kv7.2/I_{KM} function *in vitro*, and possibly *in vivo*. These include: (1) preferential suppression of inhibitory interneuron function (the "interneuronopathy" hypothesis) (Catterall 2018); (2) activation of a recurrent neuron-astrocyte-neuron excitatory loop; (3) faster action potential repolarization and sodium channel repriming; and (4) overactivation of the hyperpolarization-activated nonselective cation current resulting in secondary depolarizations (Niday & Tzingounis 2018).

The molecular mechanism underlying the functional alterations associated with them have been elucidated in several variants. These mechanisms appear heterogeneous, and include: (1) reduced K^+ ion permeation mainly for the variants located within the pore domain; (2) decreased voltage sensitivity to opening for variants affecting critical gating residues in the voltage-sensing domain; (3) altered functional regulation of cytoplasmic regulators such as syntaxin-1A, Calmodulin, or PIP_2, and others; (4) mRNA instability and precocious subunit degradation by nonsense-mediated RNA

decay when the variant affects transcript splicing sites; and (5) altered subcellular distribution when the interaction with axon-targeting signals or partners is disrupted (Nappi et al 2020).

One of the variants with well-described functional alteration was found in a patient (Sadewa et. al., 2008) with a mutation in Kv7.2 into the voltage sensor (R213W), was reported and a SLFNE phenotype. This mutation was characterized by Miceli et. al., 2013 and classified as a mild loss-of-function. This mutation affects the sixth arginine of the voltage sensor, and replaces that arginine with a tryptophan, neutralizing the positive charge of the arginine. During the voltage sensor activation, the interaction between R213 (R6) and E140 (E2) is crucial for the stabilization of the voltage sensor in the active conformation. It was postulated that this mutation, with the consequent neutralization of the positive charge, is responsible for the loss-of-function effect, due to the destabilization of the active state of the voltage sensor. However, the effect of this mutation on the function of the channel is less severe than the substitution, in the same position, with a glutamine (R6Q). Miceli et. al., explain that this feature is due to the property of W residue to provide a certain degree of VSD stabilization by creating a π-π interaction with F168 residue (in S3) (Miceli et. al., 2013). Similarly, mutations in the voltage sensor can induce gain-of-function effects. Arginine in the R201 (or R2) voltage sensor is essential to the stabilization of the voltage sensor in resting conformation and partial neutralization of the positive charge (R2H) or the replacement with a negative charge (R2C) induces a strong gain of function of the ion channel (Miceli et. al., 2015). Mutations at the level of the P-loop or selectivity filter are among the mutations with the most dramatic functional effects found in Kv7.2. These mutations, such as the recurrent T274M (Orhan et. al., 2013) and G279S (Castaldo et. al., 2002) are LoF variants with dominant negative effect. Evidently, alterations at the level of the selectivity filter affecting even one of the four subunits can induce the formation of a nonfunctional channel. Indeed, these mutations are generally associated with severe clinical pictures characterized by neonatal DEE (Milh et. al., 2013). Indeed, these mutations have been inserted into mouse animal models to generate knock-in models in which the function of the Kv7.2 channel was abolished and to obtain models of *KCNQ2*-DEE (Peters et. al., 2005; Biba-Maazou et. al.,

2022). Moreover, mutations affecting the PIP_2 binding site can also affect channel functioning. As previously described, PIP_2 is crucial to couple VDS activation to pore opening (Zaydman et. al., 2013; Mandala et. al., 2023). It is known that PIP_2 binds positive charges distributed on the surface of the intracellular side; the neutralization of these charges results in an unfunctional channel and into insensitivity to PIP_2 increase levels (Pant et. al., 2021). R325G mutation, found in a patient with *KCNQ2*-DEE, leads to total loss of the current and PIP_2 insensitivity (Soldovieri et. al., 2016). Finally, several missense mutations affecting the channel function should also fall into the A and B helix and are associated both with SLFNE and DEE and disrupt CaM-Kv7.2 interaction and reduce the surface expression of the channel (Cavaretta et. al., 2014; Kim et. al., 2018; Zhang et. al., 2020). Mechanisms through which missense mutations can alter channel function and induce, consequently a pathophysiological phenotype are varied and heterogeneous. Understanding the biophysical mechanism underlying such alterations is useful for predictive purposes, as knowing how channel functions makes it possible to predict the effect of a mutation even without conducting further functional studies. The attempt to create an algorithm that can predict, based on existing functional data, of the effect of a mutation without performing functional studies has already been tried, but with refinable outcomes (Boßelmann et. al., 2022).

1.6.4 GENOTYPE-PHENOTYPE CORRELATION FOR *KCNQ3* GENE

Mutations in *KCNQ3* are also mainly associated with SLFNE e SLFIE. About 20 families (72 individuals) with SLFNE with a heterozygous *KCNQ3* pathogenic variant have been reported to date (Charlier et. al. 1998; Hirose et. al. 2000; Singh et. al. 2003; Li et. al. 2006; Li et. al. 2008; Neubauer et. al. 2008; Fister et. al. 2013; Allen et. al. 2014; Soldovieri et. al. 2014; Grinton et. al. 2015; Miceli et. al. 2015b; Maljevic et. al. 2016; Sands et. al. 2016; Piro et. al. 2019; Symonds et. al. 2019; Maghera et. al. 2020; Miceli et. al. 2020; Pijpers et. al. 2023). The percentage of families with SLFNE who have pathogenic variants in *KCNQ3* is likely less than 5% (Miceli et. al., 2010). Despite this, the relative phenotype is indistinguishable from those reported for *KCNQ2*-SLFNS (Nappi et. al., 2020). Moreover, biallelic variants have been identified in three families with developmental and epileptic

encephalopathy with neonatal-onset seizures and global developmental delay (Ambrosino et. al. 2018; Kothur et. al. 2018; Lauritano et. al. 2019) demonstrating that, on the contrary to *KCNQ2*, homozygous variants in *KCNQ3* are compatible with life. *De novo* pathogenic variants also occurred in few children with DEE (Epi4K Consortium & Epilepsy Phenome/Genome Project, 2013) isolated ID (Rauch et.al., 2012) and autism spectrum disorder (Sands et. al., 2019). Variants in *KCNQ3* are rare and seem, overall, better tolerated than the corresponding variants in Kv7.2. For example, a frameshift variant in heterozygosity in Kv7.3 associated with a pathological phenotype has never been reported. Loss in homozygosity, however, of the Kv7.3 channel is associated with a rather severe picture of epilepsy and neurocognitive impairment (Ambrosino et al 2018) while, on the other hand, as already anticipated, variants inducing haploinsufficiency in Kv7.3 are virtually indistinguishable from the *KCNQ2*-SLFNE phenotype. Variants with gain of function in *KCNQ3*, on the other hand, appear to be predominantly associated with autism spectrum disorders and epileptic activity during sleep (Fig. I6.3)(Sands et. al., 2019, Nappi et. al., 2020).

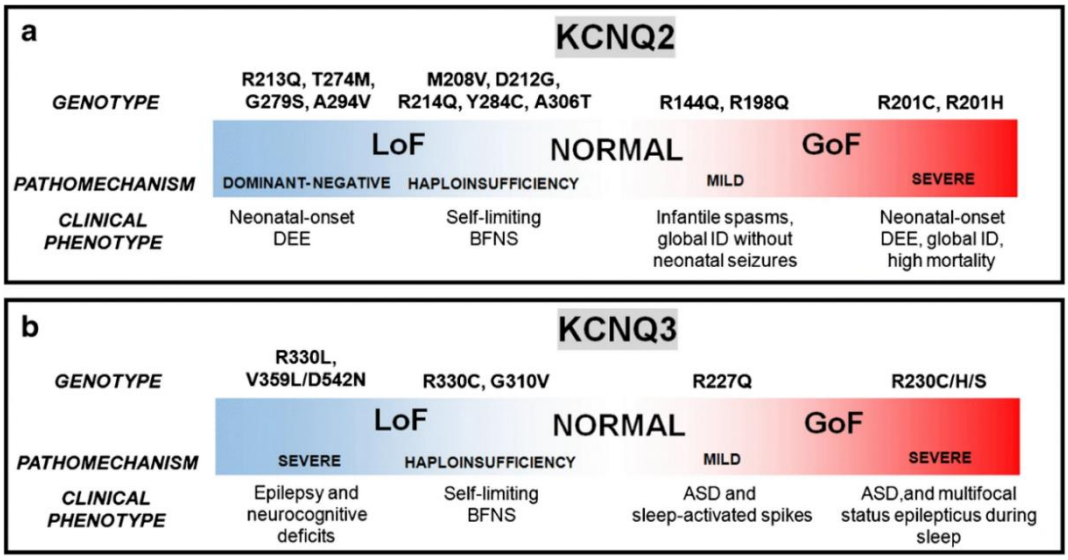

Figure I6.3 *Genotype-phenotype correlation for KCNQ2 and KCNQ3 genes.*

1.6.5 GENOTYPE-PHENOTYPE CORRELATION FOR *KCNQ5* GENE

Regarding *KCNQ5*, only 16 variants have been reported to date. Among them, there are 11 missense variants (S448I, V145G, L341I, P369R, K289N, R443Q, P369T, H576R, R359C, L692V, Q735R), 2 nonsense

variants (R178X, R443X), one intragenic duplication, one splice variant (E265_T306del) and a frameshift mutations (A301Gfs*64). (Lehman et. al., 2017; Rosti et. al., 2019; Kruger et. al., 2022; Wei et. al., 2022). The phenotype of patients with mutations in *KCNQ5* is very heterogeneous, from mild to severe neurodevelopmental disorders, absence epilepsies, drug-resistant tonic epilepsies or infantile spasms, with onset between 5 months and 5 years, but also no seizures. Hypotonia has also been reported. R359C, Q735R and E265_T306del are variants that have been identified in 3 different patient families, and have been associated with absence epilepsies, intellectual disability, myoclonic seizures and/or generalized tonic-clonic seizures. These families also report healthy carriers, suggesting that phenotypes might be influenced by other individually differing factors, such as compensatory effects, genetic background or environmental determinants. (Kruger et. al., 2022). Genotype-Phenotype correlation for *KCNQ5* will be discussed later in this work (see discussion).

2. AIMS

Mutations in neuronal Kv7 channels cause both loss-of-function and gain-of-function effects on channel function. Despite the progress made in the past years in the establishment of genotype-phenotype correlations for Kv7-related disorders, there is still a gap in the understanding of how some pathogenic variants in these genes affect channels function and, ultimately, clinical phenotypes. For instance, whilst the reduction of repolarizing K^+ current consequent to LoF in Kv7.2, Kv7.3 and Kv7.5 might explain the neuronal hyperexcitability leading to epilepsy and/or developmental delay, the mechanisms by which increased M-current activity cause such phenotype are still elusive. Therefore, elucidating the changes in the biophysical properties prompted by GoF variants is crucial to get insight in the pathogenesis of the disease and possible therapeutic approaches.

In the present work we used mutagenesis, electrophysiology, biochemical, and molecular dynamic techniques to investigate the functional and structural consequences of six pathogenic variants, found in six unrelated patients, occurring in the PD of Kv7.2, Kv7.3 and Kv7.5 channels (Table A1). All of these variants are missense *de novo* variants that occur heterozygously in the patients. Three of these variants are novel whereas three others were already reported in the literature without functional characterization. Patient variants characterization could define new subcategories of patients, representing the rationale for planning, improving and guiding personalized drug therapies for DEE. This work also moved by the identification and characterization of potential new pharmacological approaches, aimed to restore the *in vitro* altered phenotype.

PATIENT NUMBER	GENE	cDNA VARIANT	AMINOACID ALTERATION	ZYGOSITY	INHERITANCE PATTERN	PHENOTYPE	REFERENCE
Novel reported patient							
1	KCNQ5	1040G>A	G347S	Heterozygosity	De novo	DEE; severe ID	Reported us by Dr. Gaetan Lesca
2	KCNQ5	1041G>C	G347A	Heterozygosity	De novo	Moderate to severe ID	Reported us by Dr. Gaetan Lesca
3	KCNQ2	949G>A	A317T	Heterozygosity	De novo	ASD	Reported us by Dr. Ingrid Sheffer
Patient and variants reported in literature							
4	KCNQ2	937G>A	G313R	Heterozygosity	De novo	EOEE. BS	Olson et. al.. 2017
5	KCNQ2	952C>G	L318V	Heterozygosity	De novo	IS; ESES	Gong et. al.. 2021
6	KCNQ3	1066C>T	A356T	Heterozygosity	De novo	Severe ID	DDD study. 2017

***Table A1**: Patient description for the present work.*

3. MATERIALS AND METHODS

3.1 PATIENT RECRUITMENT AND GENETIC ANALYSIS

The firsts two patients were recruited in the Pediatric Neurology and Genetics Departments of the University Hospitals of Lyon and Lille, respectively. The parents gave informed consent for the genetic study and the publication, according to the French Bioethics law. The study was approved by the Ethics and Scientific Committees of the Lyon and Lille University Hospitals (no. 542, Gene Panel for Monogenic Epilepsies). Genetic diagnosis was performed using next-generation sequencing (exome sequencing for patient 1 and gene panel for patient 2), as described (Rudolf et. al., 2020). The patient 3 carrying the *KCNQ2* A317T mutation, was recruited by Dr. Ingrid Sheffer at Epilepsy Research Centre, Department of Medicine, University of Melbourne, Australia.

3.2 SITE-DIRECTED MUTAGENESIS OF Kv7 cDNAs

Each mutation was engineered in a pcDNA3.1-Kv7.5, pcDNA3.1-Kv7.2 and pcDNA3.1-Kv7.3 plasmids encoding for the human transcript variant 2 of Kv7.5 (accession number: NM_001160130.2, CCDS55037.1), for human transcript variant 3 of Kv7.2 (accession number: NM_004518.6, CCDS13518.1) and for human transcript variant 1 of Kv7.3 (accession number: NM_004519.4, CCDS34943.1), for wild-type. For mutants, incorporation of the mutation G347S, G347A, G347R, G347E for Kv7.5, of G313S, G313R, G313E, A317T and L318V mutations for Kv7.2, and A356T mutation for Kv7.3 was performed using Quick-change SiteDirected Mutagenesis (Agilent Technologies). The mutations were engineered in each plasmid by Polymerase Chain Reaction (PCR), using a pair of primers (forward and reverse), as reported in the following table, to incorporate the desired nucleotide mutation.

MUTATION	PRIMERS	
	Forward	Reverse
Q5 G347S	5'-CCTGCCGGCATTCTTAGCTCAGGTTTTGC-3'	5'-GCAAAACCTGAGCTAAGAATGCCGGCAGG-3'
Q5 G347A	5'-CCTGCCGGCATTCTTGCCTCAGGTTTTGC-3'	5'-GCAAAACCTGAGGCAAGAATGCCGGCAGG-3'
Q5 G347R	5'- GCATTCTTCGCTCAGGTTTTGC-3'	5'- GCAAAACCTGAGCGAAGAATGC-3'
Q5 G347E	5'-CGGCATTCTTGAGTCAGGTTTTGC-3'	5'-GCAAAACCTGACTCAAGAATGCCG-3'
Q2 G313R	5'- CTGCAGGCATCTTGAGGTCTGGGTTTGCC -3'	5'- GGCAAACCCAGACCTCAAGATGCCTGCAG -3'
Q2 G313S	5'-GCATCTTGAGCTCTGGGTTTGC-3'	5'-GCAAACCCAGAGCTCAAGATGC-3'
Q2 G313E	5'- GGCATCTTGGAGTCTGGG-3'	5'- CCCAGACTCCAAGATGCC-3'
Q2 A317T	5'- GGGGTCTGGGTTTACCCTGAAGGTTCAGG-3'	5'- CCTGAACCTTCAGGGTAAACCCAGACCCC-3'
Q2 L318V	5'- GTCTGGGTTTGCCGTGAAGGTTCAGGAG-3'	5'- CTCCTGAACCTTCACGGCAAACCCAGAC-3'
Q3 A356T	5'- GGTCCGGGCTGACCCTCAAGGTGC-3'	5'- GCACCTTGAGGGTCAGCCCGGACC-3'

The following ingredients were used in the final 50 µL volume of the amplification reaction: 50 nanograms of Kv7.3-WT plasmid, 125 nanograms of primer forward and reverse, 5% DMSO, 2.5 nanograms of Pfu DNA Polymerase, 1X Pfu buffer, and 1 microliter of dNTP mix. In order to denaturize the DNA double helix (95°C for 1'), the anneal the primers to the single strand of DNA (55°C for 1'), and extend the primers (68°C for 10'), the PCR was conducted in 12 cycles, each of which included three temperature steps (Fig. 11). Following the amplification process, the reaction volume comprised both methylated (parental) and unmethylated (neosynthesized) DNA; hence, enzymatic digestion was carried out using 1 µl DpnI to eliminate the parental DNA.

3.3 BACTERIAL TRANSFORMATION AND PLASMIDIC DNA PREPARATION

After enzymatic digestion with DpnI, competent E. coli DH5α cells were transformed with the PCR product by chemical transformation procedure (30' at 4°C, heat shock at 42°C for 45'' followed by 3' at 4°C). To help the bacterial cells recover from the heat shock, the cells were incubated with 200 µl of SOC medium (2% tryptone, 0.5% yeast extract, 10 mM NaCl, 2.5 mM KCl, 10 mM MgCl2, 10 mM MgSO4, 20 mM glucose), for 45' at 37°C. Finally, the cells were seeded on LB+agar plates (containing 10 g/L of tryptone, 5 g/L of yeast extract, 5 g/L of NaCl, 15 g/L of agar) with the specific antibiotic, to which the plasmids are resistant, such as ampicillin (100 µg/µL), to allow growth only of E.coli cells transformed with pcDNA3.1 plasmids (in which Kv7.3 cDNA is present).
The plates were then incubated inverted at 37°C for about 16 hours to allow bacterial growth. Each colony grown on LB medium was inoculated into 5 mL of fresh LB medium with antibiotic selection (Amp/Kan), in accordance with the antibiotic resistance conferred by plasmids on E. coli cells, at 37°C/220 rpm overnight. Subsequently, plasmid DNA was extracted using a commercially available kit (QIAprep Spin Miniprep, QIAGEN). Successful insertion of the desired mutation was verified by direct sequencing (Eurofins, Milan, Italy). To obtain a large amount of DNA, one of the positive clones was amplified on a large scale (500 mL), and plasmid DNA was extracted using a commercially available kit (Plasmid Plus Maxi, QIAGEN). The cDNA was sequenced again in order to confirm the presence of the mutation of interest and exclude any

additional mutations in the entire coding sequence. The concentration of the cDNA suspension is then defined by Nanodrop measurement (Nanodrop One, ThermoFisher).

3.4 CELL CULTURES

Chinese Hamster Ovary (CHO) cells or Human Embryonic Kidney 293 cells (HEK 293 cells) were grown in plastic Petri dishes (100 mm, 60 mm or 40 mm, according to the different experimental needs) in DMEM (Dulbecco's Minimum Eagle Medium) supplemented with 10% Fetal Bovine Serum (FBS; decomplemented at 56°C for 30'), 1% L-glutamine (2 mM in 0.85% NaCl), 1% penicillin (50 U/mL) and 1% streptomycin (50 µg/mL) in a humidified atmosphere at 37°C with 5% CO2. Every time cells became confluent within the dishes (about every 2 days), they were split by using 1% trypsin solution and collected in novel dishes with a 1:3 dilution.

3.5 CHO CELLS PREPARATION AND WHOLE-CELL ELECTROPHYSIOLOGY

For electrophysiological experiments, CHO cells were seeded on glass coverslips. After 24h, CHO cells were transfected using Lipofectamine 2000, according to the manufacturer protocol (LifeTechnologies, Milan, Italy). In each transfection mixture, a plasmid encoding for an Enhanced Green Fluorescent Protein (pEGFP; Clontech, Palo Alto, CA) was used as transfection marker (3 µg of plasmids encoding for Kv7 cDNA + 1 µg di pEGFP).

In experiments aimed at assessing the sensitivity to PIP_2 of a given channel, co-transfection of the plasmid encoding the Kv7 channel of interest the plasmid encoding the PIP5K 1γ or Dr-VSP cDNA enzymes, in addition to the transfection marker (0.75 µg of plasmids encoding for Kv7 cDNA + 2.25 plasmid encoding for the enzyme + 1 µg of pEGFP) was performed.

Macroscopic currents were recorded, after 1 day, using patch-clamp technique in the whole-cell configuration with glass micropipettes of 3–5 MΩ resistance. No compensation was performed for pipette resistance and cell capacitance. During patch clamp recordings, cells were perfused with an extracellular solution containing (in mM): 138 NaCl, 5.4 KCl, 2 CaCl2, 1 MgCl2, 10 glucose, 10 HEPES, pH 7.4 (adjusted with NaOH). The pipettes used for recordings were filled with an intracellular solution containing (in mM): 140 KCl, 2 MgCl2,

10 EGTA, 10 HEPES, 5 Mg-ATP, pH 7.4 (adjusted with KOH). The data were acquired and analyzed using a commercially available amplifier (Axopatch 200A, Axon Instruments, Foster City, CA, USA) and pCLAMP10 software (Axon Instruments). To evaluate PIP2 sensitivity of Kv7.2 A317T mutant, 100 micromolar dic8- PIP2 was added to the intracellular solution.

To generate current/voltage curves, cells were held at -80 mV, then depolarized for 1.5 s from -120 mV or from -80 mV to +20 or to +40 mV in 10 mV increments, followed by an isopotential pulse at 0 mV (Fig …). Current values recorded at the beginning of the 0 mV pulse were measured, normalized, and expressed as a function of the preceding voltage. The data obtained were then fit to a Boltzmann distribution of the following form (equation 1):

$$y = \max/[1 + \exp\,(V_{1/2} - V)/k] \qquad [1]$$

where V is the test potential, V½ the half-activation potential, and k the slope factor.

For noise analysis, 100 pulses of 500-ms duration were applied to a test voltage of 20 mV from the holding potential of −80 mV at 1 Hz frequency. Currents were low-pass filtered at 10 kHz and sampled at 100 kHz. Nonstationary noise analysis was performed according to the method of Heinemann and Conti. Variance was obtained by averaging the squared difference of consecutive records after appropriate scaling. Baseline variance was subtracted, and the variance-mean plot was fitted by the equation (equation 2):

$$\sigma^2 = \mathrm{i} < I > - \frac{< I >^2}{N} \qquad [2]$$

where σ^2 is the variance and $< I >$ is the mean current and with the free parameters i (single-channel current) and N (number of channels), without weighting points by their standard errors. The maximal open probability was calculated as $P_{\max} = < I >_{\mathrm{peak}}/(N\mathrm{i})$.

The GePulse program and the Ana program (http://users.ge.ibf.cnr.it/pusch/programs-mik.htm) were used, respectively, for data acquisition and analysis.

A stock solution (10 mM) of amitriptyline (Sigma-Aldrich, Germany) was prepared in dimethyl sulfoxide (DMSO); extracellular solution was used for subsequent drug dilutions.

Statistical significance was assessed using two-tailed unpaired Student's t test, and the threshold was set at $p < 0.05$. Errors are reported as standard errors.

3.6 MODELLING AND SIMULATIONS OF THE Kv7.2 CHANNEL WITH A STARTING CLOSED ACTIVATION GATE

To model the Kv7.2 pore with a closed activation gate (AG), we used the cryo-EM structure of the human Kv7.2 channel (PDB ID: 7CR0, apo-state) (Li et. al., 2021), characterized by a short diagonal atom-to-atom distance of ∼ 4-6 Å at the IG. The segment of each subunit defining the transmembrane pore domain (residues G215 to E330) was retained for MD simulations, while the VSDs were removed to reduce the size of the system. The CHARMM-GUI Membrane Builder server was used to prepare all necessary files for the simulations. Each of the three Kv7.2 structures was inserted in a homogeneous lipid patch of 1-palmitoyl-2-oleoyl-sn-glycero-3-phosphocholine (POPC) membrane environment and solvated with explicit water molecules. The total charge was neutralized with a 150 mM KCl solution, obtaining around 155, 000 atoms in total. In these MD simulations we used the NAMD software (Philips et. al., 2005) and the CHARMM36 (Best et. al., 2012; Huang et. al., 2013; Klauda et. al., 2010) force field for proteins and lipids, along with the CHARMM-modified TIP3P model for water molecules (Jorgensen et. al., 1983). CHARMM-compatible ionic parameters with NBFIX corrections were employed (Noskov and Roux, 2008; Luo and Roux, 2010; Venable et. al., 2013) Tetragonal periodic boundary conditions (PBCs) were applied to the simulation box to remove surface effects, and the Particle Mesh Ewald (PME) method was used to calculate long range electrostatic interactions (Steinbach et. al., 1994). Short-range electrostatic and van der Waals interactions were calculated with a 12 Å cutoff of and by applying a smooth decaying function starting to take effect at 10 Å. The CHARMM force-based switching function was employed for van der Waals interactions via the vdwForceSwitching command (Steinbach et. al., 1994). The SHAKE algorithm (Ryckaert et. al., 1977) was used to constrain covalent bonds involving hydrogen atoms (except for water molecules, where SETTLE was used) (Miyamoto et. al., 1992), allowing for an integration time step Δt=2 fs. To ensure maximum accuracy, electrostatic and van der Waals interactions were computed at each simulation step. Before production, as already done in previous works (Alberini et. al., 2021; Alberini et. al., 2023), all systems were relaxed with a ∼30 ns equilibration extending the CHARMM-GUI equilibration protocol, allowing proper hydration of solvent exposed regions of the pore cavity. Then, five statistically independent replicates of each system were simulated for 500 ns each in the NPT ensemble.

Electrostatic and van der Waals interactions were calculated with a cutoff of 12 Å and the application of a smoothing decay starting to take effect at 10 Å (Balusek et. al., 2019).

3.7 MODELING AND SIMULATIONS OF THE Kv7.2 CHANNEL WITH A STARTING OPEN ACTIVATION GATE

In the absence of an experimental structure of Kv7.2 with an open AG, we relied on homology modeling using the open human Kv7.1 (hKv7.1, PDB ID: 6V01) as a template. Our model comprises only the pore transmembrane (TM) domain (residues G215 to E330), and was constructed in two steps following a procedure similar to (Alberini et. al., 2021; Alberini et. al., 2023; Nay et. al., 2018). First, we modeled each of the four TM segments separately, using the structure prediction method included in the SWISS MODEL server (Waterhouse et. al., 2018). Then, the Kv7.2 pore domain was assembled by structurally aligning the four subunits to the template in a clockwise order viewed from extracellular side, using UCSF Chimera (Pettersen et. al., 2004). Before MD simulations, all the systems were oriented within the membrane using the OPM-PPM server (Lomize et. al., 2012). After the standard CHARMM-GUI equilibration, an additional 30 ns-long equilibration was performed with positional restraints on the protein and on the membrane atoms. At this point, to avoid the sudden occlusion of the IG, a specific equilibration procedure was designed: three independent replicates of the system were further simulated for 500 ns each by applying a set of harmonic restraints on the atomic distances between pairs of Cα atoms of residues G313 and A317 from diagonally opposed subunits, and then for 100 ns completely unrestrained. At the end of these simulations, the gate was stably open, and the final conformations were used as starting structures for five 500 ns-long MD simulations of each of the WT, G313S or A317T channel.

The pore radius of each structure was calculated using the HOLE program (Smart, 1996; Smart et. al., 1997). For replicated trajectories, average and standard deviations values were obtained from aggregating the five 500 ns-long runs and taking a snapshot every 50 ns. The structures were aligned to the starting conformation using the backbone atoms and excluding the terminal residues from 325 to 330 in each chain. The first 150 ns of each closed system were removed from the analysis to allow time for a stable hydration of the pore.

For all the HOLE calculations, AMBER van der Waals radii were adopted with a cutoff of 6 Å.

The hydration state of the different Kv7.2 pores was determined by calculating the number of water molecules along the pore axis during MD simulations. The pore axis, aligned along the z-axis, was divided into 20 intervals of 2.5 Å to map an interval of 50 Å comprising the whole cavity. In each interval, the average number of water molecules and standard deviations were calculated using VMD and Tcl scripting (Humphrey et. al., 1996). As for the pore radii calculations, the first 150 ns of each closed AG system were discarded. For replicated trajectories, the mean and standard deviation were extracted from the concatenated runs.

To monitor the conformational changes of the channel cavity during MD simulations, we calculated cross-distances between Cα atoms of pairs of diagonally opposed monomers across the pore. We used the G279 Cα atoms for the distance d1 in the SF, and the G313S and A317T Cα atoms for distances d2 and d3.

The hydrogen bond (HB) analysis in the A317T mutant was performed using VMD. HBs were defined with a cut-off distance between the heavy atoms covalently bound to a hydrogen atom of 3.3 Å, and an angle defined by the heavy atoms and the central hydrogen atom comprised between 130° and 230°.

Molecular graphics and further analysis were performed with UCSF ChimeraX (Goddard et. al., 2018; Pettersen et. al., 2021; Meng et. al., 2023), developed by the Resource for Biocomputing, Visualization, and Informatics at the University of California, San Francisco.

4. RESULTS

4.1 CLINICAL FEATURES OF THE PATIENTS

Following is the detailed clinical description of the six patients reported in this work:

Patient 1.This 10-y-old boy is the first child of unrelated parents of French origin. He was born at 37 weeks of pregnancy+5 d, with normal neonatal measures. He had plagiocephaly. Since the first months of life, he had global hypotonia. Sitting position was acquired at 1 y. At 15th month of life, he experienced several clusters of focal seizures with hypertonia of the left upper arm or of the four limbs, left deviation of the head, staring, and short loss of consciousness. Seizures were not induced by fever. Neurological examination was normal except for the global, previously known, hypotonia but with no psychomotor regression. Interictal EEG recording showed background slowing with diffuse spike waves and diphasic spikes. During drowsiness, high-amplitude spikes became multifocal. He was treated with valproate and clobazam. Brain MRI showed white matter thinning and a voluminous left temporal arachnoid cyst. Video-EEG recording showed sparse left centrotemporal spikes. A seizure was recorded, consisting of bilateral arm extension with predominance on the right side, associated with fast rhythm in the left central parietal region and with postictal slowing in the same region. The patient was operated by kysto-peritoneal derivation. Seizure frequency remained variable, up to several episodes in the same day and with periods of 2 weeks without seizures. Valproate was sequentially associated with other drugs (levetiracetam, carbamazepine, rufinamide, topiramate, vigabatrin, lamotrigine, and zonisamide) and corticosteroids. The best control was obtained with association of valproate with rufinamide and clonazepam, with multiyear seizure control. At the age of 6, lymphoblastic leukemia was diagnosed and treated with methotrexate and mercaptopurine. Currently, the child is still not walking and shows stereotypical movements, no autonomy in everyday life, and very limited language because of a severe ID. Karyotype, array comparative genomic hybridization (Array-CGH), fragile-X expansion study, and metabolic screening including very long-chain fatty acid, thyroid hormones, blood amino acid, urine organic acid, blood lactate and pyruvate, ammonemia, and Western blotting of the transferrin isoforms were normal. Trio-based exome sequencing (including DNA from the patient and unaffected parents) showed a *de novo* heterozygous

transition of *KCNQ5*: Chr6(GrCh37):g.7382 or 1040G>A,NM_001160133.1:c.1039G>A, predicted to replace a glycine (G) with a serine (S), p.G347S. *In silico* predictions (sorting intolerant from tolerant or SIFT, Polyphen-2, MutationTaster) were in favor of a deleterious effect. The combined annotation dependent depletion (CADD) score was 32. The variant was absent from the Genome Aggregation Database (gnomAD) of control individuals.

Patient 2. The patient is a 15-y-old girl, born to healthy non-related parents. She was born at term with normal growth. She walked at 18 mo and had speech delay. At the last referral at 13 years old, she had moderate to severe ID. She had mild behavioral issues with autistic features. Height was on2SD,weighton1SD,and occipitofrontal circumference (OFC) on+0.5 SD. Upon examination, she had a low hanging columella, enlarged naris, and hypertrichosis on the backside and on the arms. She also presented a pyramidal and an extrapyramidal syndrome. Initial head MRI and EEG studies around age 8 y were normal. A panel of 482 genes for neurodevelopmental disorders was performed in trio and showed a de novo heterozygous alteration in *KCNQ5* Chr6(GrCh37):g.7382 or 1041G>C NM_001160133.1:c.1040G>C, leading to the substitution of the amino acid glycine with an alanine (A), p.G347A. *In silico* predictions (SIFT, Polyphen-2, MutationTaster) were in favor of a deleterious effect. The CADD score was 26.7. The variant was absent from the gnomAD data-base of control individuals.

Patient 3. This is a male 3 years 4 months old with autism spectrum disorder, global developmental delay and no seizures. A gene-panel for monogenic epilepsies revealed a *de novo* heterozygous mutation in *KCNQ2* (c.949G>A; p.Ala317Thr). *In silico* predictions (SIFT, Polyphen-2, MutationTaster) were in favour of a deleterious effect. The variant was absent from the gnomAD database of control individuals.

Patient 4 The mutation c.937G>A (G313R) was found in *KCNQ2* gene in a patient with early-onset epileptic encephalopathy and bust suppression, reported in Olson et. al., 2017 (Patient 9). Seizures occurred at the second day after birth and the patient died at the third month of life.

Patient 5 The mutation *KCNQ2* L318V (c.952C>G) was reported in Gong et. al., 2021 (Case 6). That patient is a male patient of 4,3 years old. He reported spasms with onset at the 5th month and epileptiform discharges. He was seizure-free since the 10th month, when the seizures were controlled by adrenocorticotrophic

hormone. The EEG normalized between 12 and 22 months of life. Epileptiform discharges in the Rolandic region occurred at the age of 22 months and evolved into epileptic encephalopathy with electrical status epilepticus during sleep (ESES) at 27 months without seizures. That patient also showed hypsarrhythmia, psychomotor and developmental regression, language delay and impairment of fine motor skills. He also reported agenesis of the corpus callosum and pathologic jaundice.

Patient 6 The third variant is in *KCNQ3* gene and is leading the A356T substitution (c.1066C>T), corresponding to A317T in Kv7.2, that was identified in a large cohort of patient with ID; the patient described is a female with severe ID, abnormal repetitive mannerisms, absent speech, autistic behavior and no seizures (Deciphering Developmental Disorders Study, 2017; Satterstrom et. al., 2020).

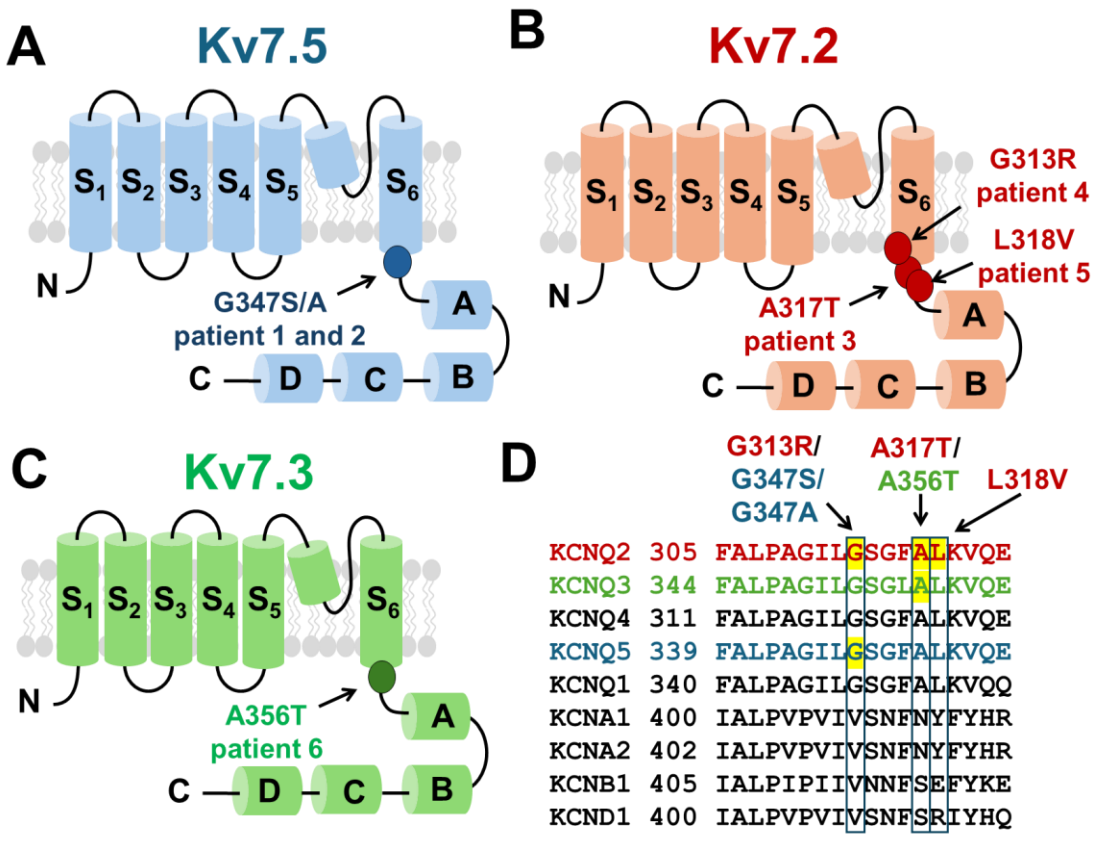

***Figure R1**: Topological representation of mutations found in patients. Figure is showing the location of (A) G347S, G347A variants in Kv7.5 found respectively in patient 1 and 2, (B) A317T, G313R and L318V found respectively in patient 3, 4 and 5 and (C) A356T variant topological location, found in patient 6. (D) Alignment of the bottom part of S6 in Kv7 and others Kv channels; The amino acids highlighted in yellow are the mutated ones, and the inscriptions show the amino acid substitution.*

4.2 CHARACTERIZATION OF Kv7.5 G347S VARIANT IN HOMOMERIC AND HETEROMERIC CONFIGURATION AND OF THE CORRESPONDING MUTATIONS IN Kv7.2 (G313S)

The patients 1 and patient 2 carried two *KCNQ5* variants affecting the first glycine (G347) within the -GSG- motif localized at the distal end of the S6 transmembrane segment of Kv7.5 subunits. In this context, G347 is denoted as G1, with the corresponding variants designated as G1S and G1A (refer to Fig. R1A, B).This region is highly conserved among Kv7 channels and represents the narrow part of the pore domain (Sun and MacKinnon 2017).

Kv7.5 channels expressed in cells exhibited small voltage-dependent K^+-selective currents, activating around -60/-50 mV with a relatively slow time course of activation (Fig. R1C). At a holding voltage of -80 mV, Kv7.5 channels remained closed. Replacement of the G1 residue with serine (Kv7.5 G1S) or alanine (Kv7.5 G1A) led to a more than 10-fold increase in the currents carried by Kv7.5 channels (observe Fig. R1C, D). Boltzmann analysis demonstrated a hyperpolarization of 13 and 9 mV in the $V_{½}$ of the voltage-dependent component in Kv7.5 G1S and Kv7.5 G1A channels, respectively (Fig. R1E). Notably, in both Kv7.5 G1S and Kv7.5 G1A channels, a significant proportion remained open even at highly hyperpolarized membrane potential values (-120 mV) (Fig. R1E, Table R1). Therefore, to quantify the instantaneous tonic current, we measured the ratio between the currents measured at the beginning of the depolarization step (time indicated by A in Fig. R1F) and those at the end of the 0 mV depolarization (time indicated by B in Fig. R1F). In particular, A and B represent time points at which instantaneous and steady-state currents were measured (Figure R1F), respectively; (B − A)/B × 100 represents the fraction of voltage- and time-dependent current (I_{VDEP}); whereas the fraction of voltage-independent, instantaneous current (I_{INST}) was calculated as (A/B) × 100 (or 1 − I_{VDEP}).

In the Kv7.2 wild type channels, the I_{INST} was close to zero, whereas it represents almost 50% of the total current in both mutants. (Table R1).

These findings collectively suggest that G1S and G1A variants in Kv7.5 channels enhance maximal current density, hyperpolarize activation gating, and prevent the closure of a substantial fraction of channels, indicating a gain-of-function (GoF) *in vitro* phenotype.

The reversal potential (V_{rev}) estimated from tail current measurements after depolarization to +20 mV for Kv7.5, Kv7.5 G1S, or Kv7.5 G1A channels was

−76.2 ± 0.7, −76.6 ± 0.7, or −76.7 ± 0.8 mV (p>0.05 for both mutants when compared to wild-type Kv7.5 channels).

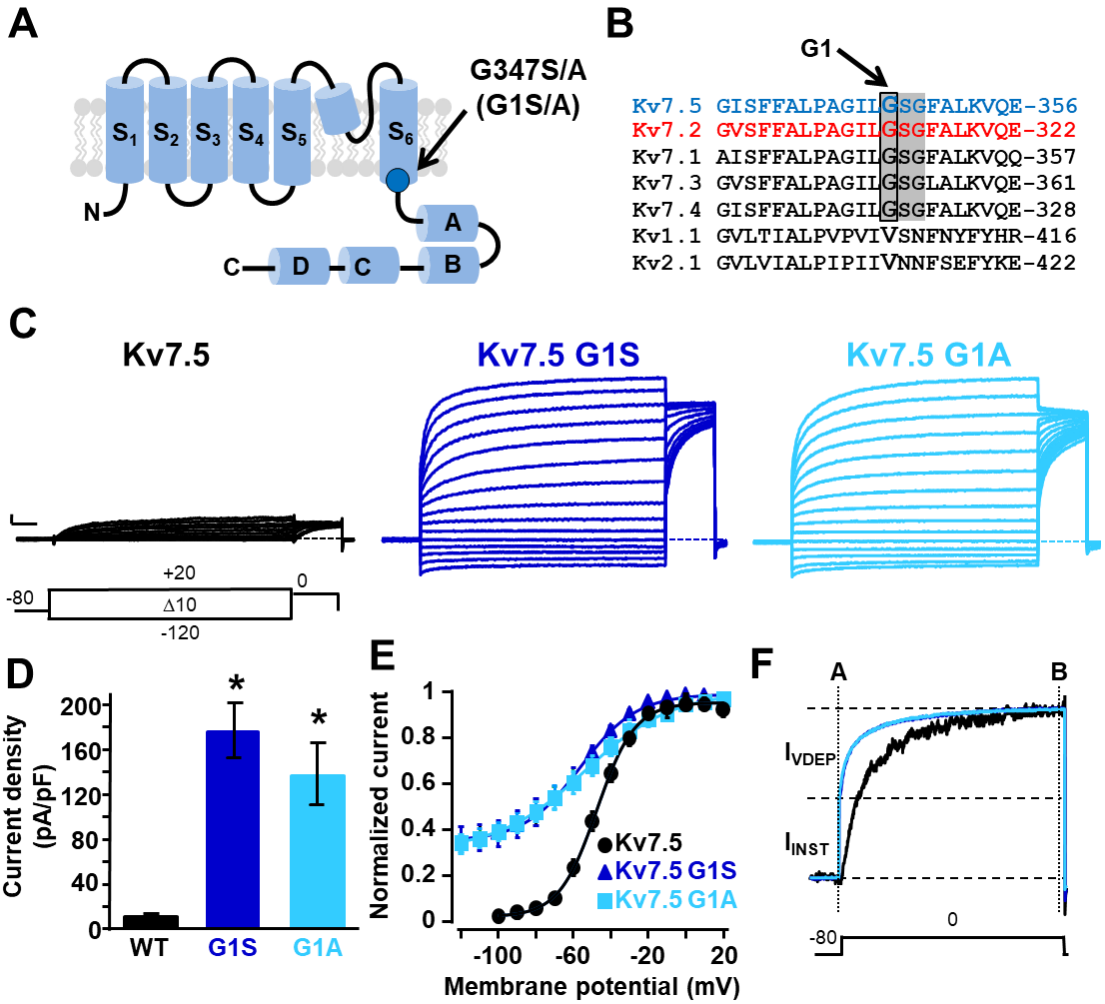

***Figure R1**: Functional characterization of homomeric Kv7.5 G1S and G1A variants. (A) Topological representation of G1 amino acid into Kv7 subunit; (B) Alignment of Kv7 and other Kv channels (https://www.ebi.ac.uk/Tools/psa/), showing -GSG- motif into the shaded region and G1 conservation, indicated by the arrow and the box, among Kv7 channels. (C) Current responses to the reported membrane depolarization protocol of Kv7.5 (Black), Kv7.5 G1S (Dark blue) and Kv7.5 G1A (Light blue) homomeric channels. (D) Normalized current densities. Statistical significance (see methods) are indicated by the asterisk. (E) Conductance to voltage curves from Kv7.5, Kv7.5 G1S and Kv7.5 G1A. Continuous lines are Boltzmann fits of the experimental data. (F) Instantaneous current at 0 mV are indicated as "I_{INST}", and voltage dependent current are indicated as "I_{VDEP}".*

To determine if the instantaneous current corresponds to a potassium current, experiments were conducted using rapid voltage ramps at hyperpolarized voltages, following a methodology previously described for Kv7.1 channels exhibiting similar functional characteristics (Boulet et. al., 2007). The findings indicated a shift in the reversal potential (V_{rev}) from -80.7 ± 1.0 to -58.6 ± 1.3 mV

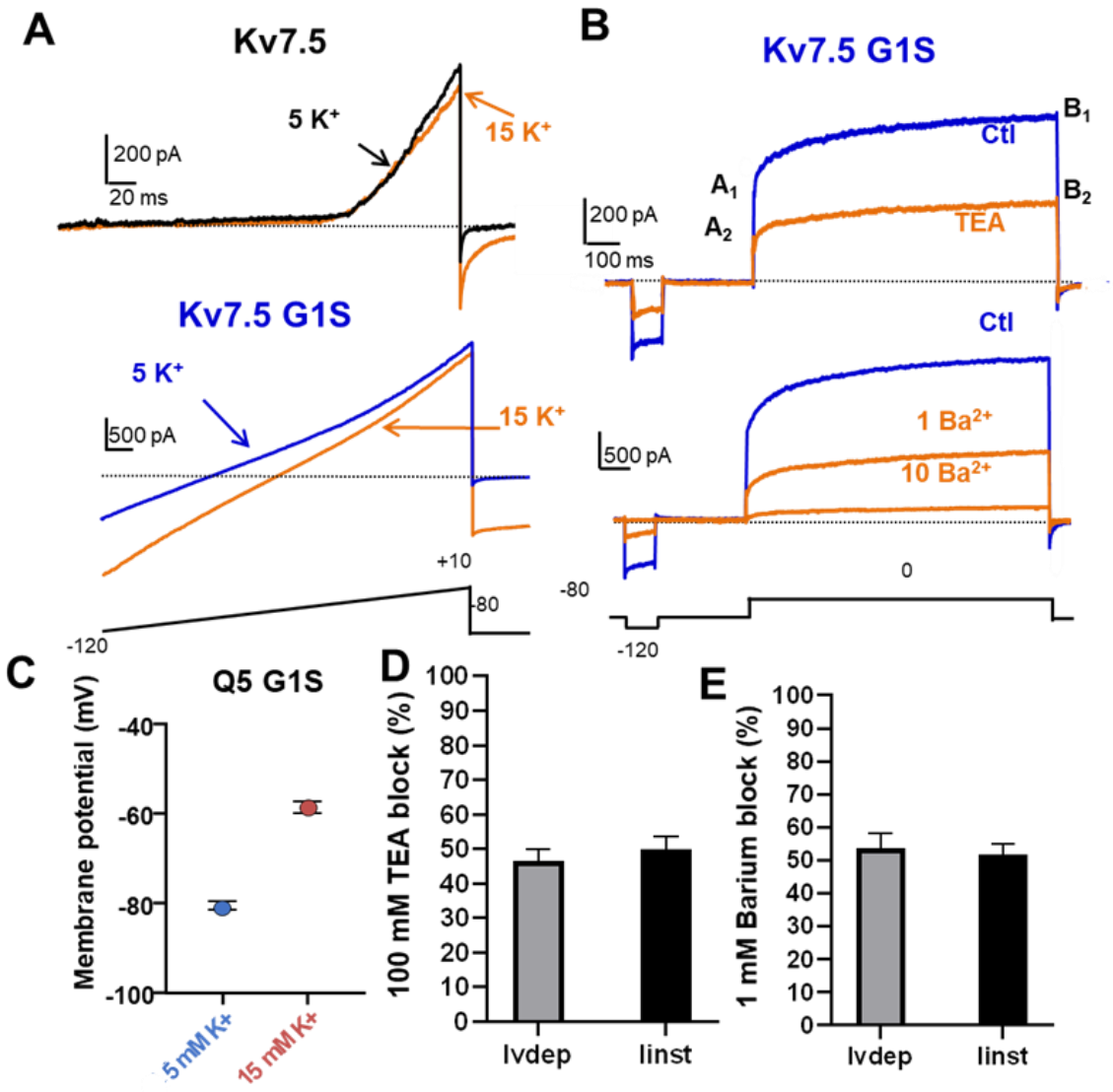

***Figure R2**: Functional characterization of Kv7.5 G1S instantaneous current component. (A) Ramp currents from Kv7.5 and Kv7.5 G1S channels using the voltage protocol shown at the bottom in 5 and 15 mM extracellular K+ ions. (B) Effect of extracellular 100 mM TEA (Upper) or 1 to 10 mM Ba2+e (Lower) on Kv7.5 G1S currents recorded with the voltage protocol shown at the bottom. Instantaneous currents are measured as described before, with A2 and B2 referring to the treated condition (C) Reversal potential for Kv7.5-mediated currents in corresponding potassium extracellular concentration. (D, E) Comparison of percentage of block for instantaneous and voltage-dependent component by 100 mM extracellular TEA and 1 mM Barium.*

upon transitioning from an extracellular solution containing 5 mM K+ to one with 15 mM K+ (Fig. R2A, C). These values closely resembles the expected shift in the Nernst potential for a K^+-selective current.

Additionally, both I_{INST} and I_{VDEP} exhibited comparable sensitivity to block by extracellularly applied tetraethylammonium (TEA_e; 100 mM) or barium (Ba^{2+}_e; 1 to 10 mM) ions at depolarizing potentials. Remarkably, consistent blocking percentages were observed at -120 mV, a membrane potential where currents are primarily carried by I_{INST}, with 100 mM TEA_e, 1 mM Ba^{2+}_e, and 10 mM Ba^{2+}_e

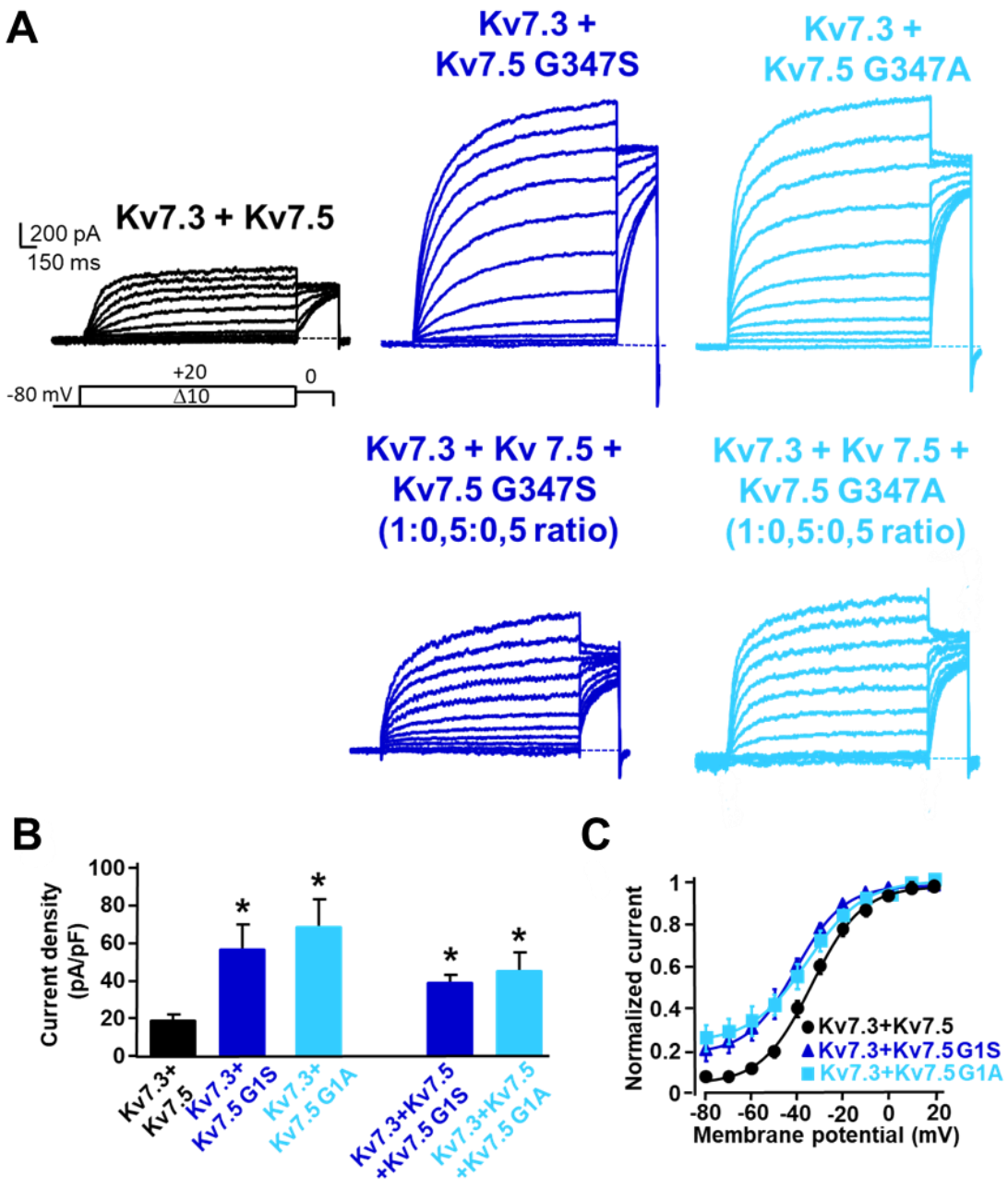

***Figure R3**: Functional characterization of Kv7.3/Kv7.5 G1S and Kv7.3/Kv7.5 G1A heteromeric channel properties. (A) Macroscopic currents recorded in CHO cells transfected with reported Kv7.3/Kv7.5 cDNA constructs ratio. (B) Quantification of current densities recorded from cells transfected with the indicated cDNA constructs. Asterisks indicate values significantly different (*p < 0.05) from their respective control (Kv7.3 + Kv7.5). (C) Conductance/voltage curves for the currents recorded from cells transfected with the indicated cDNA constructs. Continuous lines are Boltzmann fits of the experimental data.*

showing blockages of 51.1 ± 3.0, 59.8 ± 3.2, and 86.4 ± 4.5%, respectively ($p > 0.05$). All these findings provide strong support that both I_{INST} and I_{VDEP} currents were carried through the same pore domain. Kv7.5 can form heteromeric channels with Kv7.3 subunits (Lerche et. al., 2000; Schroeder et. al., 200); therefore, in the next experiments the cDNA encoding for Kv7.5 G1S or Kv7.5 G1A subunits were cotransfected with Kv7.3 or a combination of Kv7.3 and Kv7.5 cDNAs. CHO cells transfected with Kv7.3+Kv7.5 G1S or Kv7.3+Kv7.5 G1A plasmids (cDNA ratio 1:1), displayed a remarkable three-fold increase in maximum current density compared to those transfected with Kv7.3+Kv7.5 (Fig. R3A, B, Table R1) and with the presence of a voltage-independent current component, constituting approximately 20% at -80 mV. The depolarization-activated component in cells expressing G1S or G1A mutant subunits exhibited a small but statistically significant hyperpolarizing shift of $V_{½}$ (Table R1).

To mimic the genetic balance of a heterozygous individual with a mutant *KCNQ5* allele, CHO cells were co-transfected with Kv7.3+Kv7.5+Kv7.5 G1S or Kv7.3+Kv7.5+Kv7.5 G1A at a 1:0.5:0.5 cDNA ratio. Under these conditions, cells expressing Kv7.3+Kv7.5+Kv7.5 G1S or Kv7.3+Kv7.5+ Kv7.5 G1A exhibited a two-fold increase in current density compared to those expressing Kv7.3/Kv7.5 (Fig. R3B). However, in Kv7.3 + Kv7.5 + Kv7.5 G1S- or Kv7.3+Kv7.5+Kv7.5 G1A-

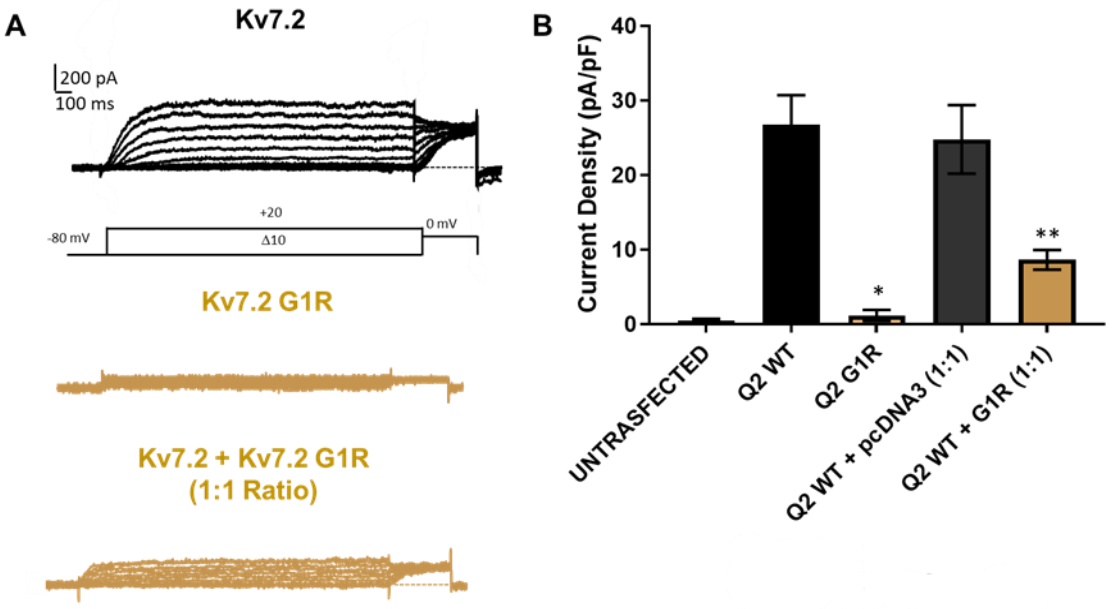

***Figure R4**: Functional characterization of Kv7.2 G1R variant (A) Macroscopic currents recorded with reported cDNA constructs ratio in CHO transfected cells. (B) Quantification of current densities recorded from cells transfected with the indicated cDNA constructs. Single asterisks indicate values significantly different (*p < 0.05) from Kv7.2 wild-type and double asterisks (**) report significant values when compared with Kv7.2 + pcDNA (1:1).*

transfected cells no discernible difference in the fraction of I_{INST} or $V_{½}$ could be detected when compared with Kv7.3+Kv7.5 (Table R1).

Interestingly mutation at a paralogous position (G313, or G1) in Kv7.2 (patient 4 in Table A1) was reported by Olson et al. in 2017 in a patient with DEE (G313R or G1R). When expressed in CHO cells, homomeric Kv7.2 G1R mutant channels were no functional (Fig. R4A, B).

Furthermore, when the Kv7.2 G1R subunit was co-expressed with the wild-type subunit in a 1:1 ratio, it exhibited less than half the current compared to cells transfected with Kv7.2 and an empty vector in the same ratio. This observation indicates that the variant exerts a dominant-negative effect on the function of the wild-type channel, as shown in Fig. R4A, B. These results strongly indicate that the G1R variant, like most other Kv7.2 variants associated with the classical *KCNQ2*-DEE phenotype, caused significant dominant-negative loss-of-function (LoF) effects *in vivo*. To investigate whether the contrasting *in vitro* phenotypes were attributed to specific amino acid substitutions within the G1 region or the Kv7 subunit context (Kv7.2 vs. Kv7.5), we introduced the G1R variant into Kv7.5 and the G1S substitution into Kv7.2. The examination of natural variants between these two channels revealed that the substitution of G1S in Kv7.2 led to a more than 10-fold increase in current density. This substitution also triggered the emergence of a voltage-independent component, constituting approximately 20% of the total current, along with a leftward shift of the $V_{½}$ of the voltage-dependent component by 40 mV (refer to Fig. R5A, C, D). In contrast, the Kv7.5 G1R substitution completely abolished channel function, as evident in Fig. R5B. Likewise, the G1E substitution rendered both Kv7.5 and Kv7.2 channels non-functional (see Fig. R5A, B, C). This observation implies that the unique GoF effect resulting from the replacement of G by S residue cannot be replicated by introducing large, positively or negatively charged side chains such as those provided by residues R or E, respectively.

These findings indicate that the replacement of the first G residue within the GSG motif with S residues (GoF) or R or E residues (Loss-of-Function, LoF) introduces qualitatively similar functional consequences into both Kv7.2 and Kv7.5 subunits,

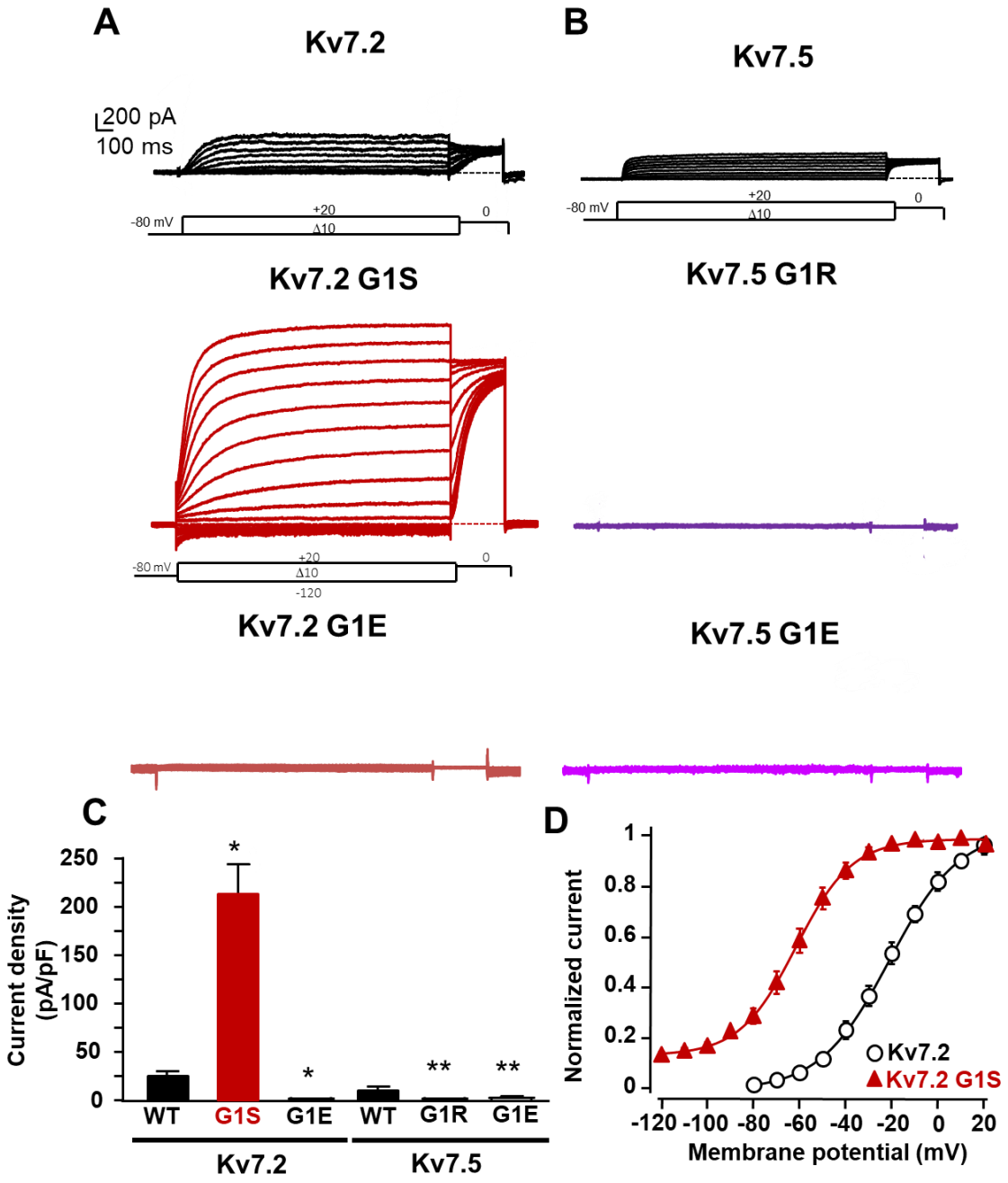

***Figure R5**: Functional characterization of non-natural variants in Kv7.2 and Kv7.5, that have not been identified in patients (A) Macroscopic currents recorded from Kv7.2, Kv7.2 G1S and Kv7.2 G1E. (B) Macroscopic currents recorded from Kv7.5, Kv7.5 G1R and Kv7.5 G1E. (C) Quantification of current densities recorded from cells transfected with the indicated cDNA constructs. Single asterisks indicate values significantly different (*p < 0.05) from Kv7.2 wild-type and double asterisks (**) report significant values when compared with Kv7.5. (D) Conductance/voltage curves for the currents recorded from cells transfected with Kv7.2 and Kv7.2 G1S constructs. Continuous lines are Boltzmann fits of the experimental data.*

suggesting that the length of the amino acid side chain can have a determinant impact in the functional phenotype of both Kv7.2 and Kv7.5.

Construct(s)	Amount cDNA (μg)	n	V1/2 (mV)	K (mV/e-fold)	I_{INST} at 0 mV (%)	Current density at 0 mV (pA/pF)
Untransfected		5	–	–	–	0.5 ± 0.2
Kv7.5	3	25	−42.0 ± 2.1	10.4 ± 0.9	3 ± 1	11.6 ± 2.0
Kv7.5 G1S	3	14	−54.8 ± 2.5*	13.5 ± 0.5*	45 ± 4*	176.5 ± 24.5*
Kv7.5 G1A	3	14	−51.4 ± 2.0*	18.7 ± 2.3*	50 ± 2*	137.6 ± 27.6*
Kv7.5 G1R	3	7	–	–	–	0.3 ± 0.1*
Kv7.5 G1E	3	7	–	–	–	0.3 ± 0.04*
Kv7.3	3	9	−37.7 ± 1.1	7.0 ± 0.3	4 ± 2	20.2 ± 2.2
Kv7.3 + Kv7.5	1.5 + 1.5	30	−35.0 ± 0.9	10.2 ± 1.0	8 ± 1	18.8 ± 2.04
Kv7.3 + Kv7.5 G1S	1.5 + 1.5	18	−42.8 ± 14.0†	11.5 ± 1.4	19 ± 4†	57.3 ± 12.7†
Kv7.3 + Kv7.5 G1A	1.5 + 1.5	12	−39.1 ± 2.1†	15.4 ± 2.4	24 ± 3†	85.5 ± 21.8†
Kv7.3 + Kv7.5 + Kv7.5 G1S	1.5 + 0.75 + 0.75	12	−32.3 ± 2.0	16.7 ± 1.9†	11 ± 3	45.6 ± 9.6†
Kv7.3 + Kv7.5 + Kv7.5 G1A	1.5 + 0.75 + 0.75	14	−38.0 ± 1.7	10.2 ± 0.7	12 ± 3	41.9 ± 7.9†
Kv7.2	3	14	−25.6 ± 2.1	12.4 ± 0.8	4 ± 1	31.9 ± 4.0
Kv7.2 G1S	3	9	−59.9 ± 4.5‡	11.7 ± 0.4	27 ± 4‡	215.1 ± 28.7‡
Kv7.2 G1E	3	10	–	–	–	1.2 ± 0.3‡
Kv7.2 G1R	3	5	–	–	–	1.2 ± 0.8‡
Kv7.2 + Kv7.2 G1R	1.5 + 1.5	18	−28.0 ± 1.9	10.6 ± 0.8	–	8.7 ± 1.3‡

***Table R1**: Biophysical properties of Kv7.5 and Kv7.2 variants in homomeric and heteromeric configurations. Symbols report statistical signfiicance as following: * $p < 0.05$ versus Kv7.5. † $p < 0.05$ versus Kv7.3 + Kv7.5; ‡ $p < 0.05$ versus Kv7.2.*

4.3 CHARACTERIZATION OF Kv7.2 A317T AND L318V VARIANTS IN HOMOMERIC AND HETEROMERIC CONFIGURATION

The variant A317 is located at the distal end of the S6 segment of Kv7.2 channels (Fig. R6A). This mutation fall into the activation gate of the channel, a highly-

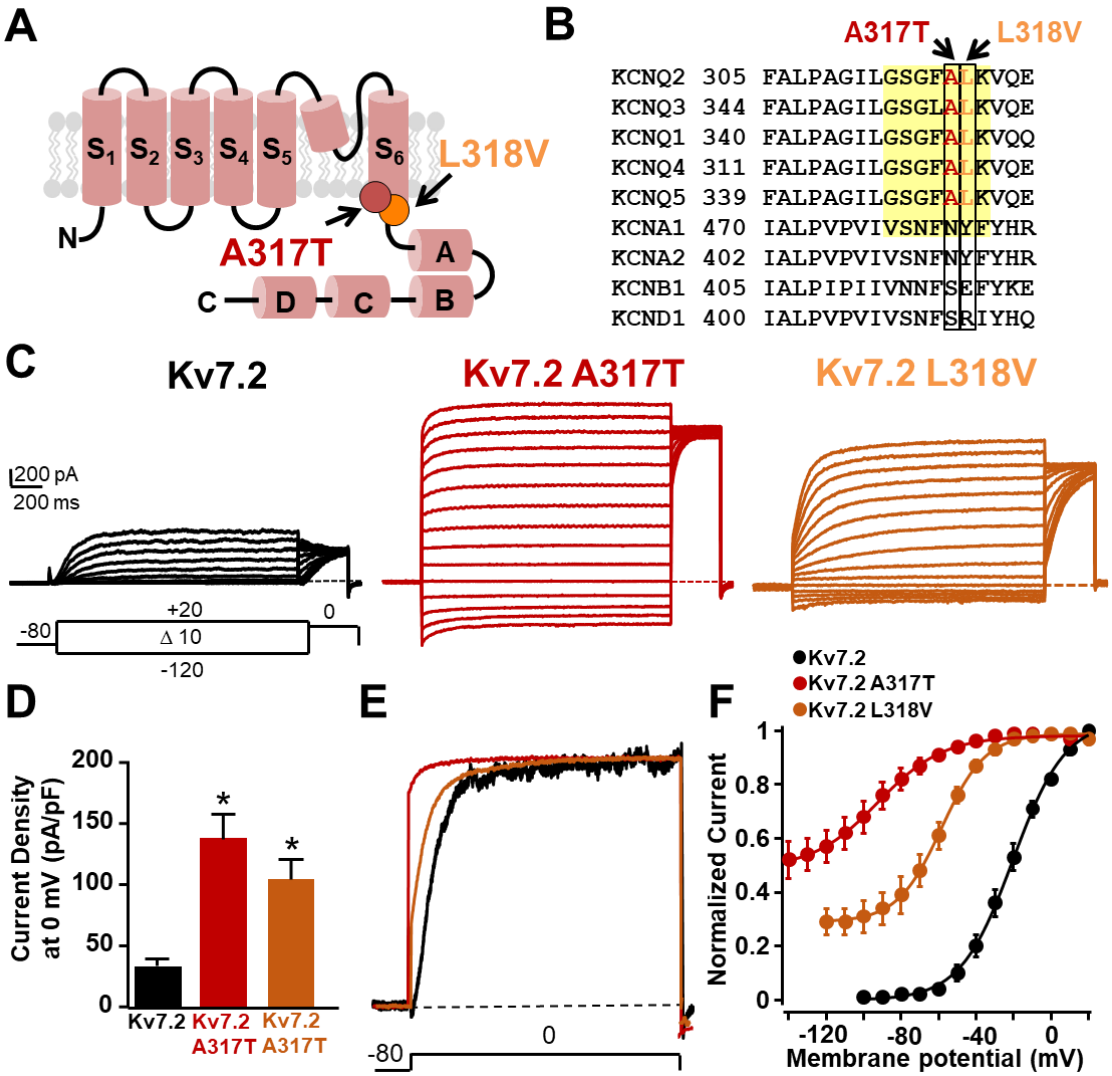

***Figure R6**: Functional characterization of Kv7.2 variants in homomeric configuration. (A) The topological location of A317T and L318V variants in the Kv7.2 subunit is illustrated. (B) Sequence alignment of the bottom part of the S6 segments of the indicated Kv subunits (https://www.ebi.ac.uk/Tools/psa/). The yellow region highlights the AG region in Kv7 members, with the A317T and L318V residues, and its paralogous counterparts in Kv channels indicated by the boxes. (C) Macroscopic currents from Kv7.2, Kv7.2 A317T, and Kv7.2 L318V homomeric channels are shown in response to the indicated voltage protocol. (D) Quantification of current densities recorded from cells transfected with the indicated cDNA constructs. Asterisks indicate values significantly different (*p<0.05) from Kv7.2. (E) Superimposed normalized current traces from Kv7.2 (black), Kv7.2 A317T (red), and Kv7.2 L318V (orange) homomeric channels are displayed. It is worth remarking on the time course of activation and the evident presence of tonic current at the beginning of the pulse. (F) Conductance/voltage curves for the indicated homomeric channels are provided, with continuous lines representing Boltzmann fits of the experimental data.*

conserved region across Kv7 channels recognized as the region that faces the most dramatic reorganizations during the opening of the pore (Fig. R6A,B). Within the same Kv7.2 AG, the variant L318V was identified in a patient with infantile spasms with hypsarrhythmia and without neonatal seizures (Patient 5 in Table A1, case 6 in Gong et. al., 2020). To evaluate the effect of the newly identified mutation (A317T) and the already described variant (L318V) on the channel function, homomeric Kv7.2, Kv7.2 A317T or Kv7.2 L318V were expressed on Chinese Hamster ovary (CHO) cells. Cells were stimulated by depolarizing potentials from -140/-120 mV to +20 mV in 10 mV incremental depolarizing pulses, and macroscopic current were recorded with the whole-cell configuration of the patch-clamp technique.

As shown in Figure R6C, cells expressing Kv7.2 channels generate a voltage-dependent K^+-selective current with current density, calculated at 0 mV, of 31.4 ± 4.5 pA/pF (Figure R6D, Table 1). These currents activate at around -50/-40 mV with a rather slow time course of activation and deactivation. $V_{½}$ and the slope of the I/V relationship (k) were -20.13±1.09 mV and 12.03 ± 0.49 mV/e-fold, respectively (Figure R6C, Table R2). At the holding voltage of -80 mV, the Kv7.2 channels were closed and the ratio between the currents calculated at the beginning of the depolarization step and those at the end of the 0 mV depolarization was close to 0 (Figure R6E, Table R2).

Both homomeric Kv7.2 A317T and Kv7.2 L318V mutant channels showed a significant increase of the maximal current by 3-4-fold, compared with Kv7.2 channels (Figure R6C, D, Table R2). Moreover, in both homomeric Kv7.2 A317T and Kv7.2 L318V channels, as already observed in Kv7.5 G1S/A variants, the activation process include two clearly-distinct components: an instantaneous voltage-independent one, followed by a slower voltage- and time-dependent component (Figure R6E and Table R2). The instantaneous voltage-independent components account for about 80% and 30% of the total current, for Kv7.2 A317T and Kv7.2 L318V respectively. Fitting I/V curves with Boltzmann equation (see Methods) showed that the $V_{½}$ of the voltage-dependent component in Kv7.2 A317T and Kv7.2 L318V channels was hyperpolarized by 70 mV and 40 mV (Fig. R6F), respectively. Despite such dramatic changes in voltage-dependent gating, both mutants channels retained their selectivity for K^+ ions; indeed, the reversal potential of the currents from Kv7.2, Kv7.2 A317T and Kv7.2 L318V channels was close to that of a K^+-selective pore (-75 mV in our experimental conditions).

Since the M-current in neurons are mainly formed by Kv7.2/Kv7.3 heteromeric channel, and to replicate *in vitro* the genetic combination occurring in the affected family members who are heterozygous for the pathogenic allele, functional studies were also carried out upon transfection of cDNAs of Kv7.2+Kv7.2A317T+Kv7.3 and Kv7.2+Kv7.2L318V+Kv7.3 at a cDNA ratio of 0.5:0.5:1 (Fig. R7A). In these conditions, there was a significant increase in 50% of current density (Fig. R7B) and a shift in voltage dependency in hyperpolarizing direction by 20 mV for both groups, when compared to Kv7.2+Kv7.3 heteromeric channels (Figure R7C). Overall, these results suggested that both A317T and L318V mutations enhanced maximal current density, both in homomeric and heteromeric configurations, increased current density, hyperpolarized activation gating and prevented closing of a significant fraction of channels, all effects being more dramatic in Kv7.2 A317T variant and consistent with a gain-of-function (GoF) *in vitro* phenotype.

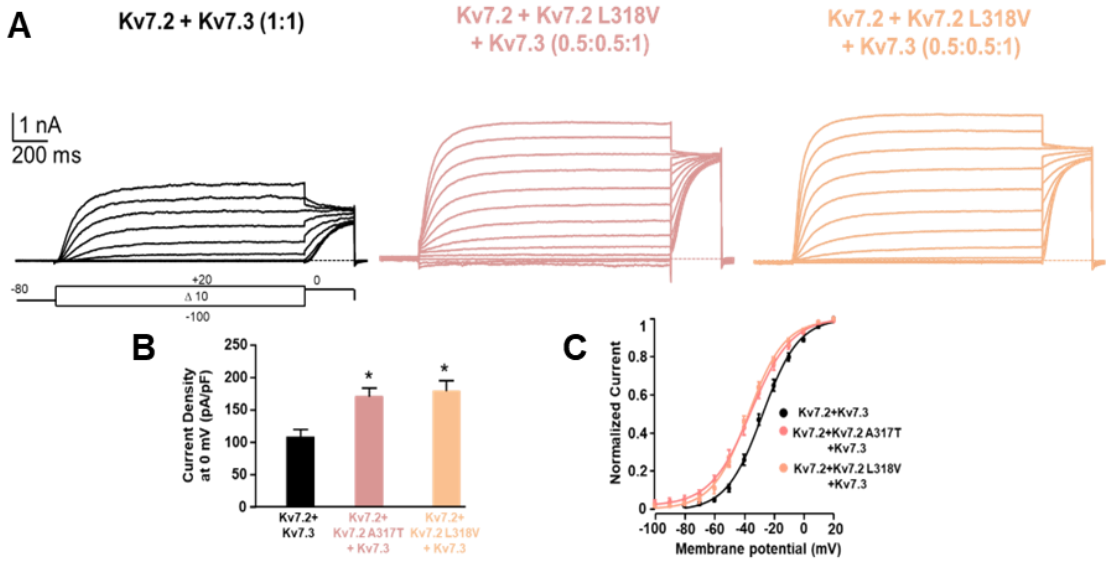

***Figure R7**: Functional characterization of Kv7.2 variants in heteromeric configuration (A) Macroscopic currents recorded from CHO cells transfected with indicated cDNA ratios in response to the indicated voltage protocol are shown. (B) Quantification of current densities recorded from cells transfected with the indicated cDNA constructs. Asterisks indicate values significantly different (*p<0.05) from Kv7.2+Kv7.3. (C) Conductance/voltage curves for the indicated heteromeric channels are provided, with continuous lines representing Boltzmann fits of the experimental data.*

4.4 CHARACTERIZATION OF Kv7.3 A356T VARIANT IN HOMOMERIC AND HETEROMERIC CONFIGURATION

The A317 residue in Kv7.2 corresponds to the A356 residue in highly homologous Kv7.3 (Fig. R6B); the Kv7.3 A356T variant has been described in a patient with severe ID, delayed language and no seizures (Patient 6 in table A1) (patient DDD4K.02558). However, no functional data is available for Kv7.3 channels carrying this variant. To understand the role of this residue in the biophysical properties of Kv7.3 channels, the functional properties of Kv7.3 A356T subunit channels were investigated. Heterologous expression of wild-type Kv7.3 subunits led to the appearance of small voltage-dependent K^+-selective currents with a density at 0 mV of 25.1±5.9 pA/pF. By contrast, homomeric Kv7.3 A356T mutant channels were not functional and the current density values were not statistically

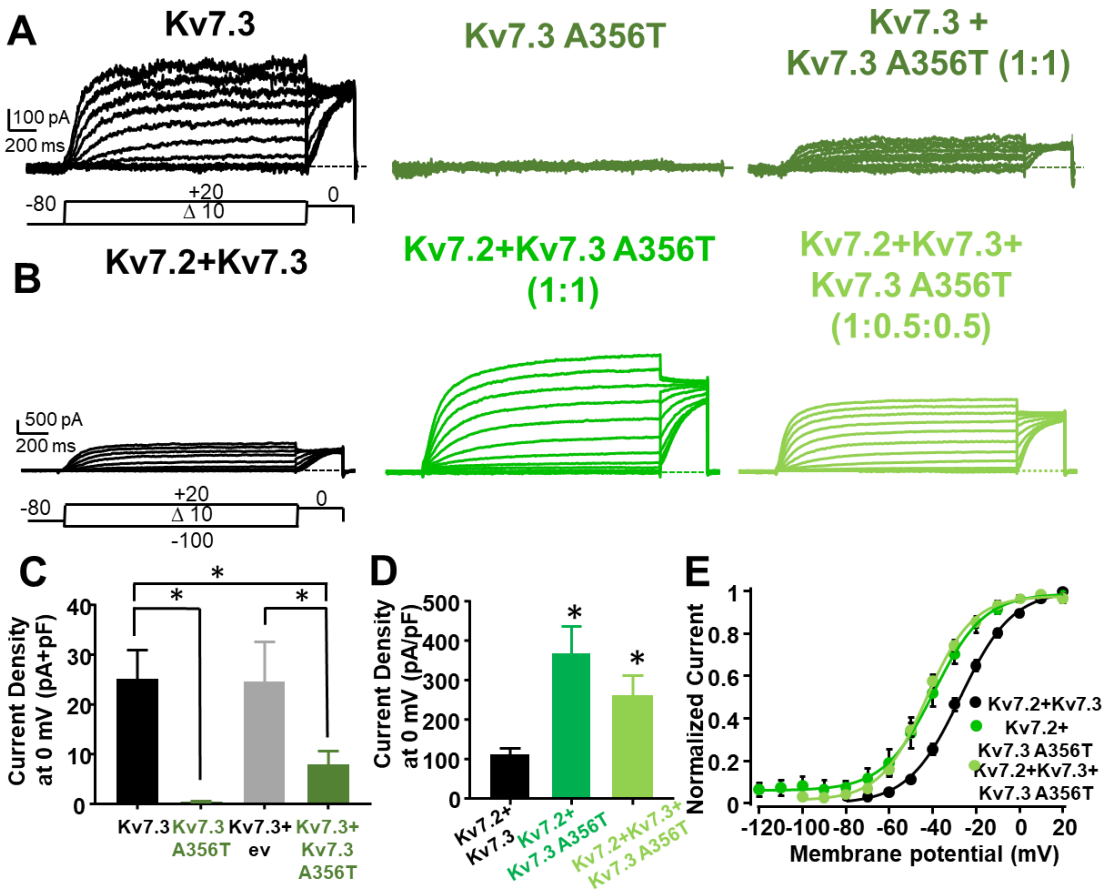

***Figure R8**: Functional characterization of Kv7.3 variants in both homomeric and heteromeric assemble. (A) Current traces from Kv7.3, Kv7.3 A356T and Kv7.3 co-expressed with A356T cDNA at 1:1 ratio. (B) Current traces of heteromeric configurations containing Kv7.3 A356T mutation at different ratios. (C, D) Quantification of current densities recorded from cells transfected with the indicated cDNA constructs. Asterisks indicate values significantly different (* $p < 0.05$) from their respective control. (E) Conductance/voltage curves for the indicated homomeric and heteromeric channels are shown, with continuous lines representing Boltzmann fits of the experimental data.*

different from untransfected CHO cells (Figure R8A, B; Table R2). When Kv7.3 A356T mutant subunit was co-transfected with Kv7.3 in 1:1 ratio, a small current was recorded and the current density was significantly lower when compared with cells transfected with half amount of Kv7.3 cDNA (cells transfected with Kv7.3 plus empty vector at the same ratio 1:1), suggesting a possible dominant-negative effect (Figure R8A, C). Surprisingly, a completely opposite effect was observed when cells were co-transfected with Kv7.2+Kv7.3 A356T (1:1 ratio) or Kv7.2+Kv7.3+Kv7.3 A356T (0.5:0.5:1 ratio); indeed, a marked increase in current density by 3/4-times (Figure R8B, D) and a shift in voltage dependency in hyperpolarizing direction in 10 mV, when compared to Kv7.2+Kv7.3 was observed (Figure R8E). In contrast with the variant A317T in Kv7.2, the variant A356T in Kv7.3 displayed a more complex mechanism, showing a LoF effect in homomeric configuration and a GoF effect in heteromeric configuration.

	cDNA trasfection (µg)	n	$V_{½}$ (mV)	k	pA/pF at 0 mV	Iinst/Iss	% TEA block
Untransfected		5	-	-	0,50 ± 0,20		
Kv7.2	3	25	-20.13 ± 1.09	12,03 ± 0,49	31,44 ± 4.57	0.03 ± 0.01	55,43 ± 7,64 (0,3 mM, n=3)
Kv7.2 A317T	3	15	-92,93 ± 3.60*	13.60 ± 1.92	138.73 ± 20.30*	0.81 ± 0.04*	56,23 ± 3.38 (0,3 mM n=7)
Kv7.2 L318V	3	8	-58.29 ± 1.28*	11,94 ± 11.12	105.26 ± 16.64*	0.33 ± 0.03*	
Kv7.2 + Kv7.3	1,5 + 1,5	20	-27.38 ± 1.23	11,38 ± 0.61	109.08 ± 11.94	0.01 ± 0.003	50,77 ± 3.19 (3 mM n=9)
Kv7.2 + Kv7.2 A317T + Kv7.3	0.75 + 0.75 + 1,5	12	-36.74 ± 2.09†	13.09 ± 2.09	177.99 ± 25.04†	0.12 ± 0.03†	54,72 ± 2.24 (3 mM n=3)
Kv7.2 + Kv7.2 L318V + Kv7.3	0.75 + 0.75 + 1,5	12	-37.51 ± 1.40†	11.98 ± 0.78	200.42 ± 46.69†	0.04 ± 0.01	50,25 ± 5.83 (3 mM n=3)
Kv7.3	3	8	-31,08 ± 1,98	9.46 ± 1.17	25.08 ± 5.94		
Kv7.3 A356T	3	8	-	-	0.42 ± 0.12‡		
Kv7.3 + pcDNA3.1	1,5 + 1,5	6	-34.37 ± 2.34	6.75 ± 0.66	24.68 ± 7.84		
Kv7.3 + Kv7.3 A356T	1,5 + 1,5	8	-34.61 ± 1.23	6.54 ± 0.67	7.88 ± 2.68‡		
Kv7.2 + Kv7.3 A356T	1,5 + 1,5	9	-41.64 ± 3.26	11.98 ± 0.66	371.91 ± 64.95‡	0.08 ± 0.03‡	51.87 ± 4.10 (3 mM n=5)
Kv7.2 + Kv7.3 + Kv7.3 A356T	0.75 + 0.75 + 1,5	9	-44.02 ± 1.21	11.77 ± 1.23	261.60 ± 50.25‡	0.05 ± 0.01‡	49,25 ± 3.06 (3 mM n=7)

***Table R2**: Biophysical properties of Kv7.2 and Kv7.3 variants in homomeric and heteromeric configurations. Symbols report statistical signfiicance as following: * p < 0.05 versus Kv7.5. † p < 0.05 versus Kv7.3 + Kv7.5; ‡ p < 0.05 versus Kv7.2.*

4.5 CHARACTERIZATION OF SINGLE CHANNEL PROPERTIES OF Kv7.5 G347S, Kv7.2 G313S AND Kv7.2 L318V VARIANTS THROUGH NOISE ANALYSIS

The most notable effect of the G1S/A variants when incorporated into either Kv7.2 or Kv7.5 subunits and of the two variants A317T and L318V in Kv7.2 was a marked increase in macroscopic current density, which dependents on the following parameters: the number of functional channels (N), single-channel current (i), and channel opening probability (Po). Non-stationary noise analysis was employed to investigate variant-induced changes in each of these parameters. Figure R9A illustrates the average (top) and variance (bottom) of 100 pulses. Fitting the variance data with equation 2 revealed a 2.5/3-fold increase in maximal Po when the G1S variant was incorporated into Kv7.5 or Kv7.2 channels (refer to Fig. R9D), without altering membrane channel abundance or channel conductance (refer to Fig. R9B, C). These findings strongly suggest that the G1S

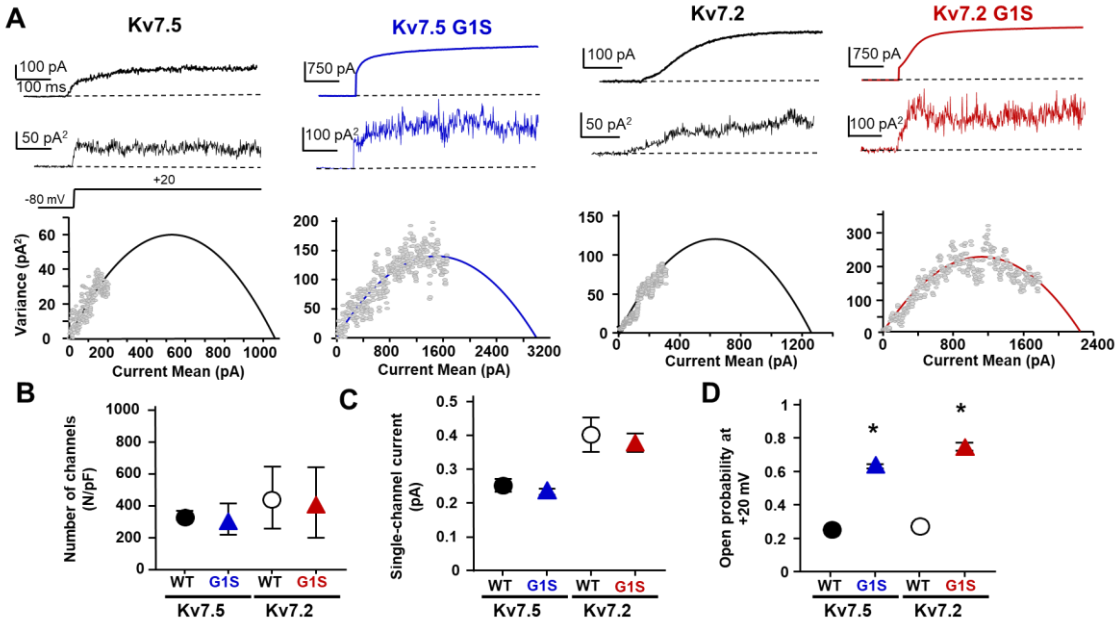

***Figure R9**: Nonstationary noise analysis of Kv7.5, Kv7.5 G1S, Kv7.2, and Kv7.2 G1S channels. (A) Representative average response to 100 pulses at +20 mV (Top), of the corresponding variance (Middle), and variance versus current mean plot (Bottom) from Kv7.5, Kv7.5 G1S, Kv7.2, and Kv7.2 G1S channels, as indicated. The continuous lines in Bottom are parabolic fits of the experimental data (Materials and Methods). Current and variance scales are 100 pA and 50 pA2 for Kv7.5, 750 pA and 100 pA2 for Kv7.5 G1S, 100 pA and 50 pA2 for Kv7.2, and 750 pA and 100 pA2 for Kv7.2 G1S. Time scale, 100 ms. Po and I estimates for the four cells shown were 0.18 and 0.20 for Kv7.5, 0.57 and 0.19 for Kv7.5 G1S, 0.25 and 0.38 for Kv7.2, and 0.79 and 0.39 for Kv7.2 G1S. (B–D) Quantification of the number of channels divided by capacitance (B), of the single-channel current (C), and (D) of the opening probability at +20 mV. Asterisks indicate values significantly different (*P < 0.05) from respective controls (Kv7.5 channels, Left; Kv7.2 channels, Right).*

substitution caused a significant increase in opening probability without affecting the number of functional channels or their conductance in both Kv7.2 and Kv7.5 subunits.

Similarly, non-stationary noise analysis were also performed for the two variants A317T and L318V in Kv7.2 For these experiments, currents from Kv7.2, Kv7.2 A317T and Kv7.2 L318V channels expressed in CHO cells were activated by 100 depolarizing pulses of 500 ms duration to +20 mV at a frequency of 1 Hz, after a 200 ms pre-pulse at -120 mV. Potential artifacts due to current rundown (<20%) were minimized by measuring the differences in the current on successive

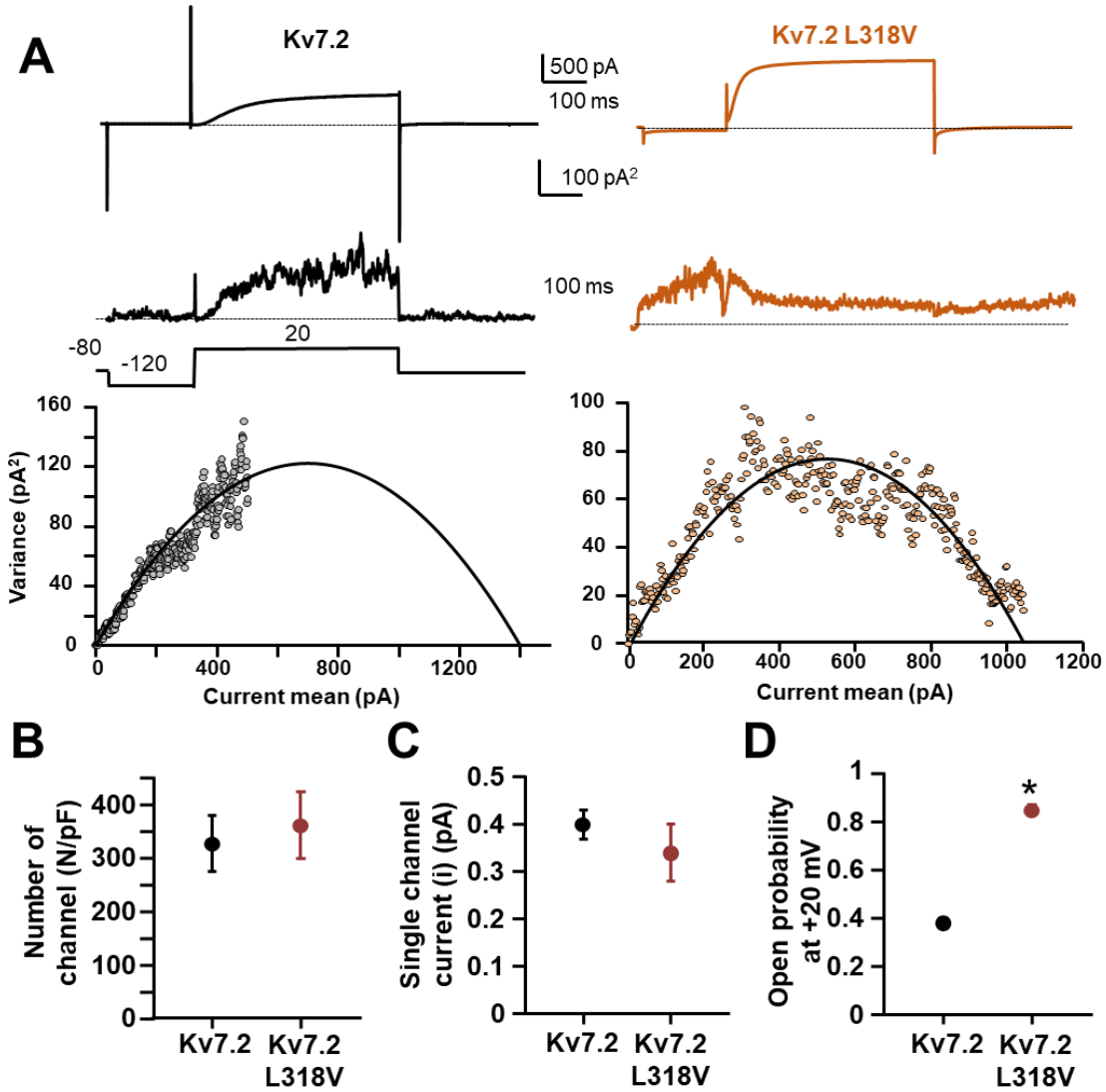

***Figure R10**: Nonstationary noise analysis of Kv7.5, Kv7.5 G1S, Kv7.2, and Kv7.2 G1S channels. (A) Representative average response to 100 pulses at +20 mV (top) of the corresponding variance (bottom), and (B) variance versus current mean plot from Kv7.2 and Kv7.2 L318V. The continuous lines in variance/mean plots are parabolic fits of the experimental data (see Materials and Methods). C–E. Quantification of the number of channels divided by capacitance (C), of the single-channel current (D), and of the opening probability at +20 mV (E). Asterisks indicate values significantly different (*p < 0.05) when compared to control (Kv7.2).*

sweeps between consecutive pulses (Sigg et al., 1994). The small amount of the time-dependent current observed in the Kv7.2 A317T variant does not allow to obtain a valid variance distribution; therefore this mutant channel was not used for further analysis (data not shown). In figure R10A and R10B the mean current, the respective variance, and the correlation between the average current and the variance for Kv7.2 and Kv7.2 L318V channels are shown. Fitting the variance data with equation 2 (as described in the Methods) failed to reveal difference in the number of functional channels (Fig. R9B) or single channel current (Fig. R10C) between wild-type Kv7.2 and Kv7.2 L318V channels. Whereas, a 2.5/3-fold increase in maximal Po was observed in the mutant channels, when compared to Kv7.2 channels (Fig. R10D).

Altogether, these data suggest that the Kv7.2 L318V mutant channels caused a strong GoF phenotype by increasing channel opening probability without major changes in the number of functional channels or their unitary conductance.

4.6 EFFECT OF THE G313S (G1S) AND A317T VARIANTS ON PIP_2-DEPENDENT CURRENT MODULATION

Given that the opening of all Kv7 members requires phosphatidylinositol 4,5-bisphosphate (PIP_2), an investigation was conducted to determine whether the G1S-induced increase in Kv7.5 Po was due to altered channel regulation by PIP_2. Resting PIP_2 levels were either decreased by co-expressing a voltage-sensitive phosphatase from Danio rerio (DrVSP) or increased by co-expressing the PIP2-synthesizing enzyme PIP5K. In CHO cells expressing DrVSP, depolarization to +100 mV time-dependently reduced Kv7.2 currents by 60% after 2 seconds, while currents carried by Kv7.2 G1S channels exhibited reduced sensitivity to inhibition upon DrVSP activation at all time points investigated, being inhibited by only 10% of the starting value after 2 seconds.

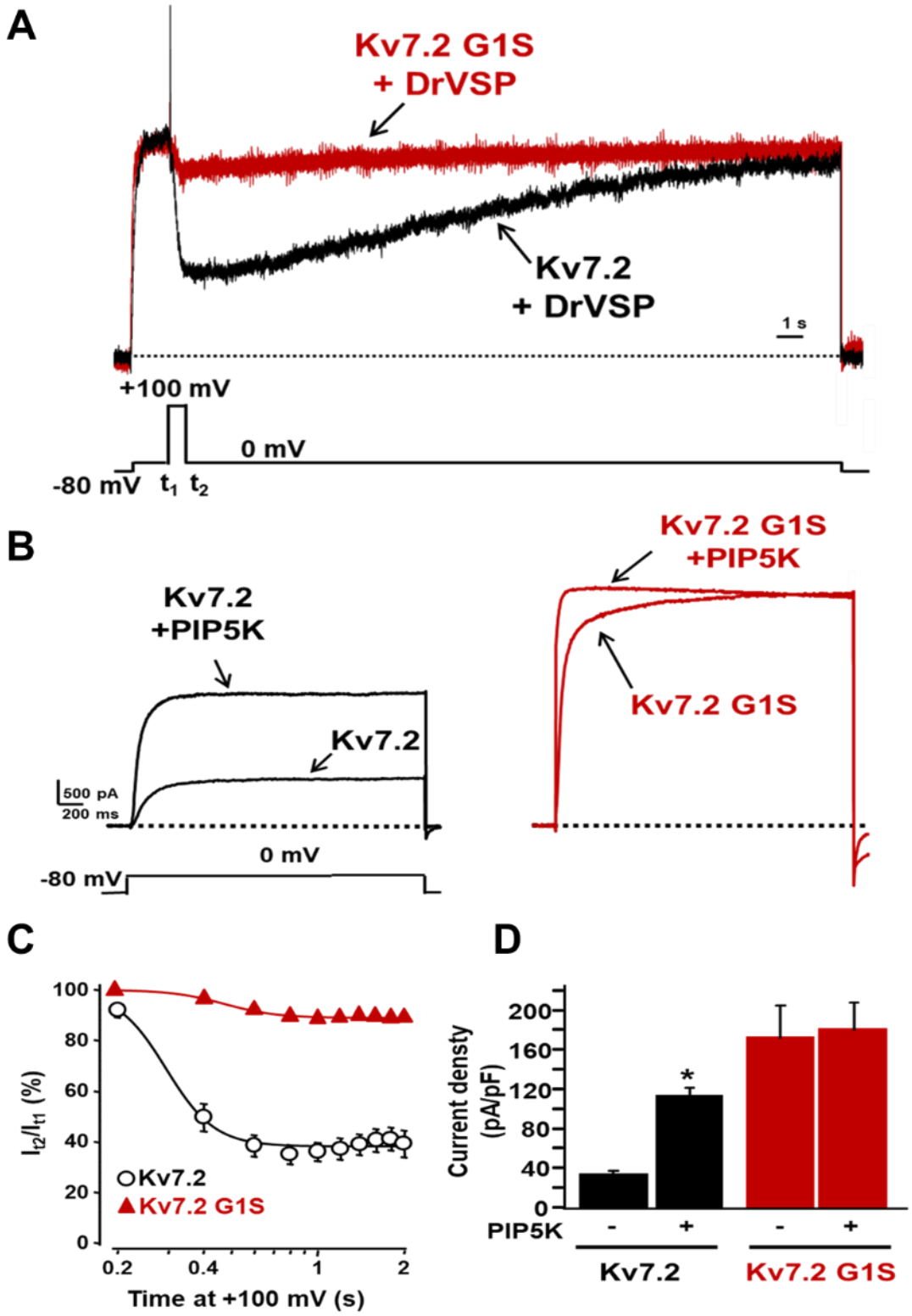

***Figure R11**: Effect of DrVSP or PIP5K on Kv7.2 and Kv7.2 G1S homomeric channels. (A) Currents recorded in response to the indicated voltage protocol in cells expressing DrVSP and Kv7.2 or Kv7.2 G1S channels. (B) Macroscopic currents recorded in response to the indicated voltage protocol in cells expressing Kv7.2 or Kv7.2 G1S channels in the absence or presence of PIP5K. (C) Time-dependent current decrease in cells coexpressing the indicated channels and DrVSP, expressed as the ratio between the current values recorded at 0 mV immediately after (t2) and before (t1) the Dr-VSP–activating +100 mV depolarizing step. (D) Current densities at 0 mV from cells expressing Kv7.2 or Kv7.2 G1S channels alone or in combination with PIP5K, as indicated. The asterisk indicates a value significantly different (*P < 0.05) from Kv7.2 currents.*

Conversely, increasing cellular PIP_2 levels by PIP5K co-expression caused a 3-

fold enhancement in Kv7.2 peak currents, along with a negative shift in their half-activation potential. When PIP5K was co-expressed with Kv7.2 G1S channels, no increase in maximal currents occurred (Fig R11B, D). Kv7 channel opening is strongly regulated by the presence of intracellular phosphatidylinositol 4,5-bisphosphate (PIP_2). This phospholipid is essential for the coupling of the VSDs and pore domains for the opening of Kv7 channels (Pant et al., 2021; Sun and MacKinnon, 2020; Zaydman et al., 2013). Several binding regions of PIP_2 in Kv7 channels, including the bottom part of the S6 segment. To investigate the sensitivity of the Kv7.2 A317T and Kv7.2 L318V currents to PIP_2 modulation, the PIP_2 levels were increased by addition of 100 micromolar of the water soluble analogous Dic8- PIP_2 in the intracellular solution or decreased by co-expressing a voltage-sensitive phosphatase from Danio rerio (DrVSP) which transiently reduces cellular PIP_2 levels when activated by strong depolarizations.

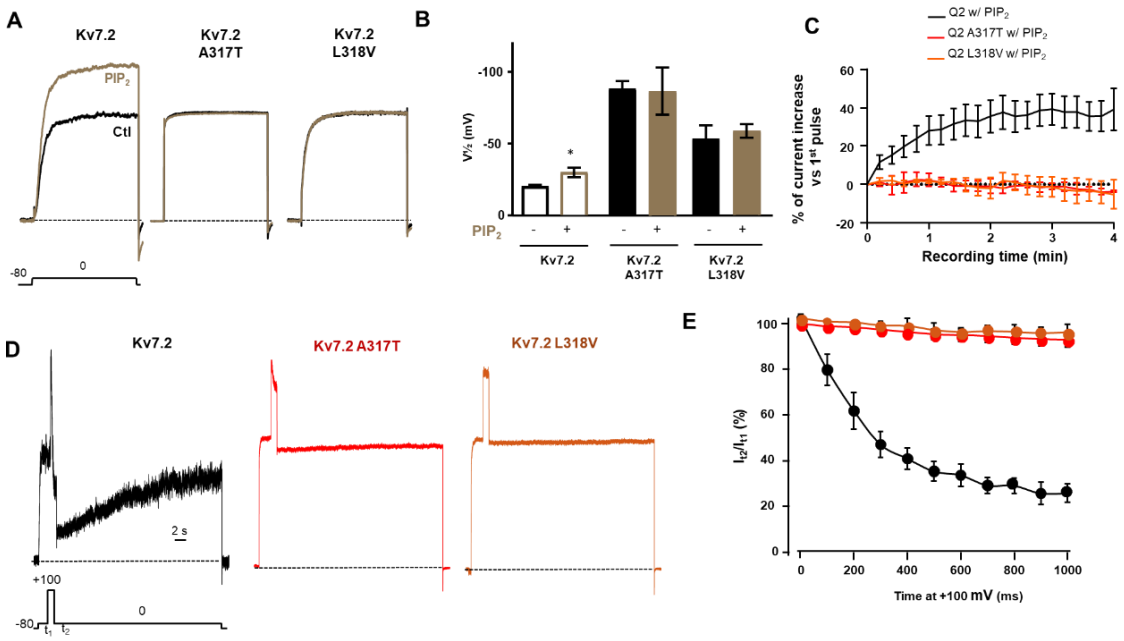

***Figure R12**: Effect of PIP2 on Kv7.2, Kv7.2 A317T and Kv7.2 L318V homomeric channels. (A) Macroscopic currents recorded in presence of 100 μM Dic8-Pip2 in the intracellular pipette solution. Black traces reports normalized currents at the beginning of the recording and yellow traces report normalized current after 4 minutes recording. (B) V½ values recorded at the beginning of the recording and after 4 minutes recording with 100 μM Dic8-PIP_2 at the intracellular solution. The asterisk indicates a value significantly different (*p<0.05).(C) Time-corse of current percentage increase of Kv7.2 wt, Kv7.2 A317T and Kv7.2 L318V recording with 100 micromolar Dic8-PIP_2 intracellularly. (D) Currents recorded in response to the indicated voltage protocol in cells expressing DrVSP and Kv7.2, Kv7.2 A317T or Kv7.2 L318V channels. Time scale, 2 s. (E) Time dependent current decrease in cells coexpressing the indicated channels and DrVSP, expressed as the ratio between the current values recorded at 0 mV immediately after (t2) and before (t1) the Dr-VSP–activating +100 mV depolarizing step.*

Increasing cellular PIP_2 levels by Dic8-PIP_2 induces an enhancement in Kv7.2 peak currents, together with a negative shift in their half-activation potential after 4 minutes of recording. By contrast, the increase of PIP_2 levels by Dic8-PIP_2 intracellularly did not affect Kv7.2 A317T-and Kv7.2 L318V-mediated currents and no shift in the half-activation potential occurred (Figure R12A and R12B). Moreover, in CHO cells expressing Dr-VSP, depolarization to +100 mV time-dependently reduced Kv7.2 currents by 80% after 1 second; by contrast, currents carried by Kv7.2 A317T and Kv7.2 L318V channels showed no inhibition upon DrVSP activation at all time points investigated (Figure R12C and R12D). These data suggest that the introduction of the two variants A317T and L318V in Kv7.2 are completely insensitive to PIP_2 modulation.

4.7 MD SIMULATIONS OF THE TWO GoF VARIANTS IN Kv7.2 CHANNEL

To gain insight into the molecular mechanism underlying the two GoF variants G313S and A317T, we resorted to all-atom MD simulations. In addition to the A317T mutation we run MD also for G313S, which was shown to induce GoF via an increase in single channel opening probability. We simulated the WT and mutant protein pores in two distinct conformations, each with a different degree of activation gate (AG) opening, quantified by cross-distances between pairs of Cα atoms from diagonally opposed subunits. Three distances were used in total, one to characterize the selectivity filter (SF) via the atoms of G279 (d1), and two for the AG, using the atoms of G313 (d2) and A317 (d3). The first conformation, derived from the cryo-EM structure of the human Kv7.2 (hKv7.2, PDB ID: 7CR0), shows a conductive filter (d1=8.03 Å) and a constricted gate, with d2 = 11.67 Å and d3 = 13.68 Å (Fig. R13A). The second

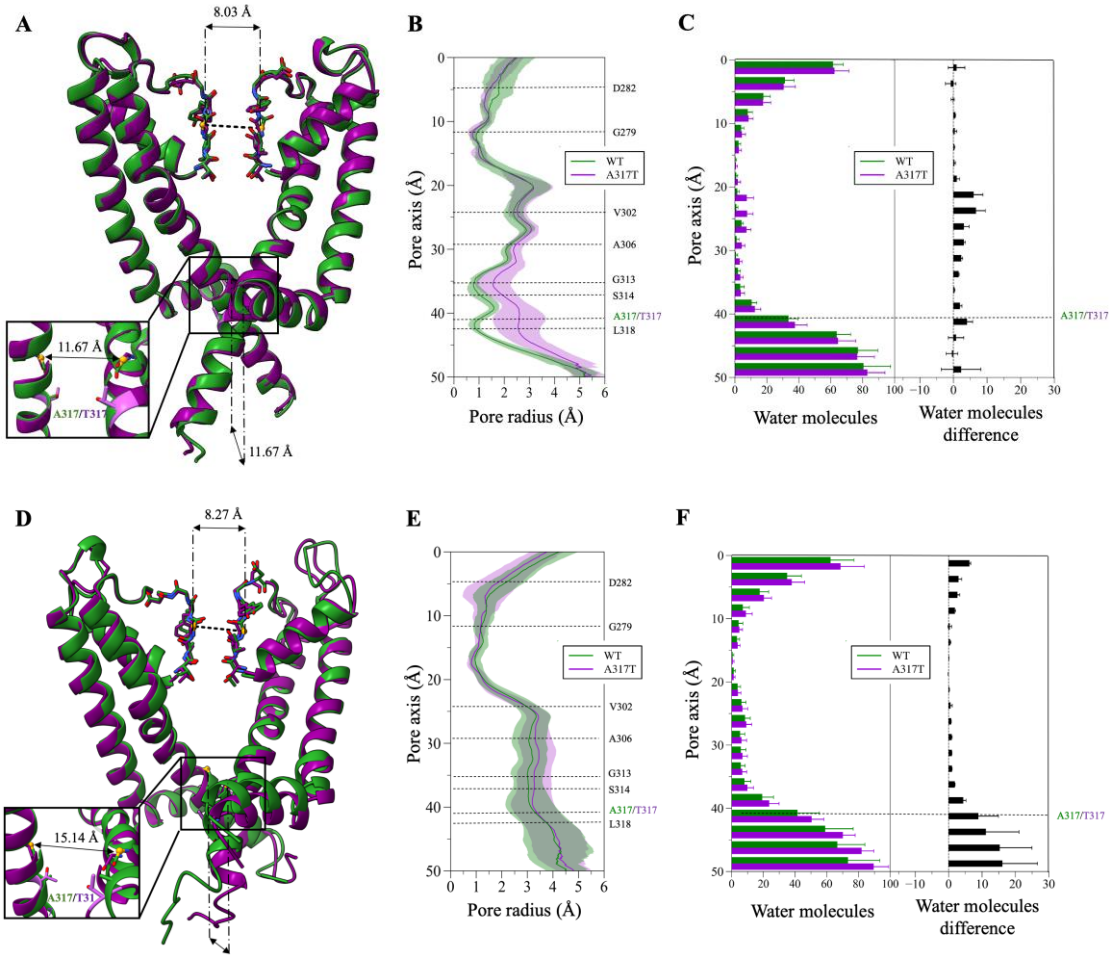

***Figure R13**: Molecular modeling of A317T variant in Kv7.2 channel (A) Superposition of WT (green) and A317T (purple) Kv7.2 closed structures after equilibration and before MD production simulations. (B) Channel radius profiles along the pore axis of the two proteins, averaged over all simulated replicas. Shaded regions indicate standard deviations. (C) Distribution of water molecules along the channel axis. Average and standard deviations are calculated over all replicas. (D-F) Same as (A-C) but for the open structures.*

conformation, with a similar filter size (d1=7.92 Å) but a wider AG (d2=13.55 Å and d3=19.54 Å; Fig. R13D), was homology modelled using the open hKv7.1 structure (Sun and MacKinnon 2020) (PDB ID: 6V01) as template.

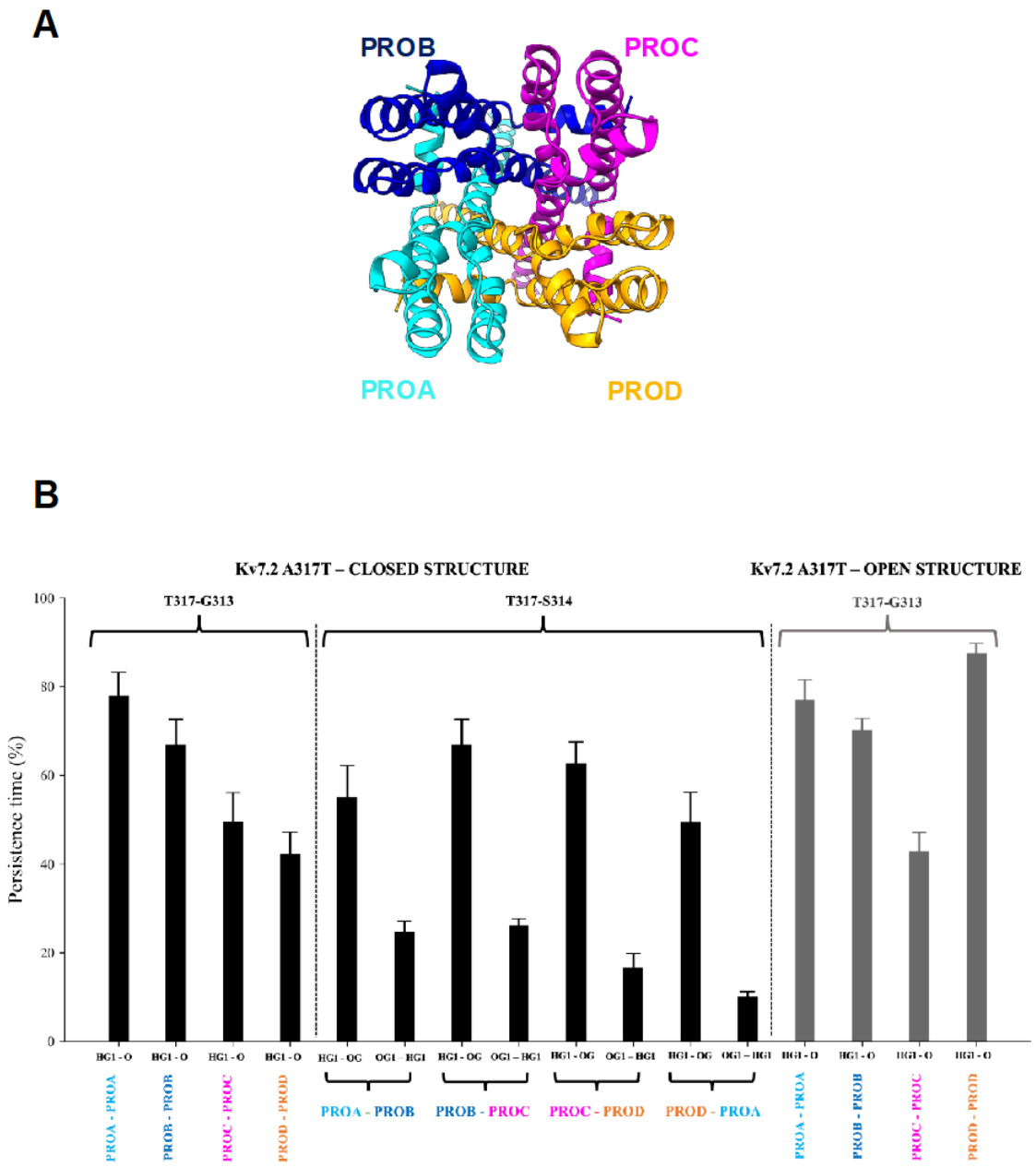

***Figure R14**: HBs formed by the mutated residue in the A317 Kv7.2 channel simulations. (A) Extracellular view of the pore, indicating the four subunits labels. (B) Persistence of the HBs (reported as percentage of the aggregated simulation time) in the closed (black bars) and open (gray bars) structure simulations, classified based on the atoms involved and the subunits they belong to. Atom names follow the PDB CHARMM notation: O is the backbone amide oxygen, HG1 the hydrogen atom bound to an oxygen in γ position with respect to the backbone amide carbon atom, OG the hydroxyl oxygen in serine (oxygen atom in γ position with respect to the backbone amide carbon atom), and OG1 the hydroxyl oxygen in threonine (again with oxygen atom in γ position with respect to the backbone amide carbon atom).*

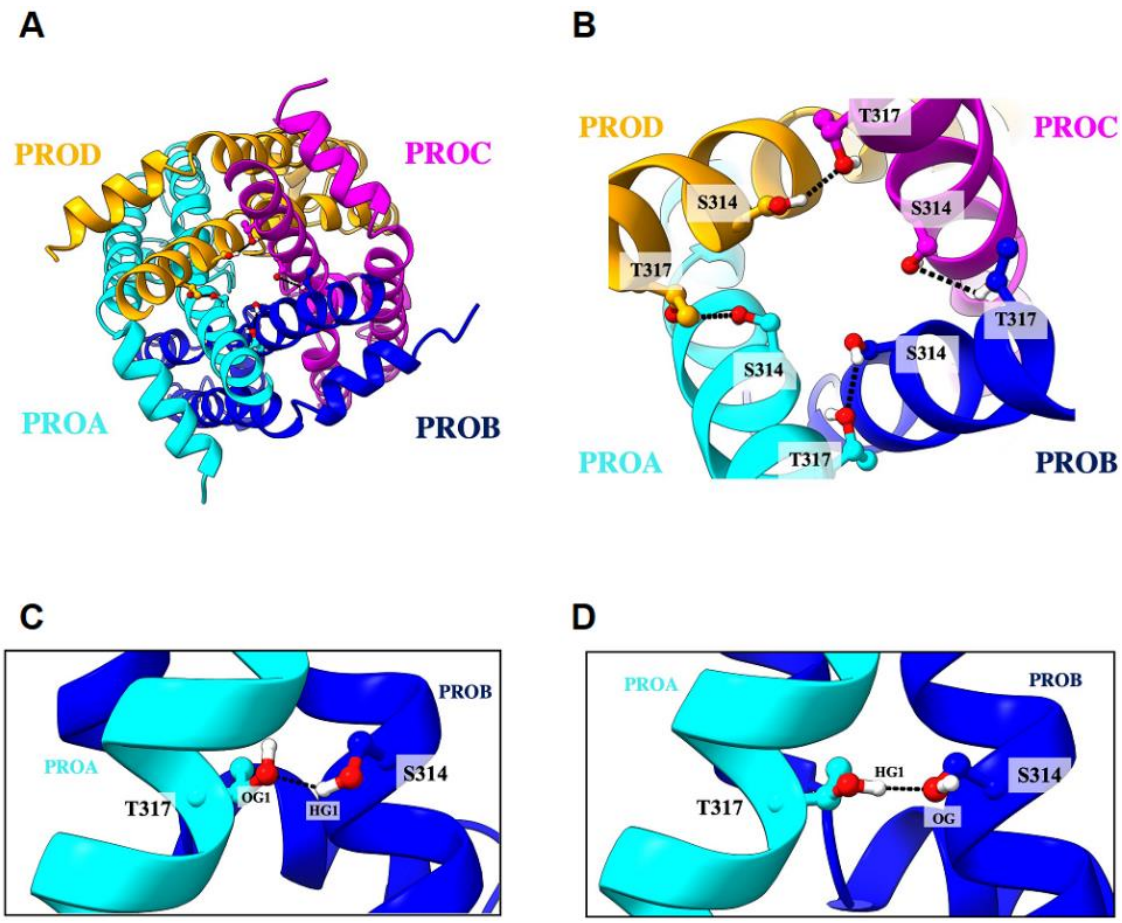

***Figure R15**: (A) Snapshot of the Kv7.2 pore with a closed IG, viewed from the cytosol. Equilibrated structure at t = 160 ns of an MD run. The sidechains of the T317-S314 pairs, belonging to two different and adjacent subunits, are shown in ball and sticks style. (B) Enlarged view of the interaction described in panel (A). (C) and (D) Representative structures showing the HBs formed between the T317-S314 sidechains, extracted from the MD simulations.*

The channels were embedded in explicit POPC membrane bilayers, solvated with water and ions, and simulated in five independent replicates for both closed and open AG conformations, obtaining a cumulative time length of more than 15 μs. All protein structures were found to be stable during the MD simulations and did not deviate substantially from the starting conformations, as evidenced by backbone Root Mean Square Deviations (RMSDs) averaged over the replicas, which are stationary around values between 2.5 and 3 Å.

To investigate the impact of the mutations on the protein structure, we first looked at the size of the channel pore along the simulated trajectories. As for the WT channel, the open and closed pore radius profiles, averaged over the replicas, nicely superimpose to those of the corresponding experimental structures, confirming that the pore geometry is maintained over the simulations. When we compared the pore profiles of A317T to those of the WT, the results for the closed

and open AG structures differed (Figure R13). In the mutant, the variation induces a widening of the AG, from above the level of G313 down to the cytoplasmic termini, which is particularly evident in correspondence of the mutated residue A317T (Figure R13A, B). This localized broadening of the pore makes it more accessible to water, as shown by the average number of water molecules computed along the channel axis (Figure R13C). The difference is most noticeable in the central cavity region, particularly around V302, where the WT system is essentially dry, while A317T accommodates about eight water molecules. We see both traits as consistent with a GoF, since a broadened gate could facilitate the transition of the mutated channel towards the open state, and the concomitant increased hydration of the cavity may promote ion permeation.

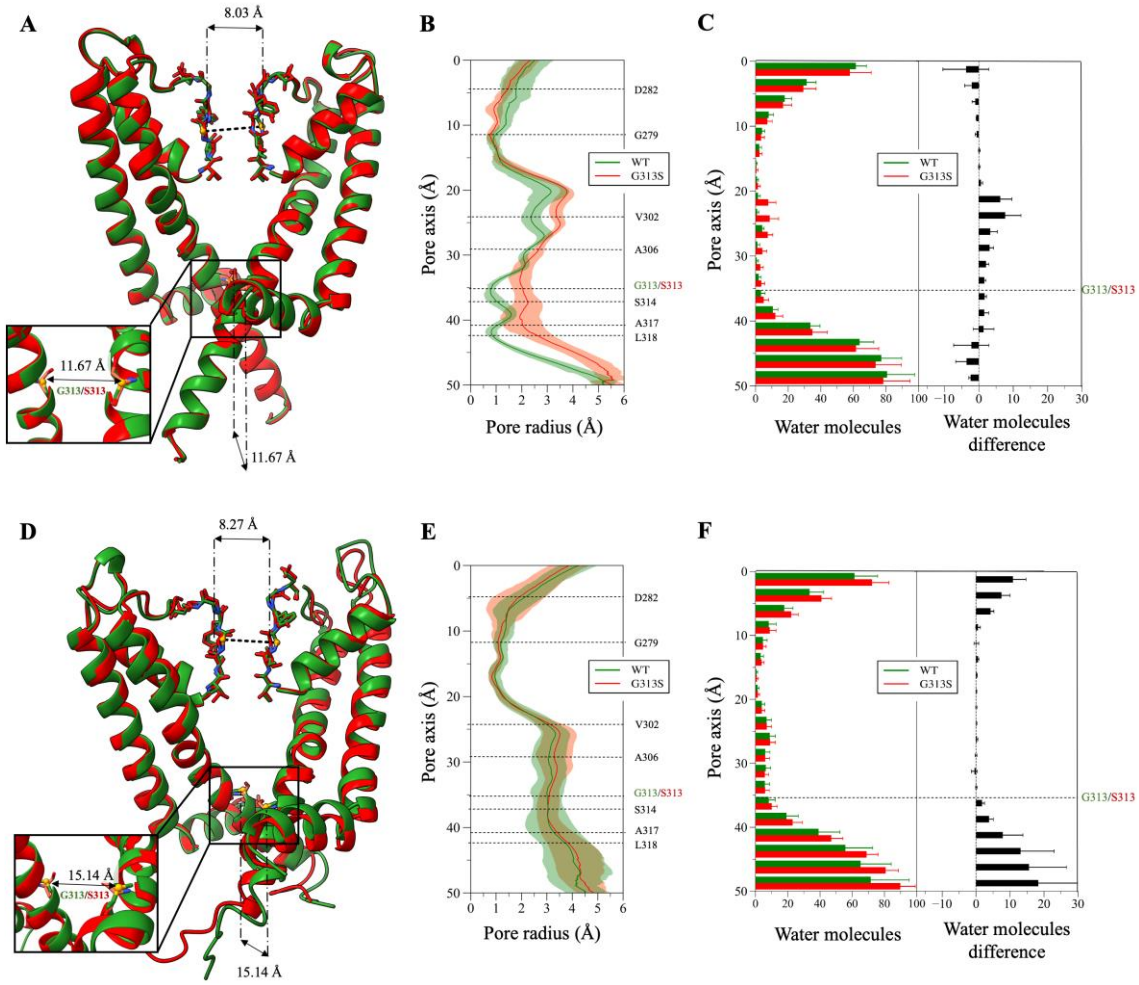

***Figure R16**: Molecular modeling of G313S variant in Kv7.2 channel (A)Superposition of WT (green) and G313S (red) Kv7.2 closed structures after equilibration and before MD production simulations. (B) Channel radius profiles along the pore axis of the two proteins averaged over all simulated replicas. Shaded regions indicate standard deviations. (C) Distribution of water molecules along the channel axis. Average and standard deviations are calculated over all replicas. (D-F) Same as (A-C) but for the open structures.*

In contrast, the WT and A317T open structures trajectories showed no difference in pore profiles (Figure R13D, E) or hydration of the central cavity (Figure R13F). In line with the enhanced hydrophilicity of the substitution, more water molecules entered the cytoplasmic side of the mutated pore, at A317T and below, but the difference remained limited to that region.

Given the AG rearrangement in the closed A317T channel, we searched for interactions involving the mutated amino acid that could be responsible for stabilizing it. We found that the threonine side chains form hydrogen bonds (HBs) with S314 from adjacent subunits (average persistence time of 55.0%, 66.8%, 62.7% and 49.4% for the four pairs of chains), occasionally competing with HBs to G313 of their same helices (Figures R14 and R15). Hence, the substituted threonine is directly involved in inter-chain bonds that cause the partial widening

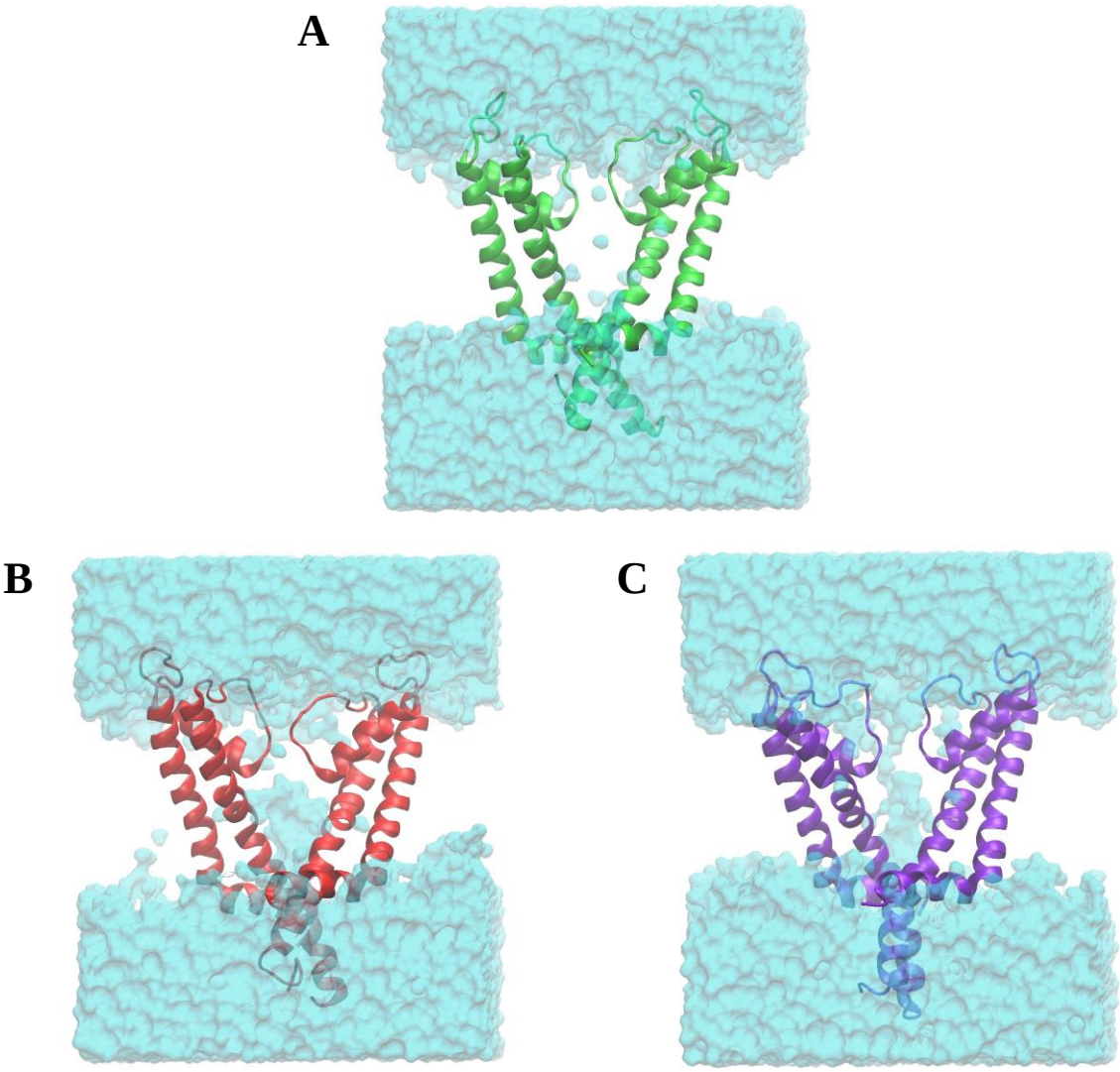

Figure R17*: Representative snapshots showing pore cavity hydration in WT (A), G313S (B), and A317T (C) Kv7.2. For each system we report an equilibrated structure extracted at 150 ns. Water molecules are represented as cyan surfaces. Lipid molecules and ions are not reported for clarity.*

of the closed AG, generating a conformation that might be more likely to become fully open. In the latter configuration, the T317-S314 interaction between chains is absent, and the threonine mostly connects to G313 from the same subunit.

To verify that the structural effects caused by A317T do not depend on the membrane model, we performed additional simulations of the mutated closed channel embedded in bilayers of different lipid composition (pure POPE, POPG, DMPC, and a mixture POPC-CHOL-PIP2). We then looked at the pore size in the closed and open G313S Kv7.2, and obtained results that are in remarkable agreement to those of A317T (Figure R16): the mutation induces a widening of the closed AG (at the level of G313S and A317) and, in this case, also of the central cavity (around V302), associated to an increased hydration of this region; conversely, in the open conformation, no major difference is detected in pore size or central cavity hydration. A comparison between three representative snapshots from the WT, G313S and A317T closed AG simulations is reported in (Figure R17), highlighting differences in pore opening and cavity hydration.

4.8 10 MICROMOLAR AMITRIPTYLINE RESTORES Kv7.2/7.3 CURRENT LEVELS IN HETEROMERIC CHANNELS CARRYING Kv7.2 A317T OR Kv7.2 L318V MUTANT SUBUNITS

Amitriptyline is a tricyclic antidepressant with analgesic properties due to the serotonin and norepinephrine reuptake inhibition, which also targets some voltage-gated ion channels and receptors. In addition, amitriptyline is able to block Kv7.2 or Kv7.3 channels (Punke et. al., 2007). Recently was described its ability to restore the normal function in heteromeric Kv7.2+Kv7.3 channels carrying a mild GoF variant when expressed in CHO cells (Miceli et. al., 2022). Bases on this study, , we evaluated the ability of amitriptyline (10 µM) to restore the normal current levels in cells transfected with Kv7.2+Kv7.2 A317T+Kv7.3 and Kv7.2+Kv7.2 L318V+Kv7.3 at 0.5:0.5:1 ratio, since this *in vitro* condition is that

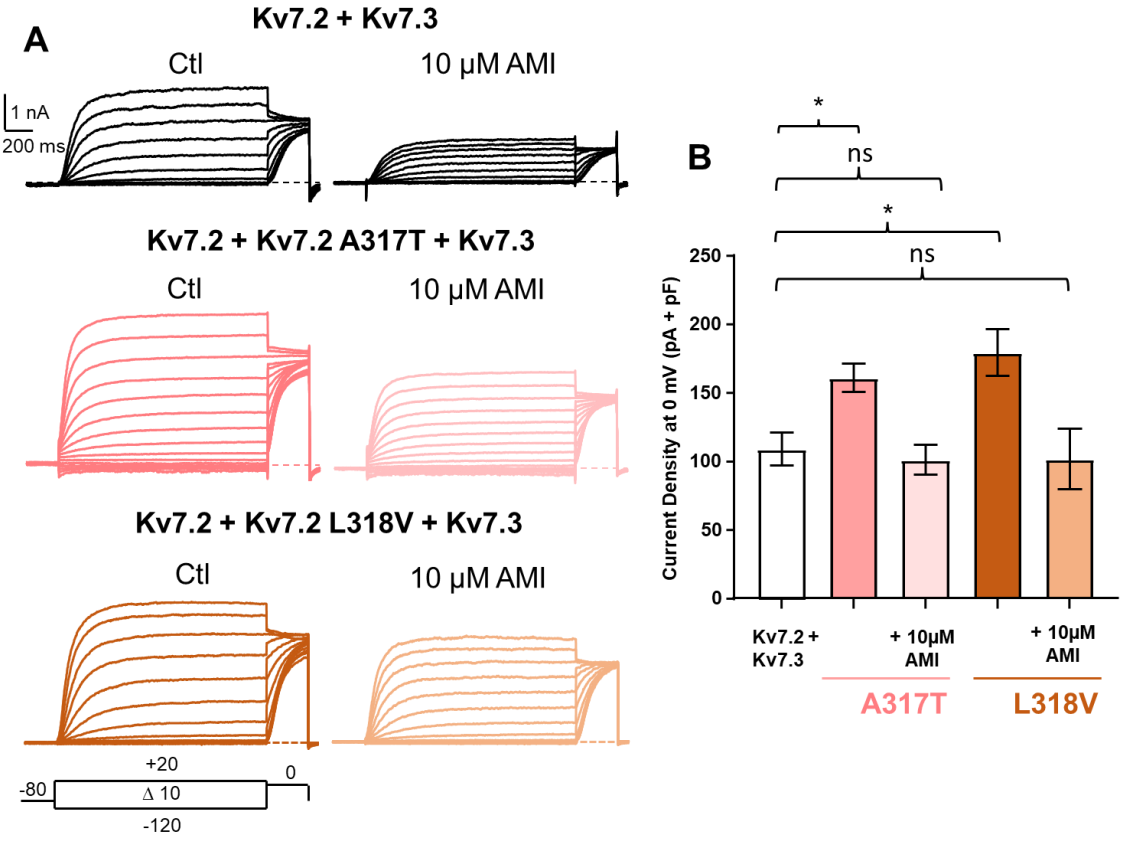

***Figure R18**: Functional effect of application of 10 micromolar Amitriptyline; (A) Macroscopic currents from Kv7.2, Kv7.2 A317T, and Kv7.2 L318V homomeric channels are shown in response to the indicated voltage protocol, with and without 10 micromolar Amitriptyline. (B) Quantification of current densities recorded from cells transfected with the indicated cDNA constructs, in presence and in absence of 10 micromolar Amitriptyline. Asterisks indicate values significantly different (*p<0.05) from Kv7.2 + Kv7.3 wt.*

mostly resemble the patient functional phenotype (Fig. R18A). The results obtained revealed that amitriptyline 10 μM was able to reduce the current level of Kv7.2+Kv7.2 A317T+Kv7.3 and Kv7.2+Kv7.2 L318V+Kv7.3 at those of Kv7.2+Kv7.3 channels (Fig. R18B). These data indicates the possible use of amitriptyline as a potential treatment in patients carrying these Kv7.2 GoF variants.

5. DISCUSSION

5.1 PHENOTYPIC SPECTRUM AND GENOTYPE–PHENOTYPE CORRELATIONS IN *KCNQ5*-RELATED DISORDERS

The *KCNQ2*, *KCNQ3* and *KCNQ5* genes contribute to the molecular heterogeneity of I_{KM} in specific neuronal subpopulations at distinct developmental periods (Lerche et. al., 2000; Schroeder et. al., 2000; Nappi et. al., 2020). However, while several hundred mutations in *KCNQ2* and *KCNQ3* have been identified over the last two decades in patients with developmental and/or epileptic diseases, the firsts four photogenic variants in *KCNQ5* were reported in 2017 (Lehman et. al., 2017). Since then, a total of 16 variants have been identified in 21 patients (Lehman et. al., 2017; Rosti et. al., 2019; Krüger et. al., 2022; Wei et. al., 2022). These variants, found in heterozygosity, include missense, nonsense and frameshift variants. Moreover, three of these mutations (R359C, Q735R and E265_T306del) were transmitted from one of the affected parents following a classical autosomal dominant inheritance (Krüger et. al., 2022), while the others occurred *de novo*.

Functional studies revealed that most of these variants are LoF (11/16), causing a reduction of current density and/or a rightward shift of the $V_{½}$ value; whereas 5 are GoF, showing an increase of current density and/or a leftward shift of the $V_{½}$ value.

The clinical phenotype of patients carrying LoF variants include: absence epilepsies with or without GTCS and/or myoclonus (11/16) and mild to severe ID (10/16); whereas the 5 patients with GoF variants showed: epileptic phenotypes (3/5), no seizures (2/5), mild to severe ID (5/5) and autism (2/5) (Wei et. al., 2022; Lehman et. al., 2017). Although the limited number of *KCNQ5* pathogenic variants, it seem that LoF variants are predominantly associated with absence epilepsy phenotypes whereas GoF variants are associated with developmental and/or epileptic phenotypes, mild to profound intellectual disability, and, more rarely, autism.

The GoF phenotypic characteristics closely resemble those of our two patients, one showing very limited language because of a severe ID and drug-resistant epilepsy (patient 1, G1S) and another suffering from moderate to severe ID without epilepsy (patient 2, G1A). Variants in *KCNQ5* were also identified in large cohorts of patients with neurodevelopmental disabilities (Kaplanis et. al., 2020;

Lelieveld et. al., 2016); notably, one of these patients carried the same G347S (G1S) variant reported in our patient 1, although no direct phenotype comparison is possible because of the lack of detailed clinical histories.

However, given the rarity of patients with *KCNQ5*-related disorders, neither the functional consequences caused by the mutations nor the variant localization within the channel sequence can fully predict the clinical features of patients carrying *KCNQ5* mutations; thus, no solid genotype–phenotype correlation can be currently drawn. For example, it is yet unclear why patients carrying the G1S or the G1A variants, despite the similarity in their *in vitro* functional properties, have different epilepsy phenotypes; additional genetic, epigenetic, and epistatic mechanisms likely explain such divergence.

5.2 PHENOTYPIC SPECTRUM AND GENOTYPE–PHENOTYPE CORRELATIONS IN *KCNQ2* AND *KCNQ3*-RELATED DISORDERS

For *KCNQ2* and *KCNQ3* a correlation between functional effects *in vitro* and phenotype has been established (Orhan et.al., 2014, Miceli et. al., 2015; Millichap et. al., 2017; Mulkey et. al., 2017; Sands et. al., 2019), with strong, dominant-negative LoF variants being responsible for severe clinical phenotypes and variants found in most self-limiting forms causing haploinsufficiency and milder LoF *in vitro* effects (Nappi et. al., 2020). The severe end of the *KCNQ2*-DEE spectrum is represented by the patient described in Olson et al. (Olson et. al., 2017) who died at 3 mo of age because of a very severe neonatal-onset epileptic encephalopathy and carried a *KCNQ2* variant affecting the G1 residue (G1R); consistent with previously reported data (Miceli et. al., 2013; Orhan et. al., 2014), the present functional results reveal strong, dominant-negative LoF effects prompted by the Kv7.2 G1R variant.

In the present study, we described functional properties of two strong GoF variants in Kv7.2 affecting the PD, induced by A317T and L318V substitutions. In Kv7.2, all GoF mutations (except G239S, located in S5 reported in Bayat et. al., 2024) are located within the VSD and cause a variable impairment in voltage dependence of the channel, with small (-4 mV) or larger (>-80 mV) hyperpolarizing shift. Electrophysiological recordings revealed that both mutations induced significant increase of current density in homomeric and heteromeric channels and a marked hyperpolarizing shift of the voltage-dependent activation, indicating that both A317T and L318V are inducing a GoF

effect. Interestingly, the functional properties of the L318V variant resemble those of a previously described GoF variant, R198Q; the patient carrying this variant also showed a clinical phenotype similar to the patient with the L318V mutation herein described, thus confirming the genotype-phenotype correlation. By contrast, the analysis of the functional properties and the clinical features prompted by the A317T variant do not allow us to make a clear genotype-phenotype correlation. Indeed, while causing a strong GoF effect, similar to that described for the R201C mutation, the clinical consequences of the A317T variant are relatively mild, resembling those associated with less severe GoF variants such as those affecting the R144 residue. Additional genetic factors or compensatory mechanisms exerted by other Kv7 subunits and/or K+ channels may explain the mild phenotype. The characterization of novel Kv7.2 GoF will help to clarify this issue.

Although Kv7.2 is the main locus for SLFNE and Kv7-DEE, pathogenic variants in Kv7.3 have been also identified in such patients although their clinical features are generally less severe. These variants are commonly missense and are located within the PD and result in LoF effect. More recently, pathogenic variants affecting the first two positively-charged residues within the S4 transmembrane domain of the VSD (R227Q and R230C/S/H) have been reported in individuals with developmental delay, autism spectrum disorder, and sleep-activated epileptiform discharges on EEG. Functional analysis using voltage-gated clamp recordings revealed that these variants stabilized the activated state of the channel and resulted in GoF effects on channel activity. In contrast to individuals with LoF variants in Kv7.3, and similar to Kv7.2 GoF, neonatal and infantile seizures are not a common finding in individuals with Kv7.3 GoF variants (Sands et. al., 2019). In the present study we characterized a variant in Kv7.3 (A356T), corresponding to the A317T in Kv7.2, previously identified in a patient with severe ID, delayed language and no seizures. Our functional data revealed that homomeric channels were not functional, whereas heteromeric configuration either with Kv7.2 or with both Kv7.2 and Kv7.3 induce a GoF effect, with a 3-fold increase in the maximal current and a 15 mV leftward shift in the voltage-dependence of activation; this is the first GoF variant localized within the PD of the channel. An opposite effect prompted by a Kv7.3 variant when expressed in homomeric or heteromeric configuration has been described also for another non-pathogenic variant affecting the PD (A315V) (Zaika et. al., 2008). It is likely

that the phenotype observed in the patient carrying the A356T mutation mainly depends on the GoF effects induced in heterotetrametric configuration, since Kv7.3 is expressed later than Kv7.2 (Dirkx et. al, 2020) and form heteromers in the vast majority of brain regions (Cooper et. al., 2000).

5.3 *IN VIVO* ROLE OF NEURONAL Kv7 GoF

KCNQ5-encoded Kv7.5 subunits preferentially assemble into heteromeric channels with Kv7.3, but not Kv7.2, subunits (Schroeder et. al., 2000). Whether these heteromeric channels actually exert specific action at selected neuronal sites or just decrease the amount of the more efficient Kv7.2/Kv7.3 channels (Gilling et. la., 2013) is still a matter of debate. However, irrespective of the pathophysiological relevance of the Kv7.3/Kv7.5 channels, our functional data seem to suggest that the G1S/A variants in Kv7.5 retain their ability to induce GoF effects even in heteromeric configuration with Kv7.3 subunits, although these effects were quantitatively smaller than those observed for homomeric channels. However, it is difficult to establish the exact channel composition underlying the recorded currents when Kv7.5 G1S/A subunits are coexpressed with Kv7.3 or Kv7.3/Kv7.5 subunits since at variance with Kv7.2 and Kv7.3 (Wang et. al., 1998), currents carried by Kv7.3 and Kv7.5 channels display similar maximal density, gating ($V_{½}$), and pharmacological (TEA sensitivity) properties (Lerche et. al., 2000; Schroeder et. al., 2000).

Within the central nervous system, Kv7.5 expression has been described in cell somata and dendrites in human cortex and hippocampus (Yus-Nájera et. al., 2003), in glutamatergic synapses of several rat brain stem nuclei (Huang and Trussel, 2011), and in the postsynaptic membrane of mouse vestibular calyx terminals (Spitzmaul et. al., 2013). Knock-in mice carrying a Kv7.5 dominant-negative pore variant had normal brain morphology and no seizures but displayed a reduction of the mAHP and sAHP currents in the hippocampus (Tsingounis et. al., 2010). In another strain, on the other hand, homozygous *KCNQ5* knock-out mice displayed varying degrees of both absence- and myoclonic-type seizures triggered by handling or elevation of body-temperature (Wei et. al., 2022).

Kv7.5 subunits are highly expressed in the hippocampus (Tsingounis et. al., 2010), where they contribute to shaping sharp waves and ripples activity (Trompoukis et. al., 2020), a highly synchronous population pattern arising from the CA3 region and leading to CA1 fast network oscillation (Buzsáki, 2015). We

hypothesize that the G1S and G1A mutations interfere with the crucial role of Kv7.5 in controlling this pattern of hippocampal excitability which is critically involved in memory consolidation (Buzsáki, 2015), possibly explaining the cognitive changes described in our two patients. On the other hand, it is still unclear how *KCNQ5* GoF changes triggered by the G1S variant lead to cortical hyperexcitability (Niday, and Tzingounis, 2017).

Similarly, the mechanisms by which Kv7.2 GoF variants cause neuronal hyperexcitability are not completely understood. One hypothesis is that GoF variants in Kv7.2 differentially affect neuronal behavior in distinct subtypes of neurons. For instance, it has been proposed that GoF variants selectively dampen the excitability of the inhibitory interneurons due to their high input resistance (Miceli et. al., 2015). Moreover, a recent work has shown that cortical pyramidal neurons (L2/3 layer) from transgenic mice carrying a Kv7.2 GoF variant are hyperexcitable, although hippocampal CA1 neurons from the same animal showed hypoexcitability (Varghese et. al., 2023).

Further studies are needed to decipher the complex interaction between GoF variants of potassium channels and electrical activity, in different neuronal subpopulations, during neurodevelopment (Dirkx et. al, 2020).

5.4 BIOPHYSICAL AND STRUCTURAL CONSEQUENCES OF G1 SUBSTITUTIONS

The functional results obtained suggest that in both Kv7.5 G1S/A variants caused a drastic enhancement in maximal current density consistent with a GoF *in vitro* phenotype. The appearance of a tonic voltage-independent component (I_{INST}), together with a marked hyperpolarization in activation gating and a significant reduction in channel deactivation rate of the voltage-dependent current component (I_{VDEP}), seems to account for this enhancement. No differences in K^+ selectivity and pharmacological sensitivity to pore blockers such as TEA and Ba^{2+} were observed between I_{INST} and I_{VDEP}, suggesting that both components are carried via the same permeation pathway, i.e., the central ion pore.

To provide mechanistic insight into the molecular basis for this GoF effect, nonstationary noise analysis was used to estimate N, i, and Po (Heinemann and Conti, 1992). Our measurements indicate that in Kv7.5 G1S or Kv7.2 G1S the increase in channel function is due to an increase in the opening probability of

the order of 2.5/3 times, without any significant difference in the number of the channels or the single channel conductance.

In all Kv7 subunits, the distal portion of the S6 domain plays an important role in channel gating. Indeed, within this region, the PAG motif (corresponding to the conserved PXP motif of other Kv channels) is considered as the gating hinge for pore opening (Jiang et. al. 2002; Long et. al., 2005). Cryogenic electron microscopy (Cryo-EM) studies have also revealed that in Kv7.1 channels, the signature GSG motif past the PAG motif forms the narrowest restriction along the ion conduction pathway (Sun and MacKinnon, 2020). Our results reveal that in both Kv7.2 and Kv7.5 channels, the replacement of G1 with either a hydrophilic S or a hydrophobic A increased channel function by enhancing pore opening probability, whereas large, permanently charged residues (either the positive R or the negative E) fully impeded channel function and caused LoF effects. Notably, also in Kv7.1 channels, G1A replacement caused a relative stabilization of the open state over the closed state (Boulet et. al., 2007), thus confirming the common functional role played by G1 in all Kv7 subunits. The anionic phospholipid PIP_2 acts as a critical gating modulator of Kv7 channels (Falkenburger et. al., 2010); by this mechanism, fluctuations in brain PIP_2 availability would translate into neuronal excitability changes (Kim et. al., 2016). Increased PIP_2 availability facilitates both voltage-dependent and voltage-independent transitions toward the open state. Our data suggest that, at least for Kv7.2 channels, the GoF effects introduced by the G1S variant are PIP_2-independent as mutant channels are resistant to inhibition or potentiation when PIP_2 levels are decreased or increased, respectively. It is already known that PIP2 is crucially involved in the coupling of the voltage sensor activation to the pore opening. We therefore hypothesize that the G1S/A substitutions prompt structural transitions resembling those triggered by PIP_2 binding, namely, an expansion of the S6 helices which locks Kv7 channels in a constitutively open state. Molecular dynamic studies indicated that G313S mutant is inducing a higher hydration rate of the water cavity of the pore destabilizing the closed state locking it in an open-like conformation.

5.5 BIOPHYSICAL PROPERTIES OF Kv7.2 A317T, L318V AND Kv7.3 A356T VARIANTS

In the present study we described the functional properties of two strong GoF in

Kv7.2 affecting the PD, namely A317T and L318V. Electrophysiological recordings revealed that both mutations induced a marked hyperpolarizing shift of the voltage-dependent activation (about 70 mV and 40 mV, respectively) and a significant increase of current density in homomeric channels. Non-stationary noise analysis revealed also that these changes are due to an increase in the channel open probability. Moreover currents from both mutant channels were characterized by two components: an instantaneous voltage-independent current followed by a time- and voltage-dependent current. All these properties are indicating that these variants are inducing GoF effect. Recent cryo-EM studies have better defined the structures, voltage gating and PIP_2 activation mechanisms of Kv7.1 (Sun and MacKinnon, 2020; Sun and MacKinnon, 2017; Mandala and MacKinnon 2023; Willegems et. al., 2022), Kv7.2 (Ma et. al., 2023; Li et. al., 2021) and Kv7.4 (Zheng et. al., 2022; Li et. al., 2021) channels. Opening of Kv7 channels is the consequence of highly coordinated interaction between the VSD, PD and PIP_2. In particular, PIP_2 is essential for the electromechanical coupling between VSD movement and pore opening, and depleting PIP_2 results in a closed pore with normal VSD activation (Kim et. al., 2017). Binding of PIP_2 to Kv7 channels induces large and complex rearrangement at the cytosolic part of the channels. In particular, it has been hypothesized that, upon depolarization, HA, HB, and their surrounding CaM undergo an almost 180° rotation; after this rotation the HA and S6 helices form a continuous a-helix leading to the enlargement of the AG with the opening of the PD. Molecular dynamic simulations indicate that the A317T mutation, located within the AG of the PD, seems to stabilize the open state of the channel. In particular, the formation of hydrogen bonds between the -OH group of threonine 317 and serine 314 side chains of the adjacent subunit induces a constitutive enlargement of the AG diameter and stabilizes the PD in an open-like conformation. The ability of the channel to mediate current at all membrane potentials and the presence of a tonic current component suggest that this channel may be in open conformation, even at very negative voltages. Moreover, these structural observations are consistent with our single channel results, that indicates an increase in opening probability of the pore. These structural rearrangements prompted by the A317T mutation resemble these triggered by PIP_2 binding, locking the Kv7.2 channel pore in a constitutively open state. This hypothesis is consistent with our patch clamp data showing

that modulation of PIP_2 levels did not affect Kv7.2 A317T and L318V-mediate currents. Interestingly, a substitution affecting position L351 in Kv7.1 (L351K), corresponding to L318 in Kv7.2, in the PD also renders the channel insensitive to PIP_2 depletion (Zaydman et. al., 2013).

5.6 *IN VITRO* PHARMACOLOGICAL TREATMENT OF Kv7.2 A317T AND Kv7.2 L318V VARIANTS RESCUE WILD-TYPE PHENOTYPE

Amitriptyline is a tricyclic antidepressant with analgesic properties due to the serotonin and norepinephrine reuptake inhibition, which also targets some voltage-gated ion channels and receptors, but act also as inhibitor of Kv7 channels (Punke et. al., 2007). In recent studies, amitriptyline induced a reversible and concentration-dependent inhibition of current carried by two GoF in Kv7.2 channels (Miceli et. al., 2022; Bayat et. al., 2024).

Here we report that 10 micromolar amitriptyline is able to rescue the *in vitro* phenotype of Kv7.2 A317T or L318V variants when co-expressed in the allelic ratio with Kv7.2 wt and Kv7.3 (0.5:0.5:1). These data suggest the potential use of amitriptyline for Kv7.2-GoF conditions and disturbances.

5.7 CONCLUSIONS

Assessment of the functional consequences of rare variants in ion channel genes, besides revealing pathogenic mechanisms and genotype–phenotype correlations, is critical for diagnostic evaluation, prognostic predictions, and tailored therapeutic management of patients with a wide spectrum of neurological disorders. In this work, we have functionally characterized several GoF variants in the pore region of Kv7.2, Kv7.3 and Kv7.5 channels identified in patients with developmental and/or epileptic encephalopathy, thereby further highlighting the role of Kv7.2, Kv7.3 and Kv7.5 channels in developmental and epileptic encephalopathy. Functional analysis revealed that the GoF effects were due to an increased opening probability and molecular dynamic simulations revealed an alteration in the pore structure, thus providing structure-function insights into Kv7 channel gating. The ability of amitriptyline to rescue GoF *in vitro* phenotype may represent a potential pharmacological approach to treat patients with GoF *KCNQ2* variants.

Acknowledgements

I could not have undertaken this journey without Prof. Maurizio Taglialatela; he mentored me during my PhD programme, trained me to think as a scientist and supported me during every step, particularly during the most difficult ones. Furthermore, this endeavour would not have been possible without our collaborators Dr. Gaetan Lesca and Prof. Ingrid Scheffer for pointing out patients bearing the mutations under study in this work. Moreover, Prof. Fabio Benfenati, Dr. Luca Maragliano, Dr. Giulio Alberini and Dr. Alessandro Berselli made a decisive contribution and I would thank them for producing the *in silico* molecular dynamics data and for giving me permission to include these data within my thesis.

I am also thankful to Dr. Francesco Miceli, who trained me and helped me to deal with challenges; for the same reasons, I also have to thank Dr. Vincenzo Barrese. Words cannot express my gratitude to Antonios Pantazis, in Linköping University, who hosted me in his lab and trained me as any other member of his group, and to Sara Liin, for her valuable guidance and advice. I'm extremely thankful also to Dr. Michael Pusch for hosting me in his laboratory at the Institute of Biophysics (IBF) at the National Research Center (CNR) in Genoa, and for making my experience as a precious and instructive one.

I'd like to acknowledge Lidia Carotenuto and I would thank all the members of Taglialatela's lab. I would be remiss in not mentioning for their hospitality and friendliness, Catherine Wang, Michelle Nillson and Serena Pozzi, Damon Frampton, Ali Kusai and all the other members of Pantazis' and Liin's lab for their late-night feedback sessions and moral support. Thanks also to Sara Bertelli, Paolo Zuccolini and all the guys of IBF. Finally, I am grateful to Gabriella, for her loving presence, support and help during my doctoral journey.

Bibliography

- Aggarwal, S. K., & MacKinnon, R. (1996). Contribution of the S4 segment to gating charge in the Shaker K+ channel. *Neuron*, *16*(6), 1169-1177.
- Ahern, C. A., Payandeh, J., Bosmans, F., & Chanda, B. (2016). The hitchhiker's guide to the voltage-gated sodium channel galaxy. *Journal of General Physiology*, *147*(1), 1-24.
- Alam, A., & Jiang, Y. (2009). High-resolution structure of the open NaK channel. *Nature structural & molecular biology*, *16*(1), 30-34.
- Alberini, G., Alexis Paz, S., Corradi, B., Abrams, C. F., Benfenati, F., & Maragliano, L. (2023). Molecular Dynamics Simulations of Ion Permeation in Human Voltage-Gated Sodium Channels. Journal of Chemical Theory and Computation, 19(10), 2953-2972.
- Alberini, G., Benfenati, F., & Maragliano, L. (2021). Structural Mechanism of ω-Currents in a Mutated Kv7. 2 Voltage Sensor Domain from Molecular Dynamics Simulations. Journal of Chemical Information and Modeling, 61(3), 1354-1367.
- Allen, N. M., Mannion, M., Conroy, J., Lynch, S. A., Shahwan, A., Lynch, B., & King, M. D. (2014). The variable phenotypes of KCNQ-related epilepsy. *Epilepsia*, *55*(9), e99-e105.
- Ambrosino, P., Freri, E., Castellotti, B., Soldovieri, M. V., Mosca, I., Manocchio, L., ... & Taglialatela, M. (2018). Kv7. 3 compound heterozygous variants in early onset encephalopathy reveal additive contribution of C-terminal residues to PIP 2-dependent K+ channel gating. *Molecular Neurobiology*, *55*, 7009-7024.
- Anderson, P. A., & Greenberg, R. M. (2001). Phylogeny of ion channels: clues to structure and function. *Comparative Biochemistry and Physiology Part B: Biochemistry and Molecular Biology*, *129*(1), 17-28.
- Armstrong, C. M., & Bezanilla, F. (1973). Currents related to movement of the gating particles of the sodium channels. *Nature*, *242*(5398), 459-461.
- Babu, Y. S., Bugg, C. E., & Cook, W. J. (1988). Structure of calmodulin refined at 2.2 Å resolution. *Journal of molecular biology*, *204*(1), 191-204.

- Bähring, R., & Covarrubias, M. (2011). Mechanisms of closed-state inactivation in voltage-gated ion channels. *The Journal of physiology*, *589*(3), 461-479.
- Bal, M., Zhang, J., Zaika, O., Hernandez, C. C., & Shapiro, M. S. (2008). Homomeric and heteromeric assembly of KCNQ (Kv7) K+ channels assayed by total internal reflection fluorescence/fluorescence resonance energy transfer and patch clamp analysis. *Journal of Biological Chemistry*, *283*(45), 30668-30676.
- Balusek, C., Hwang, H., Lau, C. H., Lundquist, K., Hazel, A., Pavlova, A., ... & Gumbart, J. C. (2019). Accelerating membrane simulations with hydrogen mass repartitioning. Journal of chemical theory and computation, 15(8), 4673-4686.
- Bayat, A., Iavarone, S., Miceli, F., Jakobsen, A. V., Johannesen, K. M., Nikanorova, M., ... & Møller, R. S. (2024). Phenotypic and functional assessment of two novel *KCNQ2* gain-of-function variants Y141N and G239S and effects of amitriptyline treatment. *Neurotherapeutics*, *21*(1), e00296.
- Berkovic, S. F., Heron, S. E., Giordano, L., Marini, C., Guerrini, R., Kaplan, R. E., ... & Scheffer, I. E. (2004). Benign familial neonatal-infantile seizures: characterization of a new sodium channelopathy. *Annals of neurology*, *55*(4), 550-557.
- Best, R. B., Zhu, X., Shim, J., Lopes, P. E., Mittal, J., Feig, M., & MacKerell Jr, A. D. (2012). Optimization of the additive CHARMM all-atom protein force field targeting improved sampling of the backbone ϕ, ψ and side-chain χ1 and χ2 dihedral angles. *Journal of chemical theory and computation*, *8*(9), 3257-3273.
- Bezanilla, F. (2000). The voltage sensor in voltage-dependent ion channels. *Physiological reviews*, *80*(2), 555-592.
- Bezanilla, F., & Armstrong, C. M. (1972). Negative conductance caused by entry of sodium and cesium ions into the potassium channels of squid axons. *The Journal of General Physiology*, *60*(5), 588-608.
- Bhattacharjee, A., & Kaczmarek, L. K. (2005). For K+ channels, Na+ is the new Ca2+. *Trends in neurosciences*, *28*(8), 422-428.
- Biba-Maazou, N., Becq, H., Pallesi-Pocachard, E., Sarno, S., Granjeaud, S., Montheil, A., ... & Aniksztejn, L. (2022). Time-limited alterations in

cortical activity of a knock-in mouse model of *KCNQ2*-related developmental and epileptic encephalopathy. *The Journal of Physiology*, *600*(10), 2429-2460.

- Bocksteins, E. (2016). Kv5, Kv6, Kv8, and Kv9 subunits: No simple silent bystanders. *Journal of General Physiology*, *147*(2), 105-125.
- Boßelmann, C. M., Hedrich, U. B., Müller, P., Sonnenberg, L., Parthasarathy, S., Helbig, I., ... & Pfeifer, N. (2022). Predicting the functional effects of voltage-gated potassium channel missense variants with multi-task learning. *EBioMedicine*, *81*.
- Boulet, I. R., Labro, A. J., Raes, A. L., & Snyders, D. J. (2007). Role of the S6 C-terminus in *KCNQ1* channel gating. *The Journal of physiology*, *585*(2), 325-337.
- Brown, D. A., & Adams, P. R. (1980). Muscarinic suppression of a novel voltage-sensitive K+ current in a vertebrate neurone. Nature, 283(5748), 673-676.
- Buzsáki, G. (2015). Hippocampal sharp wave-ripple: A cognitive biomarker for episodic memory and planning. *Hippocampus*, *25*(10), 1073-1188.
- Castaldo, P., del Giudice, E. M., Coppola, G., Pascotto, A., Annunziato, L., & Taglialatela, M. (2002). Benign familial neonatal convulsions caused by altered gating of *KCNQ2*/*KCNQ3* potassium channels. *The Journal of Neuroscience*, *22*(2), RC199.
- Catterall, W. A. (2016). Dravet syndrome: a sodium channel interneuronopathy. *Ion Channels in Health and Disease*, 85-111.
- Cavaretta, J. P., Sherer, K. R., Lee, K. Y., Kim, E. H., Issema, R. S., & Chung, H. J. (2014). Polarized axonal surface expression of neuronal KCNQ potassium channels is regulated by calmodulin interaction with *KCNQ2* subunit. *PloS one*, *9*(7), e103655.
- Chang, A., Abderemane-Ali, F., Hura, G. L., Rossen, N. D., Gate, R. E., & Minor, D. L. (2018). A calmodulin C-lobe Ca2+-dependent switch governs Kv7 channel function. *Neuron*, *97*(4), 836-852.
- Chang, A., Abderemane-Ali, F., Hura, G. L., Rossen, N. D., Gate, R. E., & Minor, D. L. (2018). A calmodulin C-lobe Ca2+-dependent switch governs Kv7 channel function. *Neuron*, *97*(4), 836-852.

- Charlier, C., Singh, N. A., Ryan, S. G., Lewis, T. B., Reus, B. E., Leach, R. J., & Leppert, M. (1998). A pore mutation in a novel KQT-like potassium channel gene in an idiopathic epilepsy family. *Nature genetics*, *18*(1), 53-55.
- Chen, L., Zhang, Q., Qiu, Y., Li, Z., Chen, Z., Jiang, H., ... & Yang, H. (2015). Migration of PIP2 lipids on voltage-gated potassium channel surface influences channel deactivation. *Scientific Reports*, *5*(1), 15079.
- Choveau, F. S., De la Rosa, V., Bierbower, S. M., Hernandez, C. C., & Shapiro, M. S. (2018). Phosphatidylinositol 4, 5-bisphosphate (PIP2) regulates *KCNQ3* K+ channels by interacting with four cytoplasmic channel domains. *Journal of Biological Chemistry*, *293*(50), 19411-19428.
- Clay, J. R., & Shlesinger, M. F. (1983). Effects of external cesium and rubidium on outward potassium currents in squid axons. *Biophysical Journal*, *42*(1), 43-53.
- Cooper, E. C., Aldape, K. D., Abosch, A., Barbaro, N. M., Berger, M. S., Peacock, W. S., ... & Jan, L. Y. (2000). Colocalization and coassembly of two human brain M-type potassium channel subunits that are mutated in epilepsy. *Proceedings of the National Academy of Sciences*, *97*(9), 4914-4919.
- Cooper, E. C., Harrington, E., Jan, Y. N., & Jan, L. Y. (2001). M channel *KCNQ2* subunits are localized to key sites for control of neuronal network oscillations and synchronization in mouse brain. *Journal of Neuroscience*, *21*(24), 9529-9540.
- Cordero-Morales, J. F., Cuello, L. G., Zhao, Y., Jogini, V., Cortes, D. M., Roux, B., & Perozo, E. (2006). Molecular determinants of gating at the potassium-channel selectivity filter. *Nature structural & molecular biology*, *13*(4), 311-318.
- Cordero-Morales, J. F., Gracheva, E. O., & Julius, D. (2011). Cytoplasmic ankyrin repeats of transient receptor potential A1 (TRPA1) dictate sensitivity to thermal and chemical stimuli. *Proceedings of the National Academy of Sciences*, *108*(46), E1184-E1191.
- Cuello, L. G., Jogini, V., Cortes, D. M., Pan, A. C., Gagnon, D. G., Dalmas, O., ... & Perozo, E. (2010). Structural basis for the coupling

between activation and inactivation gates in K+ channels. *Nature*, *466*(7303), 272-275.

- Deamer, D., Dworkin, J. P., Sandford, S. A., Bernstein, M. P., & Allamandola, L. J. (2002). The first cell membranes. *Astrobiology*, *2*(4), 371-381.
- Deciphering Developmental Disorders Study. Prevalence and architecture of de novo mutations in developmental disorders. Nature 542, 433–438 (2017).
- Delmas, P., & Brown, D. A. (2005). Pathways modulating neural KCNQ/M (Kv7) potassium channels. *Nature Reviews Neuroscience*, *6*(11), 850-862.
- Devaux, J. J., Kleopa, K. A., Cooper, E. C., & Scherer, S. S. (2004). *KCNQ2* is a nodal K+ channel. *Journal of Neuroscience*, *24*(5), 1236-1244.
- Devaux, J., Dhifallah, S., De Maria, M., Stuart-Lopez, G., Becq, H., Milh, M., ... & Aniksztejn, L. (2017). A possible link between KCNQ 2-and STXBP 1-related encephalopathies: STXBP 1 reduces the inhibitory impact of syntaxin-1A on M current. *Epilepsia*, *58*(12), 2073-2084.
- Devinsky, O., Vezzani, A., O'Brien, T. J., Jette, N., Scheffer, I. E., de Curtis, M., & Perucca, P. (2018). Epilepsy (primer). *Nature Reviews: Disease Primers*, *4*(1).
- Dirkx, N., Miceli, F., Taglialatela, M., & Weckhuysen, S. (2020). The role of Kv7. 2 in neurodevelopment: insights and gaps in our understanding. *Frontiers in Physiology*, 1240.
- Döring, F., Derst, C., Wischmeyer, E., Karschin, C., Schneggenburger, R., Daut, J., & Karschin, A. (1998). The epithelial inward rectifier channel Kir7. 1 displays unusual K+ permeation properties. *Journal of Neuroscience*, *18*(21), 8625-8636.
- Doyle, D. A., Cabral, J. M., Pfuetzner, R. A., Kuo, A., Gulbis, J. M., Cohen, S. L., ... & MacKinnon, R. (1998). The structure of the potassium channel: molecular basis of K+ conduction and selectivity. *science*, *280*(5360), 69-77.
- Eckey, K., Wrobel, E., Strutz-Seebohm, N., Pott, L., Schmitt, N., & Seebohm, G. (2014). Novel Kv7. 1-phosphatidylinositol 4, 5-

bisphosphate interaction sites uncovered by charge neutralization scanning. *Journal of biological chemistry*, *289*(33), 22749-22758.

- Epi4K Consortium., Epilepsy Phenome/Genome Project. De novo mutations in epileptic encephalopathies. Nature 501, 217–221 (2013).
- Etxeberria, A., Aivar, P., Rodriguez-Alfaro, J. A., Alaimo, A., Villace, P., Gomez-Posada, J. C., ... & Villarroel, A. (2008). Calmodulin regulates the trafficking of *KCNQ2* potassium channels. *The FASEB Journal*, *22*(4), 1135-1143.
- Feller, S. E., Zhang, Y., Pastor, R. W., & Brooks, B. R. (1995). Constant pressure molecular dynamics simulation: The Langevin piston method. The Journal of chemical physics, 103(11), 4613-4621.
- Fernández-Mariño, A. I., Tan, X. F., Bae, C., Huffer, K., Jiang, J., & Swartz, K. J. (2023). Inactivation of the Kv2. 1 channel through electromechanical coupling. *Nature*, *622*(7982), 410-417.
- Fidzinski, P., Korotkova, T., Heidenreich, M., Maier, N., Schuetze, S., Kobler, O., ... & Jentsch, T. J. (2015). *KCNQ5* K+ channels control hippocampal synaptic inhibition and fast network oscillations. *Nature communications*, *6*(1), 6254.
- Fisher, R. S., Acevedo, C., Arzimanoglou, A., Bogacz, A., Cross, J. H., Elger, C. E., ... & Wiebe, S. (2014). ILAE official report: a practical clinical definition of epilepsy. *Epilepsia*, *55*(4), 475-482.
- Fister, P., Soltirovska-Salamon, A., Debeljak, M., & Paro-Panjan, D. (2013). Benign familial neonatal convulsions caused by mutation in *KCNQ3*, exon 6: a European case. *European Journal of Paediatric Neurology*, *17*(3), 308-310.
- Gałecka, S., Kulawiak, B., Bednarczyk, P., Singh, H., & Szewczyk, A. (2021). Single channel properties of mitochondrial large conductance potassium channel formed by BK-VEDEC splice variant. *Scientific reports*, *11*(1), 10925.
- Gao, Y., Yechikov, S., Vazquez, A. E., Chen, D., & Nie, L. (2013). Distinct roles of molecular chaperones HSP90α and HSP90β in the biogenesis of *KCNQ4* channels. *PloS one*, *8*(2), e57282.
- Ghosh, A., Malavasi, E. L., Sherman, D. L., & Brophy, P. J. (2020). Neurofascin and Kv7. 3 are delivered to somatic and axon terminal

surface membranes en route to the axon initial segment. *Elife*, *9*, e60619.

- Gifford, J. L., Walsh, M. P., & Vogel, H. J. (2007). Structures and metal-ion-binding properties of the Ca2+-binding helix–loop–helix EF-hand motifs. *Biochemical Journal*, *405*(2), 199-221.
- Gilling, M., Rasmussen, H. B., Calloe, K., Sequeira, A. F., Baretto, M., Oliveira, G., ... & Tommerup, N. (2013). Dysfunction of the heteromeric KV7. 3/KV7. 5 potassium channel is associated with autism spectrum disorders. *Frontiers in genetics*, *4*, 54.
- Goddard, T. D., Huang, C. C., Meng, E. C., Pettersen, E. F., Couch, G. S., Morris, J. H., & Ferrin, T. E. (2018). UCSF ChimeraX: Meeting modern challenges in visualization and analysis. *Protein Science*, *27*(1), 14-25.
- Gong, P., Xue, J., Jiao, X., Zhang, Y., & Yang, Z. (2021). Genetic etiologies in developmental and/or epileptic encephalopathy with electrical status epilepticus during sleep: cohort study. *Frontiers in Genetics*, *12*, 607965.
- González, C., Baez-Nieto, D., Valencia, I., Oyarzún, I., Rojas, P., Naranjo, D., & Latorre, R. (2012). K+ channels: function-structural overview. Comprehensive physiology, 2(3), 2087-2149.
- Gonzalez, C., Lopez-Rodriguez, A., Srikumar, D., Rosenthal, J. J., & Holmgren, M. (2011). Editing of human KV1. 1 channel mRNAs disrupts binding of the N-terminus tip at the intracellular cavity. Nature Communications, 2(1), 436.
- Grinton, B. E., Heron, S. E., Pelekanos, J. T., Zuberi, S. M., Kivity, S., Afawi, Z., ... & Berkovic, S. F. (2015). Familial neonatal seizures in 36 families: clinical and genetic features correlate with outcome. *Epilepsia*, *56*(7), 1071-1080.
- Gu, N., Vervaeke, K., Hu, H., & Storm, J. F. (2005). Kv7/KCNQ/M and HCN/h, but not KCa2/SK channels, contribute to the somatic medium after-hyperpolarization and excitability control in CA1 hippocampal pyramidal cells. *The Journal of physiology*, *566*(3), 689-715.
- Guo, R., Zeng, W., Cui, H., Chen, L., & Ye, S. (2014). Ionic interactions of Ba2+ blockades in the MthK K+ channel. *Journal of General Physiology*, *144*(2), 193-200.

- Halliwell, J. V., & Adams, P. R. (1982). Voltage-clamp analysis of muscarinic excitation in hippocampal neurons. Brain research, 250(1), 71-92.
- Heinemann, S. H., & Conti, F. (1992). [7] Nonstationary noise analysis and application to patch clamp recordings. In Methods in enzymology (Vol. 207, pp. 131-148). Academic Press.
- Hernandez, C. C., Zaika, O., & Shapiro, M. S. (2008). A carboxy-terminal inter-helix linker as the site of phosphatidylinositol 4, 5-bisphosphate action on Kv7 (M-type) K+ channels. *The Journal of general physiology*, *132*(3), 361-381.
- Hibino, H., Inanobe, A., Furutani, K., Murakami, S., Findlay, I. A. N., & Kurachi, Y. (2010). Inwardly rectifying potassium channels: their structure, function, and physiological roles. *Physiological reviews*, *90*(1), 291-366.
- Hille, B. (1972). The permeability of the sodium channel to metal cations in myelinated nerve. *The Journal of general physiology*, *59*(6), 637-658.
- Hille, B. (2001). Ion Channels of Excitable Membranes Third Edition.
- Hirose, S., Zenri, F., Akiyoshi, H., Fukuma, G., Iwata, H., Inoue, T., ... & Mitsudome, A. (2000). A novel mutation of *KCNQ3* (c. 925T→ C) in a Japanese family with benign familial neonatal convulsions. *Annals of Neurology: Official Journal of the American Neurological Association and the Child Neurology Society*, *47*(6), 822-826.
- Hite, R. K., Yuan, P., Li, Z., Hsuing, Y., Walz, T., & MacKinnon, R. (2015). Cryo-electron microscopy structure of the Slo2. 2 Na+-activated K+ channel. *Nature*, *527*(7577), 198-203.
- Hodgkin, A. L., & Huxley, A. F. (1952). A quantitative description of membrane current and its application to conduction and excitation in nerve. *The Journal of physiology*, *117*(4), 500.
- Hoshi, N., Zhang, J. S., Omaki, M., Takeuchi, T., Yokoyama, S., Wanaverbecq, N., ... & Higashida, H. (2003). AKAP150 signaling complex promotes suppression of the M-current by muscarinic agonists. *Nature neuroscience*, *6*(6), 564-571.
- Hoshi, T., Zagotta, W. N., & Aldrich, R. W. (1990). Biophysical and molecular mechanisms of Shaker potassium channel inactivation. *Science*, *250*(4980), 533-538.

- Hoshi, T., Zagotta, W. N., & Aldrich, R. W. (1991). Two types of inactivation in Shaker K+ channels: effects of alterations in the carboxy-terminal region. *Neuron*, *7*(4), 547-556.
- Hou, P., Kang, P. W., Kongmeneck, A. D., Yang, N. D., Liu, Y., Shi, J., ... & Cui, J. (2020). Two-stage electro–mechanical coupling of a KV channel in voltage-dependent activation. *Nature communications*, *11*(1), 676.
- Howard, R. J., Clark, K. A., Holton, J. M., & Minor, D. L. (2007). Structural insight into KCNQ (Kv7) channel assembly and channelopathy. *Neuron*, *53*(5), 663-675.
- Huang, H., & Trussell, L. O. (2011). *KCNQ5* channels control resting properties and release probability of a synapse. *Nature neuroscience*, *14*(7), 840-847.
- Huang, J., & MacKerell Jr, A. D. (2013). CHARMM36 all-atom additive protein force field: Validation based on comparison to NMR data. *Journal of computational chemistry*, *34*(25), 2135-2145.
- Huang, Y., Ma, D., Yang, Z., Zhao, Y., & Guo, J. (2023). Voltage-gated potassium channels KCNQs: Structures, mechanisms, and modulations. *Biochemical and Biophysical Research Communications*, 149218.
- Humphrey, W., Dalke, A., & Schulten, K. (1996). VMD: visual molecular dynamics. *Journal of molecular graphics*, *14*(1), 33-38.
- Iannotti, F. A., Barrese, V., Formisano, L., Miceli, F., & Taglialatela, M. (2013). Specification of skeletal muscle differentiation by repressor element-1 silencing transcription factor (REST)-regulated Kv7. 4 potassium channels. *Molecular biology of the cell*, *24*(3), 274-284.
- Jan, L. Y., & Jan, Y. N. (1992). Structural elements involved in specific K+ channel functions. *Annual review of physiology*, *54*(1), 537-555.
- Jan, L. Y., & Jan, Y. N. (1997). Voltage-gated and inwardly rectifying potassium channels. *The Journal of physiology*, *505*(2), 267-282.
- Jencks, W. P. (1987). *Catalysis in chemistry and enzymology*. Courier Corporation.
- Jentsch, T. J. (2000). Neuronal KCNQ potassium channels: physislogy and role in disease. *Nature Reviews Neuroscience*, *1*(1), 21-30.

- Jiang, Y., Lee, A., Chen, J., Cadene, M., Chait, B. T., & MacKinnon, R. (2002). Crystal structure and mechanism of a calcium-gated potassium channel. *Nature*, *417*(6888), 515-522.
- Jorgensen, W. L., Chandrasekhar, J., Madura, J. D., Impey, R. W., & Klein, M. L. (1983). Comparison of simple potential functions for simulating liquid water. *The Journal of chemical physics*, *79*(2), 926-935.
- Kadamur, G., & Ross, E. M. (2013). Mammalian phospholipase C. *Annual review of physiology*, *75*, 127-154.
- Kanaumi, T., Takashima, S., Iwasaki, H., Itoh, M., Mitsudome, A., & Hirose, S. (2008). Developmental changes in *KCNQ2* and *KCNQ3* expression in human brain: possible contribution to the age-dependent etiology of benign familial neonatal convulsions. *Brain and Development*, *30*(5), 362-369.
- Kang, P. W., Westerlund, A. M., Shi, J., White, K. M., Dou, A. K., Cui, A. H., ... & Cui, J. (2020). Calmodulin acts as a state-dependent switch to control a cardiac potassium channel opening. *Science advances*, *6*(50), eabd6798.
- Kaplanis, J., Samocha, K. E., Wiel, L., Zhang, Z., Arvai, K. J., Eberhardt, R. Y., ... & Retterer, K. (2020). Evidence for 28 genetic disorders discovered by combining healthcare and research data. *Nature*, *586*(7831), 757-762.
- Kim, D. M., & Nimigean, C. M. (2016). Voltage-gated potassium channels: a structural examination of selectivity and gating. Cold Spring Harbor perspectives in biology, 8(5), a029231.
- Kim, E. C., Zhang, J., Pang, W., Wang, S., Lee, K. Y., Cavaretta, J. P., ... & Chung, H. J. (2018). Reduced axonal surface expression and phosphoinositide sensitivity in Kv7 channels disrupts their function to inhibit neuronal excitability in *KCNQ2* epileptic encephalopathy. *Neurobiology of disease*, *118*, 76-93.
- Kim, R. Y., Pless, S. A., & Kurata, H. T. (2017). PIP2 mediates functional coupling and pharmacology of neuronal KCNQ channels. *Proceedings of the National Academy of Sciences*, *114*(45), E9702-E9711.
- Kiss, L., & Korn, S. J. (1998). Modulation of C-type inactivation by K+ at the potassium channel selectivity filter. *Biophysical Journal*, *74*(4), 1840-1849.

- Klauda, J. B., Venable, R. M., Freites, J. A., O'Connor, J. W., Tobias, D. J., Mondragon-Ramirez, C., ... & Pastor, R. W. (2010). Update of the CHARMM all-atom additive force field for lipids: validation on six lipid types. *The journal of physical chemistry B*, *114*(23), 7830-7843.
- Kothur, K., Holman, K., Farnsworth, E., Ho, G., Lorentzos, M., Troedson, C., ... & Bennetts, B. (2018). Diagnostic yield of targeted massively parallel sequencing in children with epileptic encephalopathy. *Seizure*, *59*, 132-140.
- Krüger, J., Schubert, J., Kegele, J., Labalme, A., Mao, M., Heighway, J., ... & Lerche, H. (2022). Loss-of-function variants in the *KCNQ5* gene are implicated in genetic generalized epilepsies. *EBioMedicine*, *84*.
- Kruse, M., Hammond, G. R., & Hille, B. (2012). Regulation of voltage-gated potassium channels by PI (4, 5) P2. *Journal of general physiology*, *140*(2), 189-205.
- Kuenze, G., Duran, A. M., Woods, H., Brewer, K. R., McDonald, E. F., Vanoye, C. G., ... & Meiler, J. (2019). Upgraded molecular models of the human *KCNQ1* potassium channel. *PloS one*, *14*(9), e0220415.
- Lam, J., Coleman, N., Garing, A. L. A., & Wulff, H. (2013). The therapeutic potential of small-conductance KCa2 channels in neurodegenerative and psychiatric diseases. *Expert opinion on therapeutic targets*, *17*(10), 1203-1220.
- Lauritano, A., Moutton, S., Longobardi, E., Tran Mau-Them, F., Laudati, G., Nappi, P., ... & Taglialatela, M. (2019). A novel homozygous *KCNQ3* loss-of-function variant causes non-syndromic intellectual disability and neonatal-onset pharmacodependent epilepsy. *Epilepsia Open*, *4*(3), 464-475.
- Lehman, A., Thouta, S., Mancini, G. M., Naidu, S., van Slegtenhorst, M., McWalter, K., ... & Claydon, T. (2017). Loss-of-function and gain-of-function mutations in *KCNQ5* cause intellectual disability or epileptic encephalopathy. *The American Journal of Human Genetics*, *101*(1), 65-74.
- Lelieveld, S. H., Reijnders, M. R., Pfundt, R., Yntema, H. G., Kamsteeg, E. J., de Vries, P., ... & Gilissen, C. (2016). Meta-analysis of 2,104 trios provides support for 10 new genes for intellectual disability. *Nature neuroscience*, *19*(9), 1194-1196.

- Lerche, Christian, et al. "Molecular cloning and functional expression of *KCNQ5*, a potassium channel subunit that may contribute to neuronal M-current diversity." *Journal of Biological Chemistry* 275.29 (2000): 22395-22400.
- Lesage, F., & Lazdunski, M. (2000). Molecular and functional properties of two-pore-domain potassium channels. *American Journal of Physiology-Renal Physiology*, *279*(5), F793-F801.
- Li, H. Y., Tang, B. S., Yan, X. X., Guo, J. F., Shen, L., Song, Y. M., ... & Yang, Q. A. (2006). Clinical and mutational analysis of *KCNQ3* gene in a Chinese family with benign familial neonatal convulsions. *Zhonghua yi xue yi Chuan xue za zhi= Zhonghua Yixue Yichuanxue Zazhi= Chinese Journal of Medical Genetics*, *23*(4), 374-377.
- Li, H., Li, N., Shen, L., Jiang, H., Yang, Q., Song, Y., ... & Tang, B. (2008). A novel mutation of *KCNQ3* gene in a Chinese family with benign familial neonatal convulsions. *Epilepsy research*, *79*(1), 1-5.
- Li, K., Jiang, Q., Bai, X., Yang, Y. F., Ruan, M. Y., & Cai, S. Q. (2017). Tetrameric assembly of K+ channels requires ER-located chaperone proteins. *Molecular Cell*, *65*(1), 52-65.
- Li, T., Wu, K., Yue, Z., Wang, Y., Zhang, F., & Shen, H. (2021). Structural basis for the modulation of human *KCNQ4* by small-molecule drugs. *Molecular Cell*, *81*(1), 25-37.
- Li, X., Zhang, Q., Guo, P., Fu, J., Mei, L., Lv, D., ... & Guo, J. (2021). Molecular basis for ligand activation of the human *KCNQ2* channel. *Cell Research*, *31*(1), 52-61.
- Li, Y., Gamper, N., Hilgemann, D. W., & Shapiro, M. S. (2005). Regulation of Kv7 (KCNQ) K+ channel open probability by phosphatidylinositol 4, 5-bisphosphate. *Journal of Neuroscience*, *25*(43), 9825-9835.
- Li, Y., Langlais, P., Gamper, N., Liu, F., & Shapiro, M. S. (2004). Dual phosphorylations underlie modulation of unitary KCNQ K+ channels by Src tyrosine kinase. *Journal of Biological Chemistry*, *279*(44), 45399-45407.
- Li, Y., Um, S. Y., & McDonald, T. V. (2006). Voltage-gated potassium channels: regulation by accessory subunits. *The Neuroscientist*, *12*(3), 199-210.

- Lipinsky, M., Tobelaim, W. S., Peretz, A., Simhaev, L., Yeheskel, A., Yakubovich, D., ... & Attali, B. (2020). A unique mechanism of inactivation gating of the Kv channel family member Kv7. 1 and its modulation by PIP2 and calmodulin. *Science advances*, *6*(51), eabd6922.
- Liu, W., & Devaux, J. J. (2014). Calmodulin orchestrates the heteromeric assembly and the trafficking of *KCNQ2/3* (Kv7. 2/3) channels in neurons. *Molecular and Cellular Neuroscience*, *58*, 40-52.
- Lockless, S. W., Zhou, M., & MacKinnon, R. (2007). Structural and thermodynamic properties of selective ion binding in a K+ channel. *PLoS biology*, *5*(5), e121.
- Lomize, M. A., Pogozheva, I. D., Joo, H., Mosberg, H. I., & Lomize, A. L. (2012). OPM database and PPM web server: resources for positioning of proteins in membranes. *Nucleic acids research*, *40*(D1), D370-D376.
- Long, S. B., Campbell, E. B., & MacKinnon, R. (2005). Crystal structure of a mammalian voltage-dependent Shaker family K+ channel. *Science*, *309*(5736), 897-903.
- Luo, Y., & Roux, B. (2010). Simulation of osmotic pressure in concentrated aqueous salt solutions. *The journal of physical chemistry letters*, *1*(1), 183-189.
- Ma, D., Zheng, Y., Li, X., Zhou, X., Yang, Z., Zhang, Y., ... & Guo, J. (2023). Ligand activation mechanisms of human *KCNQ2* channel. *Nature Communications*, *14*(1), 6632.
- MacKinnon, R. (1995). Pore loops: an emerging theme in ion channel structure. *Neuron*, *14*(5), 889-892.
- MacKinnon, R. (2004). Potassium channels and the atomic basis of selective ion conduction (Nobel Lecture). *Angewandte Chemie International Edition*, *43*(33), 4265-4277.
- Maghera, J., Li, J., Lamothe, S. M., Braun, M., Appendino, J. P., Au, P. B., & Kurata, H. T. (2020). Familial neonatal seizures caused by the Kv7. 3 selectivity filter mutation T313I. *Epilepsia Open*, *5*(4), 562-573.
- Maljevic, S., Vejzovic, S., Bernhard, M. K., Bertsche, A., Weise, S., Döcker, M., ... & Syrbe, S. (2016). Novel *KCNQ3* mutation in a large family with benign familial neonatal epilepsy: a rare cause of neonatal seizures. *Molecular Syndromology*, *7*(4), 189-196.

- Mandala, V. S., & MacKinnon, R. (2023). The membrane electric field regulates the PIP2-binding site to gate the *KCNQ1* channel. *Proceedings of the National Academy of Sciences*, *120*(21), e2301985120.
- Martinac, B., Saimi, Y., & Kung, C. (2008). Ion channels in microbes. *Physiological reviews*, *88*(4), 1449-1490.
- Martyna, G. J., Tobias, D. J., & Klein, M. L. (1994). Constant pressure molecular dynamics algorithms. The Journal of chemical physics, 101(5), 4177-4189.
- Meng, E. C., Goddard, T. D., Pettersen, E. F., Couch, G. S., Pearson, Z. J., Morris, J. H., & Ferrin, T. E. (2023). UCSF ChimeraX: Tools for structure building and analysis. *Protein Science*, *32*(11), e4792.
- Miceli, F., Carotenuto, L., Barrese, V., Soldovieri, M. V., Heinzen, E. L., Mandel, A. M., ... & Sands, T. T. (2020). A novel Kv7. 3 variant in the voltage-sensing S4 segment in a family with benign neonatal epilepsy: functional characterization and *in vitro* rescue by β-hydroxybutyrate. *Frontiers in physiology*, *11*, 1040.
- Miceli, F., Millevert, C., Soldovieri, M. V., Mosca, I., Ambrosino, P., Carotenuto, L., ... & Weckhuysen, S. (2022). *KCNQ2* R144 variants cause neurodevelopmental disability with language impairment and autistic features without neonatal seizures through a gain-of-function mechanism. *EBioMedicine*, *81*.
- Miceli, F., Soldovieri, M. V., Ambrosino, P., Barrese, V., Migliore, M., Cilio, M. R., & Taglialatela, M. (2013). Genotype–phenotype correlations in neonatal epilepsies caused by mutations in the voltage sensor of Kv7. 2 potassium channel subunits. *Proceedings of the National Academy of Sciences*, *110*(11), 4386-4391.
- Miceli, F., Soldovieri, M. V., Weckhuysen, S., Cooper, E., & Taglialatela, M. (2022). *KCNQ2*-related disorders.
- Miceli, F., Striano, P., Soldovieri, M. V., Fontana, A., Nardello, R., Robbiano, A., ... & Mangano, S. (2015). A novel *KCNQ3* mutation in familial epilepsy with focal seizures and intellectual disability. *Epilepsia*, *56*(2), e15-e20.
- Miceli, F., Striano, P., Soldovieri, M. V., Fontana, A., Nardello, R., Robbiano, A., ... & Mangano, S. (2015). A novel *KCNQ3* mutation in

familial epilepsy with focal seizures and intellectual disability. *Epilepsia*, *56*(2), e15-e20.

- Milh, M., Falace, A., Villeneuve, N., Vanni, N., Cacciagli, P., Assereto, S., ... & Fassio, A. (2013). Novel compound heterozygous mutations in TBC 1 D 24 cause familial malignant migrating partial seizures of infancy. *Human mutation*, *34*(6), 869-872.
- Millichap, J. J., Miceli, F., De Maria, M., Keator, C., Joshi, N., Tran, B., ... & Taglialatela, M. (2017). Infantile spasms and encephalopathy without preceding neonatal seizures caused by *KCNQ2* R198Q, a gain-of-function variant. *Epilepsia*, *58*(1), e10-e15.
- Mitterdorfer, J., & Bean, B. P. (2002). Potassium currents during the action potential of hippocampal CA3 neurons. *Journal of Neuroscience*, *22*(23), 10106-10115.
- Miyamoto, S. & Kollman, P. A. Settle: An analytical version of the SHAKE and RATTLE algorithm for rigid water models. Journal of Computational Chemistry 13, 952–962 (1992).
- Moulton, K. S., Vakili, K., Zurakowski, D., Soliman, M., Butterfield, C., Sylvin, E., ... & Folkman, J. (2003). Inhibition of plaque neovascularization reduces macrophage accumulation and progression of advanced atherosclerosis. *Proceedings of the National Academy of Sciences*, *100*(8), 4736-4741.
- Mucha, M., Ooi, L., Linley, J. E., Mordaka, P., Dalle, C., Robertson, B., ... & Wood, I. C. (2010). Transcriptional control of KCNQ channel genes and the regulation of neuronal excitability. *Journal of Neuroscience*, *30*(40), 13235-13245.
- Mulkey, S. B., Ben-Zeev, B., Nicolai, J., Carroll, J. L., Grønborg, S., Jiang, Y. H., ... & Cilio, M. R. (2017). Neonatal nonepileptic myoclonus is a prominent clinical feature of KCNQ 2 gain-of-function variants R201C and R201H. *Epilepsia*, *58*(3), 436-445.
- Nappi, P., Miceli, F., Soldovieri, M. V., Ambrosino, P., Barrese, V., & Taglialatela, M. (2020). Epileptic channelopathies caused by neuronal Kv7 (KCNQ) channel dysfunction. *Pflügers Archiv-European Journal of Physiology*, *472*, 881-898.

- Nay, P. O. A., & CHANNEL, M. (2018). STRUCTURAL MODELLING AND MUTANT CYCLE ANALYSIS PREDICT. Chasing Men on Fire: The Story of the Search for a Pain Gene, 251.
- Neher, E., & Sakmann, B. (1976). Single-channel currents recorded from membrane of denervated frog muscle fibres. *Nature*, *260*(5554), 799-802.
- Neubauer, B. A., Waldegger, S., Heinzinger, J., Hahn, A., Kurlemann, G., Fiedler, B., ... & Sander, T. (2008). *KCNQ2* and *KCNQ3* mutations contribute to different idiopathic epilepsy syndromes. *Neurology*, *71*(3), 177-183.
- Ngugi, A. K., Bottomley, C., Kleinschmidt, I., Sander, J. W., & Newton, C. R. (2010). Estimation of the burden of active and life-time epilepsy: a meta-analytic approach. *Epilepsia*, *51*(5), 883-890.
- Niday, Z., & Tzingounis, A. V. (2018). Potassium channel gain of function in epilepsy: an unresolved paradox. *The Neuroscientist*, *24*(4), 368-380.
- Noskov, S. Y., & Roux, B. (2008). Control of ion selectivity in LeuT: two Na+ binding sites with two different mechanisms. *Journal of molecular biology*, *377*(3), 804-818.
- Noskov, S. Y., Berneche, S., & Roux, B. (2004). Control of ion selectivity in potassium channels by electrostatic and dynamic properties of carbonyl ligands. *Nature*, *431*(7010), 830-834.
- Okada, M., Zhu, G., Hirose, S., Ito, K. I., Murakami, T., Wakui, M., & Kaneko, S. (2003). Age-dependent modulation of hippocampal excitability by KCNQ-channels. *Epilepsy research*, *53*(1-2), 81-94.
- Olson, H. E., Kelly, M., LaCoursiere, C. M., Pinsky, R., Tambunan, D., Shain, C., ... & Poduri, A. (2017). Genetics and genotype–phenotype correlations in early onset epileptic encephalopathy with burst suppression. *Annals of neurology*, *81*(3), 419-429.
- Ong, S. T., Tyagi, A., Chandy, K. G., & Bhushan, S. (2022). Mechanisms underlying C-type inactivation in Kv channels: Lessons from structures of human Kv1. 3 and fly shaker-IR channels. *Frontiers in Pharmacology*, *13*, 924289.
- Orhan, G., Bock, M., Schepers, D., Ilina, E. I., Reichel, S. N., Löffler, H., ... & Maljevic, S. (2014). Dominant-negative effects of *KCNQ2* mutations

are associated with epileptic encephalopathy. *Annals of neurology*, *75*(3), 382-394.

- Otto, J. F., Yang, Y., Frankel, W. N., White, H. S., & Wilcox, K. S. (2006). A spontaneous mutation involving *KCNQ2* (Kv7. 2) reduces M-current density and spike frequency adaptation in mouse CA1 neurons. *Journal of Neuroscience*, *26*(7), 2053-2059.
- Oyrer, J., Maljevic, S., Scheffer, I. E., Berkovic, S. F., Petrou, S., & Reid, C. A. (2018). Ion channels in genetic epilepsy: from genes and mechanisms to disease-targeted therapies. *Pharmacological reviews*, *70*(1), 142-173.
- Pan, Z., Kao, T., Horvath, Z., Lemos, J., Sul, J. Y., Cranstoun, S. D., ... & Cooper, E. C. (2006). A common ankyrin-G-based mechanism retains KCNQ and NaV channels at electrically active domains of the axon. *Journal of neuroscience*, *26*(10), 2599-2613.
- Pant, S., Zhang, J., Kim, E. C., Lam, K., Chung, H. J., & Tajkhorshid, E. (2021). PIP2-dependent coupling of voltage sensor and pore domains in Kv7. 2 channel. *Communications biology*, *4*(1), 1189.
- Papazian, D. M., Schwarz, T. L., Tempel, B. L., Jan, Y. N., & Jan, L. Y. (1987). Cloning of genomic and complementary DNA from Shaker, a putative potassium channel gene from Drosophila. *Science*, *237*(4816), 749-753.
- Parsegian, V. A. (1975). Ion-membrane interactions as structural forces. *Annals of the New York Academy of Sciences*, *264*(1), 161-174.
- Perozo, E., MacKinnon, R., Bezanilla, F., & Stefani, E. (1993). Gating currents from a nonconducting mutant reveal open-closed conformations in Shaker K+ channels. *Neuron*, *11*(2), 353-358.
- Peters, H. C., Hu, H., Pongs, O., Storm, J. F., & Isbrandt, D. (2005). Conditional transgenic suppression of M channels in mouse brain reveals functions in neuronal excitability, resonance and behavior. *Nature neuroscience*, *8*(1), 51-60.
- Pettersen, E. F., Goddard, T. D., Huang, C. C., Couch, G. S., Greenblatt, D. M., Meng, E. C., & Ferrin, T. E. (2004). UCSF Chimera—a visualization system for exploratory research and analysis. *Journal of computational chemistry*, *25*(13), 1605-1612.

- Pettersen, E. F., Goddard, T. D., Huang, C. C., Meng, E. C., Couch, G. S., Croll, T. I., ... & Ferrin, T. E. (2021). UCSF ChimeraX: Structure visualization for researchers, educators, and developers. *Protein Science*, *30*(1), 70-82.
- Phillips, J. C., Braun, R., Wang, W., Gumbart, J., Tajkhorshid, E., Villa, E., ... & Schulten, K. (2005). Scalable molecular dynamics with NAMD. Journal of computational chemistry, 26(16), 1781-1802.
- Pijpers, J. A., Au, P. Y. B., Weeke, L. C., Vein, A. A., Smit, L. S., Vilan, A., ... & Peeters-Scholte, C. M. (2023). Early recognition of characteristic conventional and amplitude-integrated EEG patterns of seizures in SCN2A and *KCNQ3*-related epilepsy in neonates. *Seizure: European Journal of Epilepsy*, *110*, 212-219.
- Piro, E., Nardello, R., Gennaro, E., Fontana, A., Taglialatela, M., Mangano, G. D., ... & Mangano, S. (2019). A novel mutation in *KCNQ3*-related benign familial neonatal epilepsy: electroclinical features and neurodevelopmental outcome. *Epileptic Disorders*, *21*(1), 87-91.
- Pless, S. A., Galpin, J. D., Niciforovic, A. P., Kurata, H. T., & Ahern, C. A. (2013). Hydrogen bonds as molecular timers for slow inactivation in voltage-gated potassium channels. *Elife*, *2*, e01289.
- Plouin, P. (1994). Benign familial neonatal convulsions. *Idiopathic generalized epilepsies: clinical, experimental and genetic aspects*.
- Punke, M. A., & Friederich, P. (2007). Amitriptyline is a potent blocker of human Kv1. 1 and Kv7. 2/7.3 channels. *Anesthesia & Analgesia*, *104*(5), 1256-1264.
- Rastin, C., Schenkel, L. C., & Sadikovic, B. (2023). Complexity in Genetic Epilepsies: A Comprehensive Review. *International Journal of Molecular Sciences*, *24*(19), 14606.
- Rauch, A., Wieczorek, D., Graf, E., Wieland, T., Endele, S., Schwarzmayr, T., ... & Strom, T. M. (2012). Range of genetic mutations associated with severe non-syndromic sporadic intellectual disability: an exome sequencing study. *The Lancet*, *380*(9854), 1674-1682.
- Regev, N., Degani-Katzav, N., Korngreen, A., Etzioni, A., Siloni, S., Alaimo, A., ... & Lotan, I. (2009). Selective interaction of syntaxin 1A with *KCNQ2*: possible implications for specific modulation of presynaptic activity. *PLoS One*, *4*(8), e6586.

- Rosenhouse-Dantsker, A., & Logothetis, D. E. (2006). New roles for a key glycine and its neighboring residue in potassium channel gating. *Biophysical journal*, *91*(8), 2860-2873.
- Rosti, G., Tassano, E., Bossi, S., Divizia, M. T., Ronchetto, P., Servetti, M., ... & Puliti, A. (2019). Intragenic duplication of *KCNQ5* gene results in aberrant splicing leading to a premature termination codon in a patient with intellectual disability. *European Journal of Medical Genetics*, *62*(9), 103555.
- Roux, B. (2005). Ion conduction and selectivity in K+ channels. *Annu. Rev. Biophys. Biomol. Struct.*, *34*, 153-171.
- Rudolf, G., de Bellescize, J., de Saint Martin, A., Arzimanoglou, A., Hirsch, M. P. V., Labalme, A., ... & Lesca, G. (2020). Exome sequencing in 57 patients with self-limited focal epilepsies of childhood with typical or atypical presentations suggests novel candidate genes. European Journal of Paediatric Neurology, 27, 104-110.
- Ryckaert, J.-P., Ciccotti, G. & Berendsen, H. J. C. Numerical integration of the cartesian equations of motion of a system with constraints: molecular dynamics of n-alkanes. Journal of Computational Physics 23, 327–341 (1977).
- Safiulina, V. F., Zacchi, P., Taglialatela, M., Yaari, Y., & Cherubini, E. (2008). Low expression of Kv7/M channels facilitates intrinsic and network bursting in the developing rat hippocampus. *The Journal of physiology*, *586*(22), 5437-5453.
- Saitsu, H., Kato, M., Osaka, H., Moriyama, N., Horita, H., Nishiyama, K., ... & Matsumoto, N. (2012). CASK aberrations in male patients with Ohtahara syndrome and cerebellar hypoplasia. *Epilepsia*, *53*(8), 1441-1449.
- Salkoff, L., Butler, A., Ferreira, G., Santi, C., & Wei, A. (2006). High-conductance potassium channels of the SLO family. *Nature Reviews Neuroscience*, *7*(12), 921-931.
- Sands, T. T., Balestri, M., Bellini, G., Mulkey, S. B., Danhaive, O., Bakken, E. H., ... & Cilio, M. R. (2016). Rapid and safe response to low-dose carbamazepine in neonatal epilepsy. *Epilepsia*, *57*(12), 2019-2030.
- Sands, T. T., Miceli, F., Lesca, G., Beck, A. E., Sadleir, L. G., Arrington, D. K., ... & Cilio, M. R. (2019). Autism and developmental disability caused

by *KCNQ3* gain-of-function variants. *Annals of neurology*, *86*(2), 181-192.

- Satterstrom, F. K., Kosmicki, J. A., Wang, J., Breen, M. S., De Rubeis, S., An, J. Y., ... & Demontis, D. (2020). Large-scale exome sequencing study implicates both developmental and functional changes in the neurobiology of autism. *Cell*, *180*(3), 568-584.
- Sausbier, M., Hu, H., Arntz, C., Feil, S., Kamm, S., Adelsberger, H., ... & Ruth, P. (2004). Cerebellar ataxia and Purkinje cell dysfunction caused by Ca2+-activated K+ channel deficiency. *Proceedings of the National Academy of Sciences*, *101*(25), 9474-9478.
- Schroeder, B. C., Hechenberger, M., Weinreich, F., Kubisch, C., & Jentsch, T. J. (2000). *KCNQ5*, a novel potassium channel broadly expressed in brain, mediates M-type currents. *Journal of Biological Chemistry*, *275*(31), 24089-24095.
- Schumacher, M. A., Rivard, A. F., Bächinger, H. P., & Adelman, J. P. (2001). Structure of the gating domain of a Ca2+-activated K+ channel complexed with Ca2+/calmodulin. *Nature*, *410*(6832), 1120-1124.
- Schwake, M., Jentsch, T. J., & Friedrich, T. (2003). A carboxy-terminal domain determines the subunit specificity of KCNQ K+ channel assembly. *EMBO reports*, *4*(1), 76-81.
- Schwarz, T. L., Tempel, B. L., Papazian, D. M., Jan, Y. N., & Jan, L. Y. (1988). Multiple potassium–channel components are produced by alternative splicing at the Shaker locus in Drosophila. Nature, 331(6152), 137-142.
- Seebohm, G., Strutz-Seebohm, N., Ureche, O. N., Baltaev, R., Lampert, A., Kornichuk, G., ... & Lang, F. (2006). Differential roles of S6 domain hinges in the gating of KCNQ potassium channels. *Biophysical journal*, *90*(6), 2235-2244.
- Seoh, S. A., Sigg, D., Papazian, D. M., & Bezanilla, F. (1996). Voltage-sensing residues in the S2 and S4 segments of the Shaker K+ channel. *neuron*, *16*(6), 1159-1167.
- Sigg, D., Stefani, E., & Bezanilla, F. (1994). Gating current noise produced by elementary transitions in Shaker potassium channels. Science, 264(5158), 578-582.

- Singh, N. A., Westenskow, P., Charlier, C., Pappas, C., Leslie, J., Dillon, J., ... & Leppert, M. F. (2003). *KCNQ2* and *KCNQ3* potassium channel genes in benign familial neonatal convulsions: expansion of the functional and mutation spectrum. *Brain*, *126*(12), 2726-2737.
- Smart O.S., (1996). HOLE: A program for the analysis of the pore dimensions of ion channel structural models. *J Mol Graph*, *14*, 376.
- Smart, O. S., Breed, J., Smith, G. R., & Sansom, M. S. (1997). A novel method for structure-based prediction of ion channel conductance properties. *Biophysical Journal*, *72*(3), 1109-1126.
- Soh, H., Springer, K., Doci, K., Balsbaugh, J. L., & Tzingounis, A. V. (2022). *KCNQ2* and *KCNQ5* form heteromeric channels independent of *KCNQ3*. *Proceedings of the National Academy of Sciences*, *119*(13), e2117640119.
- Soldovieri, M. V., Ambrosino, P., Mosca, I., De Maria, M., Moretto, E., Miceli, F., ... & Taglialatela, M. (2016). Early-onset epileptic encephalopathy caused by a reduced sensitivity of Kv7. 2 potassium channels to phosphatidylinositol 4, 5-bisphosphate. *Scientific reports*, *6*(1), 38167.
- Soldovieri, M. V., Ambrosino, P., Mosca, I., Miceli, F., Franco, C., Canzoniero, L. M. T., ... & Taglialatela, M. (2019). Epileptic encephalopathy in a patient with a novel variant in the Kv7. 2 S2 transmembrane segment: clinical, genetic, and functional features. *International Journal of Molecular Sciences*, *20*(14), 3382.
- Soldovieri, M. V., Boutry-Kryza, N., Milh, M., Doummar, D., Heron, B., Bourel, E., ... & Lesca, G. (2014). Novel KCNQ 2 and KCNQ 3 Mutations in a Large Cohort of Families with Benign Neonatal Epilepsy: First Evidence for an Altered Channel Regulation by Syntaxin-1 A. *Human mutation*, *35*(3), 356-367.
- Soldovieri, M. V., Miceli, F., & Taglialatela, M. (2011). Driving with no brakes: molecular pathophysiology of Kv7 potassium channels. *Physiology*, *26*(5), 365-376.
- Soldovieri, M. V., Miceli, F., & Taglialatela, M. (2011). Driving with no brakes: molecular pathophysiology of Kv7 potassium channels. *Physiology*, *26*(5), 365-376.

- Spitzmaul, G., Tolosa, L., Winkelman, B. H., Heidenreich, M., Frens, M. A., Chabbert, C., ... & Jentsch, T. J. (2013). Vestibular role of *KCNQ4* and *KCNQ5* K+ channels revealed by mouse models. *Journal of Biological Chemistry*, *288*(13), 9334-9344.
- Steinbach, P. J., & Brooks, B. R. (1994). New spherical-cutoff methods for long-range forces in macromolecular simulation. Journal of computational chemistry, 15(7), 667-683.
- Stewart, A. P., Gómez-Posada, J. C., McGeorge, J., Rouhani, M. J., Villarroel, A., Murrell-Lagnado, R. D., & Edwardson, J. M. (2012). The Kv7. 2/Kv7. 3 heterotetramer assembles with a random subunit arrangement. *Journal of Biological Chemistry*, *287*(15), 11870-11877.
- Stocker, M., & Pedarzani, P. (2000). Differential distribution of three Ca2+-activated K+ channel subunits, SK1, SK2, and SK3, in the adult rat central nervous system. *Molecular and Cellular Neuroscience*, *15*(5), 476-493.
- Storm, J. F. (1988). Temporal integration by a slowly inactivating K+ current in hippocampal neurons. *Nature*, *336*(6197), 379-381.
- Sun, J., & MacKinnon, R. (2017). Cryo-EM structure of a *KCNQ1*/CaM complex reveals insights into congenital long QT syndrome. *Cell*, *169*(6), 1042-1050.
- Sun, J., & MacKinnon, R. (2020). Structural basis of human *KCNQ1* modulation and gating. *Cell*, *180*(2), 340-347.
- Symonds, J. D., Zuberi, S. M., Stewart, K., McLellan, A., O ‘Regan, M., MacLeod, S., ... & Wilson, M. (2019). Incidence and phenotypes of childhood-onset genetic epilepsies: a prospective population-based national cohort. *Brain*, *142*(8), 2303-2318.
- Taglialatela, M., Ficker, E., Wible, B. A., & Brown, A. M. (1995). C-terminus determinants for Mg2+ and polyamine block of the inward rectifier K+ channel IRK1. *The EMBO journal*, *14*(22), 5532-5541.
- Tan, X., Bae, C., Stix, R., Fernández-Mariño, A. I., Huffer, K., Chang, T. H., ... & Swartz, K. (2022). Structure of the Shaker Kv channel and mechanism of slow C-type inactivation. *Biophysical Journal*, *121*(3), 294a-295°.

- Tao, X., Lee, A., Limapichat, W., Dougherty, D. A., & MacKinnon, R. (2010). A gating charge transfer center in voltage sensors. *Science*, *328*(5974), 67-73.
- Thiel, G., Moroni, A., Blanc, G., & Van Etten, J. L. (2013). Potassium ion channels: could they have evolved from viruses?. *Plant physiology*, *162*(3), 1215-1224.
- Thomas, D., Plant, L. D., Wilkens, C. M., McCrossan, Z. A., & Goldstein, S. A. (2008). Alternative translation initiation in rat brain yields K2P2. 1 potassium channels permeable to sodium. *Neuron*, *58*(6), 859-870.
- Tinel, N., Lauritzen, I., Chouabe, C., Lazdunski, M., & Borsotto, M. (1998). The *KCNQ2* potassium channel: splice variants, functional and developmental expression. Brain localization and comparison with *KCNQ3*. *FEBS letters*, *438*(3), 171-176.
- Tobelaim, W. S., Dvir, M., Lebel, G., Cui, M., Buki, T., Peretz, A., ... & Attali, B. (2017). Competition of calcified calmodulin N lobe and PIP2 to an LQT mutation site in Kv7. 1 channel. *Proceedings of the National Academy of Sciences*, *114*(5), E869-E878.
- Triggle, D. J., Gopalakrishnan, M., Rampe, D., Zheng, W., Mannhold, R., Kubinyi, H., & Folkers, G. (Eds.). (2006). *Voltage-gated ion channels as drug targets* (Vol. 29). Wiley-VCH.
- Trompoukis, G., Rigas, P., Leontiadis, L. J., & Papatheodoropoulos, C. (2020). Ih, GIRK, and KCNQ/Kv7 channels differently modulate sharp wave-ripples in the dorsal and ventral hippocampus. *Molecular and Cellular Neuroscience*, *107*, 103531.
- Trudeau, M. C., Warmke, J. W., Ganetzky, B., & Robertson, G. A. (1995). HERG, a human inward rectifier in the voltage-gated potassium channel family. *Science*, *269*(5220), 92-95.
- Tzingounis, A. V., Heidenreich, M., Kharkovets, T., Spitzmaul, G., Jensen, H. S., Nicoll, R. A., & Jentsch, T. J. (2010). The *KCNQ5* potassium channel mediates a component of the afterhyperpolarization current in mouse hippocampus. *Proceedings of the National Academy of Sciences*, *107*(22), 10232-10237.
- Varghese, N., Moscoso, B., Chavez, A., Springer, K., Ortiz, E., Soh, H., ... & Tzingounis, A. V. (2023). *KCNQ2/3* Gain-of-Function Variants and

Cell Excitability: Differential Effects in CA1 versus L2/3 Pyramidal Neurons. *Journal of Neuroscience*, *43*(38), 6479-6494.

- Venable, R. M., Luo, Y., Gawrisch, K., Roux, B., & Pastor, R. W. (2013). Simulations of anionic lipid membranes: development of interaction-specific ion parameters and validation using NMR data. *The journal of physical chemistry B*, *117*(35), 10183-10192.
- Wang, H. S., Pan, Z., Shi, W., Brown, B. S., Wymore, R. S., Cohen, I. S., ... & McKinnon, D. (1998). *KCNQ2* and *KCNQ3* potassium channel subunits: molecular correlates of the M-channel. *Science*, *282*(5395), 1890-1893.
- Waterhouse, A., Bertoni, M., Bienert, S., Studer, G., Tauriello, G., Gumienny, R., ... & Schwede, T. (2018). SWISS-MODEL: homology modelling of protein structures and complexes. *Nucleic acids research*, *46*(W1), W296-W303.
- Wawrzkiewicz-Jałowiecka, A., Borys, P., & Grzywna, Z. J. (2017). Impact of geometry changes in the channel pore by the gating movements on the channel's conductance. Biochimica et Biophysica Acta (BBA)-Biomembranes, 1859(3), 446-458.
- Weckhuysen, S., Ivanovic, V., Hendrickx, R., Van Coster, R., Hjalgrim, H., Møller, R. S., ... & *KCNQ2* Study Group. (2013). Extending the *KCNQ2* encephalopathy spectrum: clinical and neuroimaging findings in 17 patients. *Neurology*, *81*(19), 1697-1703.
- Weckhuysen, S., Mandelstam, S., Suls, A., Audenaert, D., Deconinck, T., Claes, L. R., ... & De Jonghe, P. (2012). *KCNQ2* encephalopathy: emerging phenotype of a neonatal epileptic encephalopathy. *Annals of neurology*, *71*(1), 15-25.
- Wei, A. D., Wakenight, P., Zwingman, T. A., Bard, A. M., Sahai, N., Willemsen, M. H., ... & Kalume, F. K. (2022). Human *KCNQ5* de novo mutations underlie epilepsy and intellectual disability. *Journal of neurophysiology*, *128*(1), 40-61.
- Wen, H., & Levitan, I. B. (2002). Calmodulin is an auxiliary subunit of *KCNQ2/3* potassium channels. *Journal of Neuroscience*, *22*(18), 7991-8001.
- Willegems, K., Eldstrom, J., Kyriakis, E., Ataei, F., Sahakyan, H., Dou, Y., ... & Fedida, D. (2022). Structural and electrophysiological basis for the

modulation of *KCNQ1* channel currents by ML277. *Nature Communications*, *13*(1), 3760.

- Winks, J. S., Hughes, S., Filippov, A. K., Tatulian, L., Abogadie, F. C., Brown, D. A., & Marsh, S. J. (2005). Relationship between membrane phosphatidylinositol-4, 5-bisphosphate and receptor-mediated inhibition of native neuronal M channels. *Journal of Neuroscience*, *25*(13), 3400-3413.
- Wladyka, C. L., & Kunze, D. L. (2006). KCNQ/M-currents contribute to the resting membrane potential in rat visceral sensory neurons. *The Journal of physiology*, *575*(1), 175-189.
- Yang, S. B., & Jan, L. Y. (2013). Potassium channels: their physiological and molecular diversity. *Encyclopedia of biophysics. Springer, Berlin*, 1933-1941.
- Yao, X., Liu, W., Tian, S., Rafi, H., Segal, A. S., & Desir, G. V. (2000). Close association of the N terminus of Kv1. 3 with the pore region. *Journal of Biological Chemistry*, *275*(15), 10859-10863.
- Yus-Nájera, E., Santana-Castro, I., & Villarroel, A. (2002). The identification and characterization of a noncontinuous calmodulin-binding site in noninactivating voltage-dependent KCNQ potassium channels. *Journal of Biological Chemistry*, *277*(32), 28545-28553.
- Zagotta, W. N., Hoshi, T., & Aldrich, R. W. (1990). Restoration of inactivation in mutants of Shaker potassium channels by a peptide derived from ShB. *Science*, *250*(4980), 568-571.
- Zaika, O., Hernandez, C. C., Bal, M., Tolstykh, G. P., & Shapiro, M. S. (2008). Determinants within the turret and pore-loop domains of *KCNQ3* K+ channels governing functional activity. *Biophysical journal*, *95*(11), 5121-5137.
- Zara, F., Specchio, N., Striano, P., Robbiano, A., Gennaro, E., Paravidino, R., ... & Minetti, C. (2013). Genetic testing in benign familial epilepsies of the first year of life: clinical and diagnostic significance. *Epilepsia*, *54*(3), 425-436.
- Zaydman, M. A., & Cui, J. (2014). PIP2 regulation of KCNQ channels: biophysical and molecular mechanisms for lipid modulation of voltage-dependent gating. *Frontiers in physiology*, *5*, 195.

- Zaydman, M. A., Silva, J. R., Delaloye, K., Li, Y., Liang, H., Larsson, H. P., ... & Cui, J. (2013). Kv7. 1 ion channels require a lipid to couple voltage sensing to pore opening. *Proceedings of the National Academy of Sciences*, *110*(32), 13180-13185.
- Zhang, J., & Shapiro, M. S. (2012). Activity-dependent transcriptional regulation of M-type (Kv7) K+ channels by AKAP79/150-mediated NFAT actions. *Neuron*, *76*(6), 1133-1146.
- Zhang, J., & Shapiro, M. S. (2016). Mechanisms and dynamics of AKAP79/150-orchestrated multi-protein signalling complexes in brain and peripheral nerve. *The Journal of Physiology*, *594*(1), 31-37.
- Zhang, J., Kim, E. C., Chen, C., Procko, E., Pant, S., Lam, K., ... & Chung, H. J. (2020). Identifying mutation hotspots reveals pathogenetic mechanisms of *KCNQ2* epileptic encephalopathy. *Scientific reports*, *10*(1), 4756.
- Zhang, X., Bursulaya, B., Lee, C. C., Chen, B., Pivaroff, K., & Jegla, T. (2009). Divalent cations slow activation of EAG family K+ channels through direct binding to S4. *Biophysical journal*, *97*(1), 110-120.
- Zheng, Y., Liu, H., Chen, Y., Dong, S., Wang, F., Wang, S., ... & Xu, F. (2022). Structural insights into the lipid and ligand regulation of a human neuronal KCNQ channel. *Neuron*, *110*(2), 237-247.
- Zhou, M., & MacKinnon, R. (2004). A mutant KcsA K+ channel with altered conduction properties and selectivity filter ion distribution. *Journal of molecular biology*, *338*(4), 839-846.
- Zhou, X., Ma, A., Liu, X., Huang, C., Zhang, Y., Shi, R., ... & Li, S. (2006). Infantile seizures and other epileptic phenotypes in a Chinese family with a missense mutation of *KCNQ2*. *European journal of pediatrics*, *165*, 691-695.
- Zhou, Y., & MacKinnon, R. (2003). The occupancy of ions in the K+ selectivity filter: charge balance and coupling of ion binding to a protein conformational change underlie high conduction rates. *Journal of molecular biology*, *333*(5), 965-975.
- Zhou, Y., Morais-Cabral, J. H., Kaufman, A., & MacKinnon, R. (2001). Chemistry of ion coordination and hydration revealed by a K+ channel–Fab complex at 2.0 Å resolution. *Nature*, *414*(6859), 43-48.